TAMPEREEN TEKNILLINEN YLIOPISTO
TAMPERE UNIVERSITY OF TECHNOLOGY

SAYEDMOHSEN SHAHSHAHAN

CHARACTERIZATION OF FUNCTIONAL GROUPS ON THE SURFACE OF SONICATED CARBON NANOTUBES BY OPTICAL SPECTROSCOPY METHODS

Master of Science Thesis

Examiner: Professor Jyrki Vourinen
Examiner and topic approved by the Faculty Council of the Faculty of Engineering Sciences on
12th August 2015

ABSTRACT

SAYEDMOHSEN SHAHSHAHAN: Characterization of Functional Groups on the Surface of Sonicated Carbon Nanotubes by Optical Spectroscopy Methods
Tampere University of Technology
Master of Science Thesis, 106 pages, 03 appendices pages
March 2016
Master's Degree Program in Materials Science
Major: Materials Research
Examiner: Professor Jyrki Vourinen
Keywords: Characterization of Functional Groups, Carbon Nanotubes, Sonicated Carbon Nanotubes, Ultrasonication, Functionalization, Optical Spectroscopy, Fourier Transform Infrared (FTIR) Spectroscopy, Raman Spectroscopy, Dispersion of Carbon Nanotubes, Surface Chemistry of Carbon Nanotubes, Sonochemistry

Carbon nanotubes (CNTs) due to their unique properties are used in the various applications. Oftentimes for using this material as a component of a composite material, uniform dispersion of CNTs particles plays vital role in the final properties of structure. Ultrasonication technique is one of the major methods for dispersion of carbon nanotubes in a suspension. On the other side, defects and functional groups on the surface of CNTs affect on the mechanical, electrical, and thermal properties of the final product.

This study follows two major targets. The initial goal is the characterization of functional groups and defects on the surface of sonicated carbon nanotubes by helping of Fourier transform infrared (FTIR) and Raman spectroscopy. What follows is the study of relationship between sonication time and functional groups on the CNTs.

In this regard, CNTs were sonicated in Jeffamine® D-230 polyetheramine and deionized water at different times and by different amount of energy. Characterization tests revealed significant changes on the surface of CNTs during sonication process. Current study clarifies what should be expected about surface chemistry of CNTs while ultrasonication process is selected as dispersion method.

PREFACE AND ACKNOWLEDGEMENT

This master thesis was carried out at Department of Materials Science of Tampere University of Technology (TUT), during the years 2015-16. This thesis is one of the fruits of my work at the Department of Materials Science of TUT. First of all, I should to have greatest appreciation to my supervisor, **Prof. Jyrki Vourinen** for giving me this chance to work in so professional and strong group. My special gratitude goes to **M.Sc. Pasi Keinanen** who without his patience, guidance, advises, supports, and supervising never was done this thesis. I would like to express my sincere gratitude to **Dr. Alexander Efimov**, responsible of FTIR device in Department of Chemistry and Bioengineering, for his valuable assists. Current thesis is deeply indebted to him for his immense knowledge in infrared spectroscopy. Also I must explain my deep gratitude to **Dr. Nezamoddin Mirsattari**[1] who this thesis is indebted to him for his valuable consultation in surface chemistry of carbon nonotube (CNT). I wish to express my appreciation to my dear friend and colleague, **M.Sc. Mitra Akbari** who always supports me by her inspirational guidance during my master thesis and education. Also I should mention to assists of **M.Sc. Sanna Siljander** responsible of FTIR device at laboratory of the Department of Materials Science.

Further, I would like to express my utmost spiritual gratitude to my family, specially **my mother**, alone angel of my life, who it would not have been possible study in Finland without her support. Also, I should appreciate **my dear brothers, Mojtaba, Mortaza and Mohammad** who always support me during my life. At the end, thanks to my supportive friend, **Arman Dastpak** who his friendship and supports have been greatest my spiritual wealth during my master studies in Finland.

Tampere, Finland, March 2016

Mohsen Shahshahan

[1] Azad University Shahreza Branch, Isfahan, Iran

TABLE OF CONTENTS

1. INTRODUCTION 1
1.1 Motivation and challenges of Thesis 1
1.2 Thesis Outlines 2
2. THEORETICAL BACKGROUND 5
2.1 Surface Chemistry of Carbon Nanotubes 6
2.1.1 Structure, and Chemical Bonding of Carbon Nanotubes 7
2.1.2 Defects and Disorder in Carbon nanotubes 10
2.1.3 Reactivity of Carbon Nanotubes 12
2.1.4 Functional Groups on the CNT 15
2.2 Ultrasonic Dispersion of Carbon Nanotubes 16
2.3 Optical Spectroscopy Methods 18
2.3.1 Fundamental Concepts of Optical Spectroscopy 18
2.3.2 Fourier Transform Infrared (FTIR) Spectroscopy 21
2.3.3 Raman Spectroscopy 33
2.4 Study of Carbon Nanotubes Surface by Optical Spectroscopy 42
2.4.1 Characterization of Functional Groups on the Carbon Nanotubes by FTIR Spectroscopy 42
2.4.2 Characterization of Carbon Nanotubes by Raman Spectroscopy 45
3. EXPERIMENTAL 52
3.1 Materials 53
3.2 Processing 55
3.2.1 Preparation of suspension 55
3.2.2 Sonication 56
3.2.3 Separation 58
3.2.4 Drying 59
3.3 Characterization 60
3.3.1 Characterization by Fourier Transform Infrared (FTIR) Spectroscopy 60
3.3.2 Characterization by Raman Spectroscopy 64
4. RESULTS AND DISCUSSION 66
4.1 Study of Raw Materials 66
4.2 Study of CNTs Sonicated in the DIW 70
4.3 Study of CNTs Sonicated in the JD230 86
5. SUMMARY AND CONCLUSION 96
REFERENCES 99
APPENDICES 107
Appendix A: IR Absorptions by Frequency Regions 107

LIST OF FIGURES

Figure 2-1: The whole structure of theoretical background chapter. 5
Figure 2-2: Graphene sheet rolled up with different chiralities to form CNT. 6
Figure 2-3: Single wall carbon nanotube (SWCNT), double wall carbon nanotube (DWCNT), and multi wall carbon nanotube (MWCNT). 7
Figure 2-4: The sp^2-hybridization 7
Figure 2-5: Forming σ and π bonds in graphene (or CNT) resulted from sp^2 hybridization. 8
Figure 2-6: The sp^3-hybridization. 9
Figure 2-7: a) The π orbitals of graphene, b) Rearrangement of π orbitals in C_{20}. 9
Figure 2-8: Rehybridization of a carbon nanotube. 10
Figure 2-9: STM view of the point defect between two chirally-distinct segments on the CNT 10
Figure 2-10: Vacancy defects in the graphene lattice: Mono-vacancy (a) before and (b) after reconstruction. Di-vacancy (c) before and (d) after reconstruction. 11
Figure 2-11: The Stone-Wales transformation in the graphene lattice. 11
Figure 2-12: (a) A single 5-7 defect and (b) a 5-7-7-5 Stone-Wales defect. 12
Figure 2-13: Relationship between bending degree and chemical reactivity for graphene sheet, CNT and fullerene. 12
Figure 2-14: Pyramidalization angle for sp^2 and sp^3 orbitals. 13
Figure 2-15: The end cap of tube, maximum curvature, maximum reactivity. 13
Figure 2-16: sp^3- hybridized defects related to open ends terminated and functional groups. 14
Figure 2-17: Defects act as active sites. 14
Figure 2-18: Changing chemical activity as function of bending angle. 14
Figure 2-19: Functionalization possibilities for CNTs: A) defect-group functionalization, B)covalent sidewall functionalization, C) non-covalent exohedral functionalization with surfactants, D) non-covalent exohedral functionalization with polymers and E) endohedral functionalization. 15
Figure 2-20: Cavitation phenomenon by ultrasonic waves. 16
Figure 2-21: Ultrasonic dispersion process. 17
Figure 2-22: Reaction zones during ultrasonication process. 17
Figure 2-23: Simple form of a spectrometer. 19
Figure 2-24: Electromagnetic radiation regions and molecular effects. 19
Figure 2-25: Quantized vibrations of atoms. 23
Figure 2-26: Change in the dipole moment of a heteronuclear diatomic molecule. 25
Figure 2-27: Stretching and bending vibration modes. 25
Figure 2-28: Symmetric and asymmetric stretching vibrations. 26

Figure 2-29: Different types of bending vibration modes. 26
Figure 2-30: Out-of-plane and in-plane bending vibration modes. 26
Figure 2-31: Structure of FTIR spectrometer. 27
Figure 2-32: Converting interferogram to spectrum by the Fourier transform operation. 28
Figure 2-33: Formation of evanescent waves. 30
Figure 2-34: Attenuated total reflection (ATR) technique. 30
Figure 2-35: Major functional groups and bonds along IR absorption frequency regions. 32
Figure 2-36: Tangent baseline measurement. 32
Figure 2-37: Calibration graph for determination of unknown concentration. 33
Figure 2-38: Different frequencies of Raman transitions. 34
Figure 2-39: Possible optical processes in IR and Raman Spectroscopy. 35
Figure 2-40:Place of different Raman transitions in Raman spectrum. 35
Figure 2-41: symmetric and asymmetric vibration modes of CO_2 molecule. 36
Figure 2-42: Possible molecular vibrations of carbon disulphide(CS_2) along their IR and Raman peaks. 37
Figure 2-43:Major parts of Raman spectrometer. 39
Figure 2-44: FT-IR spectra of CNTs oxidized with (a) HNO_3, (b) H_2SO_4/HNO_3, (c) $HClO_4$ and (d) H_2O_2. 45
Figure 2-45: Raman Spectrum of Graphene. 46
Figure 2-46: Brillouin zone in graphene lattice. 46
Figure 2-47: The displacement pattern corresponding to the E_{2g} phonon. 46
Figure 2-48: Breathing mode for bilayer graphene. 47
Figure 2-49: Raman spectrum of SWCNT with important bands. 48
Figure 2-50: Comparison of the Raman spectra related to SWCNT, DWCNT, and MWCNT 48
Figure 2-51: Raman map images of a CNT sample, and distribution of RBM, G band and D band. 49
Figure 2-52: Raman spectra of MWCNT samples after treatment with different agents. 50
Figure 2-53: Raman spectra of the MWCNT treated by H_2SO_4, HNO_3 and HCl acids. 51
Figure 2-54: The I_G/I_D ratios of different CNTs functionalized in different mediums and acid treatment times. 51
Figure 3-1: The whole structure of experimental chapter. 52
Figure 3-2: NC7000 CNT, naked eye and TEM view. 53
Figure 3-3: Uvasol® potassium bromide, chemical structure and naked eye view. 54
Figure 3-4: Jeffamine D-230 Polyetheramine, chemical structure and naked eye view. 54
Figure 3-5: JD230-CNT (a) and DIW-CNT(b) suspensions. 55
Figure 3-6: QSonica- Q700 device. 57

Figure 3-7: Appearance of J_n series samples after sonication.....58
Figure 3-8: Appearance of W_n series samples after sonication.....58
Figure 3-9: Filtration system.....59
Figure 3-10: Samples sonicated in the JD230 (a), and DIW (b), after separation step. 59
Figure 3-11: Termaks - TS 8136 dryer. 60
Figure 3-12: CNTs sonicated in the JD230 (a), and DIW (b), after drying. 60
Figure 3-13: FTIR-ATR (BRUKER-TENSOR 27) device.....61
Figure 3-14: Diamond-ATR spectrum of sample JC by BRUKER-TENSOR 27. 62
Figure 3-15: IR spectra of the CNT/KBr samples with different ratios.....62
Figure 3-16: FTIR-ATR (Perkin-Elmer Spectrum One) device 63
Figure 3-17: IR-ATR sample preparation of functionalized CNT samples. 63
Figure 3-18: RAMAN Imaging System WITEC alpha300R. 65
Figure 4-1: IR spectrum of used KBr.....66
Figure 4-2: IR spectrum of pristine CNT (NANOCYLTM NC7000). 67
Figure 4-3: IR spectrum of JD230. 68
Figure 4-4: IR spectrum of DIW. 68
Figure 4-5: IR spectrum of sample JC. 69
Figure 4-6: IR spectrum of sample W_0. 70
Figure 4-7: IR spectrum of sample W_5. 71
Figure 4-8: IR spectrum of sample W_{10}. 72
Figure 4-9: IR spectrum of sample W_{15}. 72
Figure 4-10: IR spectrum of sample $W_{20.}$ 72
Figure 4-11: IR spectrum of sample $W_{25.}$ 73
Figure 4-12: IR spectrum of sample $W_{30.}$ 73
Figure 4-13: IR spectrum of sample W_{35}. 73
Figure 4-14: Measurement of absorption for C-H bond located at 2922 cm^{-1} in the spectrum of sample W_5. 75
Figure 4-15: Changes of the absorption of O-H bond during increasing sonication time in the DIW medium. 76
Figure 4-16: Changes of the absorption of C-H bond during increasing sonication time in the DIW medium. 77
Figure 4-17: Changes of the absorption of COOH bond during increasing sonication time in the DIW medium. 78
Figure 4-18: Changes of the absorption of C=O bond during increasing sonication time in the DIW medium. 78
Figure 4-19: Changes of the absorption of H-O-H bond (Bending mode) during increasing sonication time in the DIW medium. 79
Figure 4-20: Changes of the absorption of C-O bond during increasing sonication time in the DIW medium. 80
Figure 4-21: Raman spectrum of sample W_0. 82
Figure 4-22: Raman spectrum of sample W_4. 82

Figure 4-23: Raman spectrum of sample W_6. 82
Figure 4-24: Raman spectrum of sample W_8. 83
Figure 4-25: Raman spectrum of sample W_{10}. 83
Figure 4-26: Comparison of Raman spectra related to samples W_0, W_4, W_6, W_8, and $W_{10.}$ 83
Figure 4-27: Effect of sonication time on the I_D/I_G ratio. 84
Figure 4-28: Non-hexagonal rings, optimized geometries for absorbing functional groups. 85
4-29: IR spectrum of sample J_0 86
Figure 4-30: IR spectrum of sample J_{10}. 87
Figure 4-31: IR spectrum of sample J_{20}. 87
Figure 4-32: IR spectrum of sample J_{30}. 88
Figure 4-33: IR spectrum of sample J_{40}. 88
Figure 4-34: IR spectrum of sample J_{50}. 88
Figure 4-35: IR spectrum of sample J_{60}. 89
Figure 4-36: IR spectrum of sample J_{70}. 89
Figure 4-37: IR spectrum of sample J_{80}. 89
Figure 4-38: IR spectrum of sample J_{90}. 90
Figure 4-39: Changes of the absorption of C-H bond during increasing sonication energy in the JD230 medium. 91
Figure 4-40: Changes of the absorption of COOH group during increasing sonication energy in the JD230 medium. 92
Figure 4-41: Various events for and against functionalization during sonication. 93
Figure 4-42: Changes of the absorption of C=O bond during increasing sonication energy in the JD230 medium. 94
Figure 4-43: Changes of the absorption of C-O bond during increasing sonication energy in the JD230 medium. 95

LIST OF TABLES

Table 2-1: Comparison of Raman and IR spectroscopy for characterization of some functional groups or vibration modes along own vibration frequency. 40
Table 2-2: Information obtained according to feature of Raman peak. 41
Table 2-3: IR absorption frequencies for oxygenated functional groups on the carbon materials surface. 43
Table 2-4: IR absorption frequencies for nitrogen functional groups on the carbon materials surface. 44
Table 3-1: Important chemical and physical properties of NC7000. 53
Table 3-2: Chemical and physical properties of JD230. 54
Table 3-3: Information related to suspension preparation of JD230-CNT samples. 56
Table 3-4: Information related to suspension preparation of DIW-CNT samples. 56
Table 3-5: Information related to sonication of JD230-CNT samples. 57
Table 3-6: Information related to sonication of DIW-CNT samples. 57
Table 3-7: Sonication parameters fixed for all of the samples. 58
Table 3-8: Properties of diamond prism of BRUKER-TENSOR 27 device. 61
Table 3-9: Spectroscopic parameters of measurements by BRUKER-TENSOR 27. 61
Table 3-10: Information of sample JC. 61
Table 3-11: Properties of Di/ZnSe prism of 'Perkin-Elmer Spectrum One' device. 63
Table 3-12: Spectroscopic parameters of measurements by 'Perkin-Elmer Spectrum One' device. 63
Table 3-13: Information of IR-ATR sample preparation for non-processed specimens. 64
Table 3-14: Information of IR-ATR sample preparation for the specimens sonicated in the JD230. 64
Table 3-15: Information of IR-ATR sample preparation for the specimens sonicated in the DIW. 64
Table 3-16: Features of the Raman spectroscopy tests. 65
Table 4-1: Qualitative analysis of IR spectrum of pristine CNT (NANOCYLTM NC7000). 67
Table 4-2: Qualitative analysis of IR spectrum of JD230. 68
Table 4-3: Qualitative analysis of IR spectrum of DIW. 69
Table 4-4: Qualitative analysis of IR spectrum of sample JC. 69
Table 4-5: Qualitative analysis of IR spectrum of sample W_0. 71
Table 4-6: Qualitative analysis of IR investigations related to samples W_0, W_5, and W_{35} 74
Table 4-7: Changes of the absorption of O-H bond during increasing sonication time in the DIW medium. 75

Table 4-8: Changes of the absorption of C-H bonds during increasing sonication time in the DIW medium. 76
Table 4-9: Changes of the absorption of COOH group during increasing sonication time in the DIW medium. 77
Table 4-10: Changes of the absorption of C=O bond during increasing sonication time in the DIW medium. 77
Table 4-11: Changes of the absorption of H-O-H bond (Bending mode) during increasing sonication time in the DIW medium. 79
Table 4-12: Changes of the absorption of C-O bond during increasing sonication time in the DIW medium. 79
Table 4-13: Characteristic parameters related to Raman spectra of samples W_0, W_4, W_6, W_8, and W_{10}. 84
Table 4-14: Qualitative analysis of IR spectrum of sample J_0 86
Table 4-15: Qualitative analysis of IR measurements related to samples J_0, J_{10}, and J_{90} 90
Table 4-16: Changes of the absorption of C-H bonds during increasing sonication energy in the JD230 medium. 91
Table 4-17: Changes of the absorption of COOH group during increasing sonication energy in the JD230 medium. 92
Table 4-18: Changes of the absorption of C=O bond during increasing sonication energy in the JD230 medium. 93
Table 4-19: Changes of the absorption of C-O bond during increasing sonication energy in the JD230 medium. 94
Table 5-1: Summary of IR qualitative analysis of important samples. 97

LIST OF SYMBOLS AND ABBREVIATIONS

®	Registered trademark
a	Vector related to reciprocal lattice of graphene
$A(r)$	Frequency domain points
a_1	Unit vector of graphene
a_2	Unit vector of graphene
A_s	Absorption of standard sample
A_t	Total absorption
A_u	Absorption of unknown sample
A_v	Absorbance
c	Concentration, Speed of light
c_s	Standard concentration
c_u	Unknown concentration
d_e	The effective penetration of the IR beam
$d_{e\perp}$	Perpendicular polarization
$d_{e\parallel}$	Parallel polarization
d_p	Depth of penetration
e	Euler's number
E	Electron field, Energy
E_0	Electron field of incident electromagnetic wave
E_{el}	Electronic energy
E_{rot}	Rotational energy
E_{vib}	Vibrational energy
f	Force constant

G_1	Vector related to reciprocal lattice of graphene
G_2	Vector related to reciprocal lattice of graphene
h	Planck constant
I	Intensity of the light after interaction with sample
I_0	Intensity of the light before interacting with sample
I_D	Intensity of D band
I_G	Intensity of G band
I_r	Intensity of Reflected light
I_t	Intensity of the transmitted light
J_n	JD230-CNT sample sonicated by n KJ energy.
K	A point series which present Brillouin zone in graphene lattice
l	Path length
m	Chirality index of carbon nanotube, Mass
m_1	Mass of individual atom
m_2	Mass of individual atom
n	Chirality index of carbon nanotube, Quantum number
N	Number of atoms, Number of points formed spectrum, Number of reflections
n_c	Refractive index of the crystal
n_s	Refractive index of the sample
P	Power
q	Electrical charge
Q	Normal mode of vibration in the molecule
Q_k	Normal mode of vibration in the molecule
Q_k^0	Amplitude of vibration of the molecule

r	Distance between the charges
R_v	Reflectance
t	Time
T	Carbon nanotube axis
T_v	Transmittance
V_{as}	Asymmetrical stretching vibration
V_s	Symmetrical stretching vibration
W_n	DIW-CNT sample sonicated for n min.
$X(k)$	Time domain points
α	Polarizability
δ	Bending vibration, Optical path difference
Δ	Mirror displacement
ΔE	Energy gap
$\mathcal{E}_v$	Frequency-dependent absorptivity constant
θ	Angle of incidence of IR beam
θ_c	Critical angle
θ_P	Pyramidalization angle
$\theta_{\sigma\pi}$	Angle between σ and π orbitals
λ	Wavelength
μ	Dipole, Dipole moment, The reduced mass per molecule
v	Frequency, Stretching vibration
v_0	Frequency of laser beam
v_k	Vibration frequency of the molecule
$\bar{v}$	Raman shift, Wavenumber
$^{\circ}C$	Centigrade degree

a.u.	Arbitrary Unit
A/D	Analog to Digital
AAS	Atomic Absorption Spectroscopy
AES	Atomic Emission Spectroscopy
Arb. unit	Arbitrary unit
asym	Asymmetry
atm	Atmospheres
ATR	Attenuated Total Reflection
Br	Bromine
C	Carbon
cc	Cubic centimeter
CCDs	Charge-Coupled Devices
CCVD	Catalytic Carbon Vapor Deposition
Cl	Chlorine
cm	Centimeters
Cm	Coulomb-Meter
cm^{-1}	Inverse Centimeters
CNT	Carbon Nanotube
Co.	Company
cP	Centipoise
cps	Counts Per Second
CPU	Central Processing Unit
cSt	Centistokes
CVD	Chemical Vapour Deposition
DFT	Density Functional Theory

Di/ZnSe	Diamond - Zinc Selenide
DIW	Deionized Water
DWCNT	Double Wall Carbon Nanotube
EPL	Effective Path Length
equ.	Equation
eV	Electronvolt
FFT	Fast Fourier Transform
FTIR	Fourier Transform Infrared (Spectroscopy)
gr	Grams
g/eq	Grams per equivalent
g/ml	Grams per milliliter
h	Hour
H	Hydrogen
hrs	Hours
Hz	Hertz
IR	Infrared
J s	Joule - Second
JC	JD230-CNT
JD230	Jeffamine D-230 polyetheramine
K	Kelvin, Potassium
K/sec	Kelvin per Second
KBr	Potassium Bromide
Kg/m^3	Kilograms per cubic meter
KJ	Kilojoules
km/h	Kilometers per Hour

LBMs	Layer-Breathing Modes
m^2/g	Square meters per gram
max	Maximum
min	Minimum, Minutes
MCNT	Multi Wall Carbon Nanotube
meq/g	Milliequivalents per gram
meV	Millielectron Volt
ml	Milliliters
mm	Millimeters
mW	Milliwatts
MWCNT	Multi Wall Carbon Nanotube
N	Nitrogen
N/S	Noise -to- Signal
nm	Nanometer
Nm^{-1}	Newton – Inverse Meters
O	Oxygen
OPD	Optical Path Difference
PECVD	Plasma Enhanced Chemical Vapour Deposition
pm	Picometer
R	Chemical Radical
RBM	Radial Breathing Mode
RT	Room Temperature
s	Seconds
S	Sulfur
S/N	Signal-to-Noise

STM	Scanning Tunneling Microscope
SW	Stone-Wales
SWCNT	Single Wall Carbon Nanotube
SWNT	Single Wall Carbon Nanotube
TEM	Transmission Electron Microscope
TM	Trademark
UV	Ultraviolet
VOL	Volume
WC	DIW-CNT
wt	weight
XPS	X-ray Photoelectron Spectroscopy
ZPD	Zero Path Difference
μm	Micrometer
μSec	Microsecond

1. INTRODUCTION

7th November 1991, an article which was published in Nature (VOL 354) changed materials science world completely. “Helical microtubules of graphitic carbon” written by Sumio Iijima led to explore of carbon nanotube (CNT) [1]. This discovery opened new window in materials science. Nowadays carbonaceous nanomaterials play vital and unique role in materials science and technology. Unique and special properties of CNTs such as thermal and electrical conductivity, semiconducting behavior and good mechanical properties along light weight, provide them for vast applications.

Surface chemistry of CNTs is one of the most important factors which affects on the functional properties of them directly. Hence control of environment which the CNTs are subjected is necessary. First study in this field was started by discovering that exposure of the CNTs to NH_3, NO_2, or O_2 affects on the electrical conductivity, in the year 2000. [2,3]

As mentioned, study of surface chemistry of CNTs clarifies physicochemical properties of final product. Also functional groups located on the CNT surface boost the solubility of nanotubes in solvents. Presence of chemical species on the surface of CNTs is studied by various characterization methods. Infrared spectroscopy (IR), X-ray photoelectron spectroscopy (XPS), Raman Spectroscopy, Boehm and potentiometric titrations are most popular methods for achieving to this target. [4,5]

1.1 Motivation and challenges of Thesis

Composite technology and industry uses carbon nanotubes (CNTs) due to their unique mechanical and functional properties. For using CNTs as a component of a composite structure, uniform dispersion of these particles affects on the final properties of composite significantly. Ultrasonication method is one of the main techniques for achieving to uniform dispersion of CNTs in a suspension. But it can be not the entire story. Positive role of sonication process in creation of uniform dispersion of CNTs is one side of a coin. The other side of the coin is side effect of this process on the surface chemistry of CNTs. [6–9]

The entire target of current thesis is study on the second side of the coin. Characterization of functional groups and defects on the surface of sonicated carbon nanotubes and relationship between sonication time and functional groups on the CNTs are focused in this thesis. In other words, this research clarifies what should be expected about surface chemistry of CNTs while sonication technique is selected as dispersion method.

In the current study, Fourier transform infrared (FTIR) and Raman spectroscopy are used for characterization of functional groups and defects on the surface of CNTs respectively. Also Jeffamine® D-230 polyetheramine and deionized water are selected as liquid part of CNT suspension. In the composite industry also these two liquids are selected for forming CNT suspension. This is philosophy of selection of these liquids in this thesis. In the composite industry, polyetheramine is used for polymerizing the carboxylated CNT because of its ability to make bonds with the amino groups and carboxyl groups of CNT which creates a resin used as polymeric matrix for nanocomposite structure. Actually, Jeffamine acts as curing agent during composite processing. [10,11]

In this study, the first challenge is opacity of carbon. Opacity of carbon materials results in decrease of energy throughput, and also reduce spectral signal-to-noise (S/N) ratio in IR spectroscopy. Actually, when study of surface chemistry of carbon by IR spectroscopy is subjected, main challenge is black body absorption of carbon. [5]

To select appropriate IR spectroscopy method, an extensive study was undertaken. Either direct transmission analysis (KBr tablet method) or attenuated total reflection (ATR) method where used. Many tests revealed that direct transmission analysis method due to high opacity of carbon is not appropriate method.

Finally, the ATR method was selected despite there are serious limitations for selection of appropriate ATR prism. Diamond (Di) and Diamond - Zinc Selenide (Di/ZnSe) ATR prisms were the only available choices for current study. Because refractive indexes of carbon and these prisms are close to 2.4, obtaining the IR spectrum which enjoys high signal-to-noise (S/N) ratio and high resolution is so troublous. Most favorable ATR prism for studying surface chemistry of carbon materials is germanium prism which enjoys refractive index of 4. The more difference between refractive indexes of prism and matter leads to more S/N ratio and resolution for spectrum. [12]

Another challenge is quantitative analysis by IR spectroscopy. Generally, IR spectroscopy is not reliable method for quantitative analysis. In order to obtain reliable results in current study, IR tests were repeated several times for each individual sample.

1.2 Thesis Outlines

This thesis includes 5 chapters. Chapter 2 looks at the theoretical background including:

- Surface chemistry of carbon nanotubes,
- Ultrasonic dispersion of carbon nanotubes,
- Optical spectroscopy methods (fundamental concepts, FTIR, and Raman spectroscopy),
- Study of carbon nanotubes surface by optical spectroscopy.

Writing this part is done quite scrupulously. The considered point in writing this part is that the existential philosophy of theoretical background is expanded explanation of whatever the reader requires for the comprehending the next parts (experimental, result and discussion parts). Thus, stating inapplicable points and concepts is avoided due to broadness of the subject. Regarding this point of view, it has been tried not to be negligent in stating the principle concepts.

The other viewpoint considered in writing this part is an evolutionary and dynamic spirituality in the context. Such that, it has been tried for the preliminary paragraphs to be simple, both for the type of expressions and also for the subject, and develop the expressed points as well as the style of writing. It has been tried that a paragraph to be the prerequisite for its next one, for the reader to understand the existential philosophy of each paragraph. Hence, bringing extra words that damages the current spirituality is avoided.

The point considered in writing this part with regards to the evolutionary view is staring with the simplest concepts, leading to the most complicated notions, in such a way that a first year student of materials, physics or chemistry fields can easily use this thesis. Meanwhile, it is tried that the writing be not boring, and the primary concepts to be rapidly connected to the complicated concepts and applied principles.

Since the subject of this thesis indicates an intersecting point between various sciences such as physics, quantum chemistry, analytical chemistry, surface chemistry and materials science, the priority of the author is using the simplest expressions of complicated points, and creating continuity between these various fields of study.

For instance, if expressing $(E = h\nu)$ (Planck relation) with considering classical physics viewpoint was required in a paragraph, and expressing the same relation with quantum physics viewpoint (Planck- Einstein relation) with using the concept of photon was considered in the next paragraph, another paragraph has been written to link the two views regarding classical and modern physics.

Consequently, it has been tried that after finishing the part of theoretical background, the readers achieve to whatever the theoretical knowledge required for fulfilling similar research projects with spending the shortest time and using the least energy, by going through an attractive and non-homogeneous trend.

In chapter 3, the experimental part is explained. The first section is mainly focused on the presentation of chemical and physical properties of utilized raw materials. The second section deals with samples processing consisting of preparation of suspension, sonication, separation and drying. The last section explains the characterization methods including FTIR and Raman spectroscopy. In this part, sample preparation for spectroscopic measurements, and optimization of spectroscopic parameters will be described.

Chapter 4 representing results and discussion is most important part of this thesis. This chapter by helping qualitative and quantitative analysis of FTIR spectra and also Raman spectroscopy tries to explain effect of sonication process on the surface chemistry of CNTs. The surface reactions, attached chemical species, and relationship of amount of sonication time and energy with them are main subjects of chapter 4.

Chapter 5 summarizes the work which is carried out during current study and brings forward the conclusion. This chapter tries to summarize of significant results by a comprehensive table. The considered point in writing this part is that if reader would not have enough time for reading whole of thesis, just reading this chapter can satisfy him / her.

Finally, it is wished that current thesis takes a small step forward to the promotion of materials science.

2. THEORETICAL BACKGROUND

This chapter explains theoretical knowledge and concepts related to experimental work. Main and huge part of this chapter is related to Raman and IR spectroscopy, because the main quiddity of this thesis is based on characterization science. Figure 2-1 represents whatever that will be discussed further, schematically.

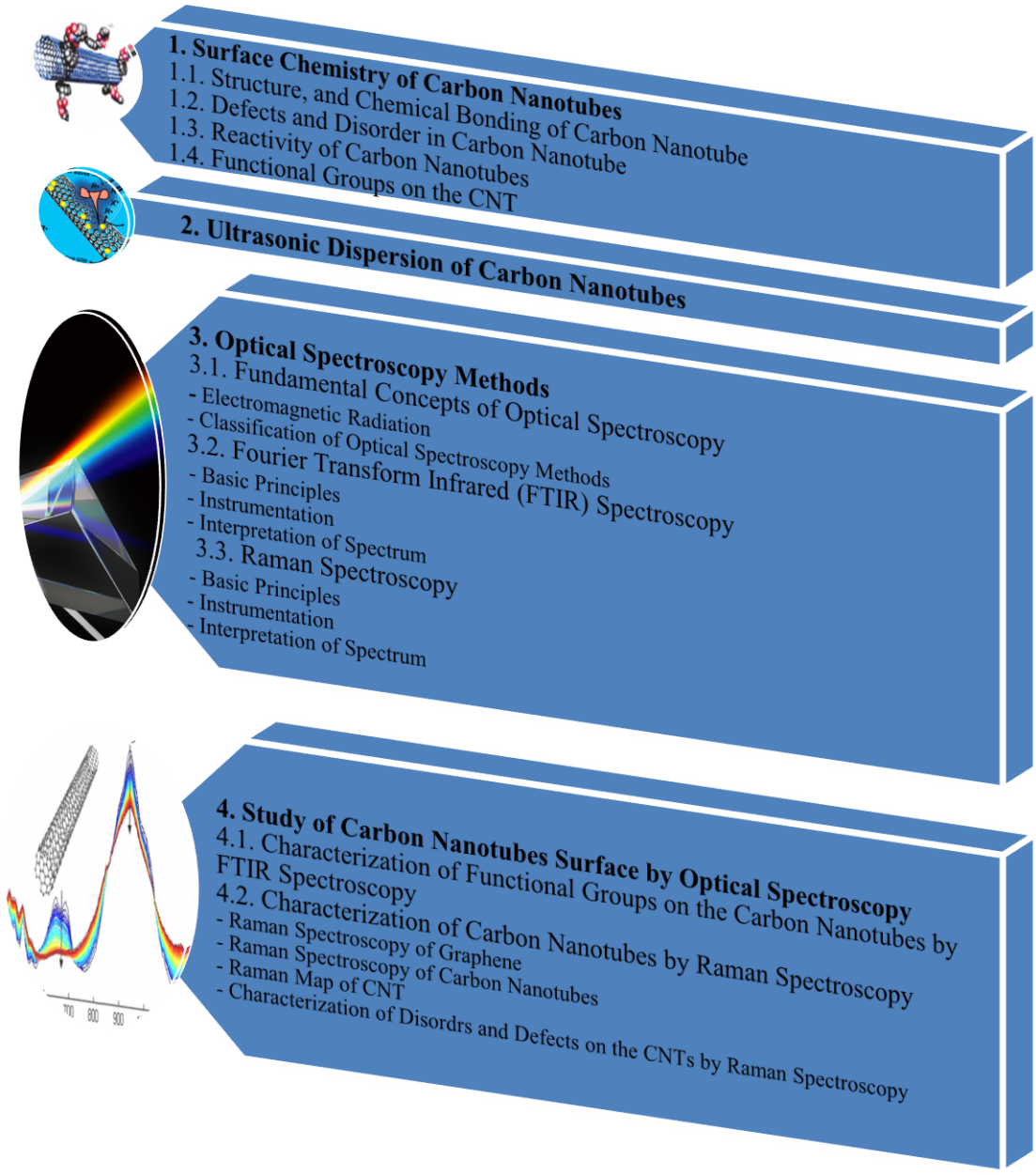

Figure 2-1: *The whole structure of theoretical background chapter* [13–15].

2.1 Surface Chemistry of Carbon Nanotubes

Carbon nanotubes (CNTs) belong to fullerene structural family. They are obtained by rolling up **graphene** sheets. The graphene sheets are rolled at special and different angles that result in different properties for the CNTs. CNT enjoys long and hollow carbon structure with diameters ranging between 1 and 100 nm. Special structure and chemical bonding make this material with unique properties such as thermal and electrical conductivity, semiconducting behavior and good mechanical properties. [16,17]

As mentioned, the graphene sheets are rolled up with special angles that lead to form the different kind of CNTs including **chiral, zigzag and armchair** as figure 2-2 shows. In the figure 2-2, letters n and m describe how the graphene sheet is rolled up for forming the nanotube; letter T presents the tube axis, and also parameters a_1 and a_2 are the unit vectors of graphene in real space. Different wrapping angles and diameters lead to different structures, or **chiralities** which determine the functional properties of carbon nanotubes. [16,18]

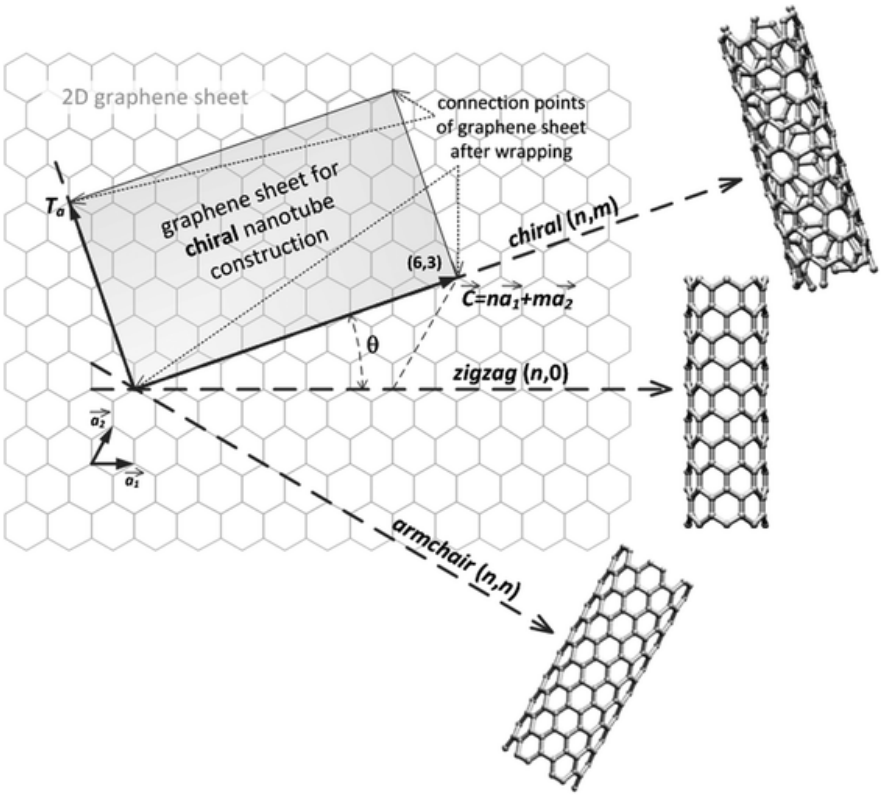

Figure 2-2: *Graphene sheet rolled up with different chiralities to form CNT* [16].

For the first time, carbon nanotubes (CNTs) were observed in 1952 by Radushkevich and Lukyanovich. But many scientific sources have cited that the carbon nanotubes are discovered by Iijima in 1991. Various methods are presented for the synthesis of CNT in scientific references. But it can be claimed that the most popular and applicable of them are chemical vapour deposition (CVD), plasma enhanced chemical vapour deposition (PECVD), arc-discharge, and laser ablation methods. The Basic classification of

CNTs based on the number of layer is including single wall carbon nanotubes (SWCNTs), double wall carbon nanotubes (DWCNTs) and multi wall carbon nanotubes (MWCNTs) as figure 2-3 shows. [19]

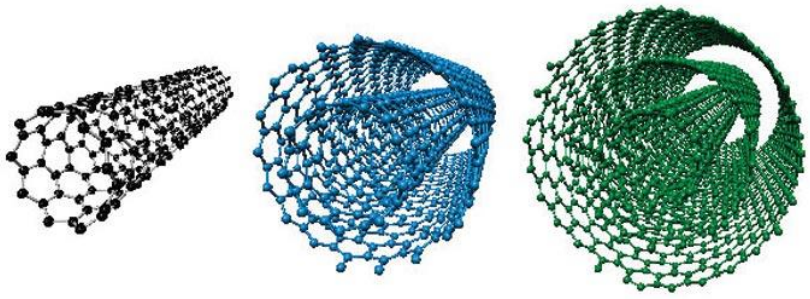

Figure 2-3: *Single wall carbon nanotube (SWCNT), double wall carbon nanotube (DWCNT), and multi wall carbon nanotube (MWCNT)* [20].

2.1.1 Structure, and Chemical Bonding of Carbon Nanotubes

Graphene is one graphitic monolayer that can be considered as basis for all new carbon allotropes. Graphene based materials (graphite and CNT) are built of **hexagons of sp^2-hybridised** carbon atoms as basic units. [17,21]

The **sp^2-hybridization** is combination of one s-orbital with two p-orbitals (p_x and p_y). Figure 2-4 shows how these orbitals form together a planar assembly with a characteristic angle of 120˚ between hybrid orbitals. [22]

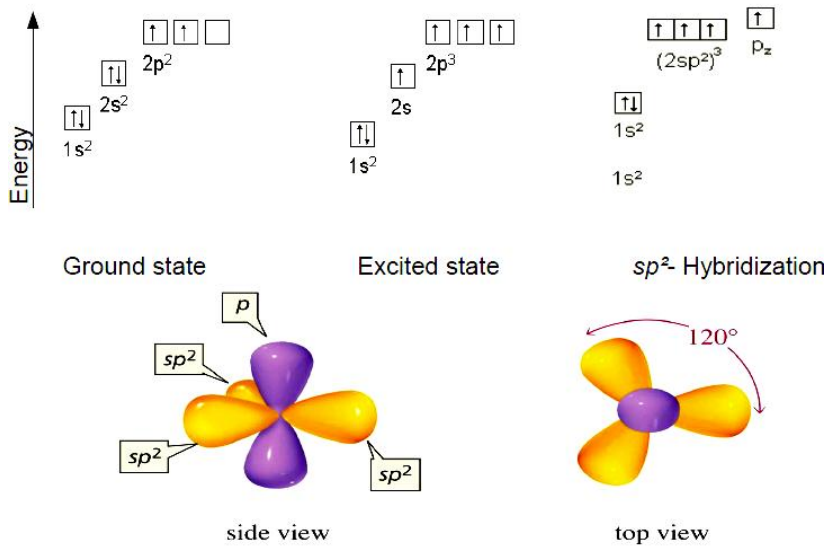

Figure 2-4: *The sp^2-hybridization* [23,24] **.**

Graphene based materials enjoy two kinds of bonds resulted from sp^2 hybridization. These kinds of bonds are known as **σ and π bonds**, presented in figure 2-5. In these

materials, a 2s electron hybridizes with two 2p electrons, forming three sp^2 orbitals which place at 120˚ than each other in an orbital plane, and one other orbital enjoying $2p_z$ configuration at 90˚ than this plane. The sp^2 orbitals create the strong σ bonds between carbon atoms that form hexagonal network in the graphene plane while the p_z or π orbitals form the weak van der Waals bonds between planes or tubes. [25–27]

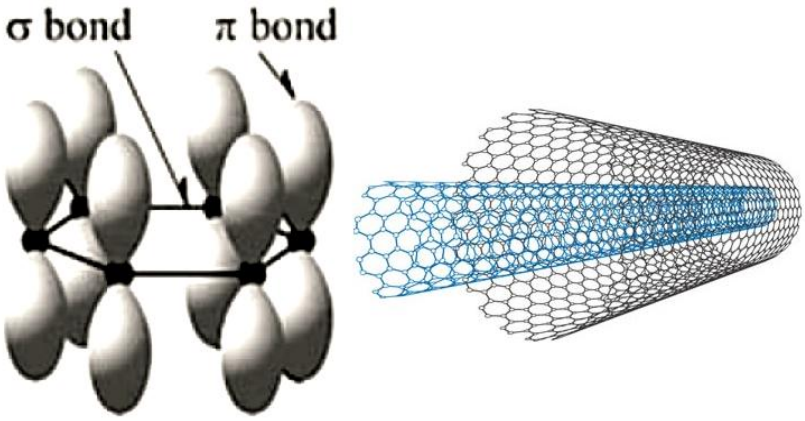

Figure 2-5: *Forming σ and π bonds in graphene (or CNT) resulted from sp^2 hybridization* [27,28].

The story of chemical bonding and hybridization in rolled carbon materials is not entire in this point. The bonding in rolled carbon materials is sp^2 primarily but high curvature in these materials leads to create some sp^3 characters. Hence chemical bonding in rolled carbon materials is considered mixture of sp^2 and sp^3 orbitals. [26]

The **sp^3-hybridization** is mixed state formed out of one s-orbital and three p-orbitals. A combination of sp^3 configuration creates a tetrahedral assembly with a characteristic angle of 109.5˚ between the hybrid orbitals according to figure 2-6. [22]

Rolling up graphene sheet to a cylindrical structure like CNT leads to change in chemical bonds and sp^2 to sp^3 **rehybridization**. The curvature resulted from rolling up leads that the π orbitals would be no longer orthogonal to the surface. Also it results in decreasing bond length between carbon atoms and changing the bond angle. In the rolled carbon materials, π and σ orbitals are no longer perpendicular to each other. In these materials, the parts of π orbitals inside and outside of the cylindrical structure (tube) rearrange. Figure 2-7 shows that the outer contribution of π orbitals is much larger than the inner one in the rolled carbon materials. [22,26]

Actually, the curvature leads to create a mixed state of σ and π orbitals. Figure 2-8 represents **wavefunctions** of a carbon nanotube. In this figure, the dark and bright regions represent positive and negative signs, respectively. The square of the wavefunction indicates the electron density. The positive and negative signs of wavefunction present bonding and antibonding orbitals respectively. [22,29]

As figure 2-8 shows, inner area of tube is seen a continuous dark ring that is related to σ bonds. But outside of the tube is seen alternating bright and dark. It indicates rear-

rangement of π orbitals as discussed before. It is clear that figure 2-8 explains that electron density in different regions of CNT is different. This phenomenon is related to rehybridization which leads to chemical bonding for CNT is explained by a mixture of sp^2 and sp^3 orbitals. [22,30]

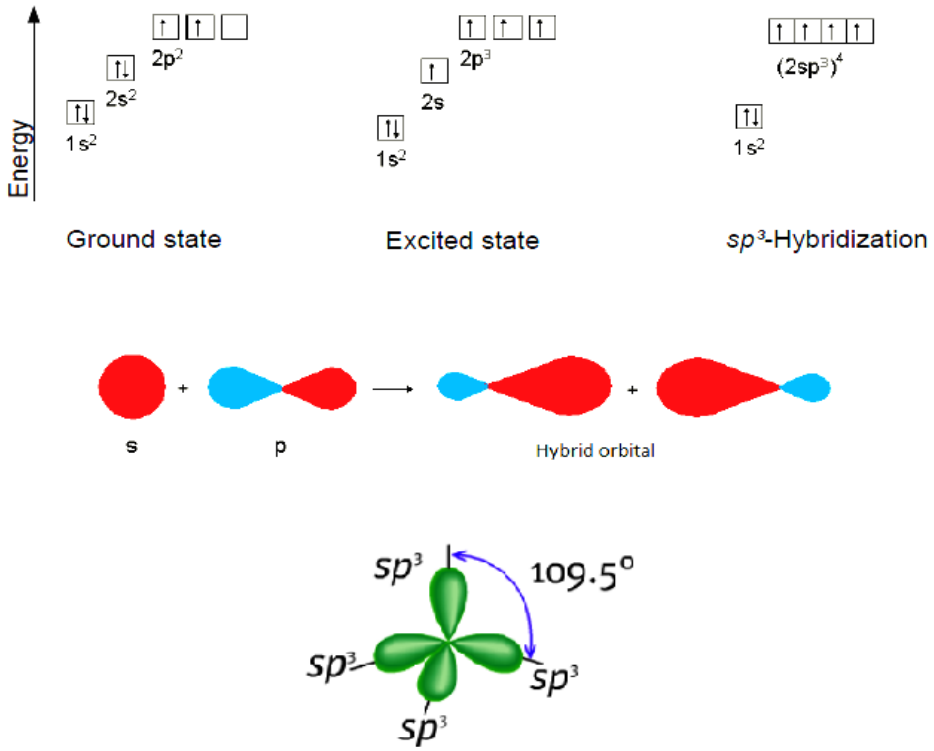

Figure 2-6: The *sp^3-hybridization* [22,23].

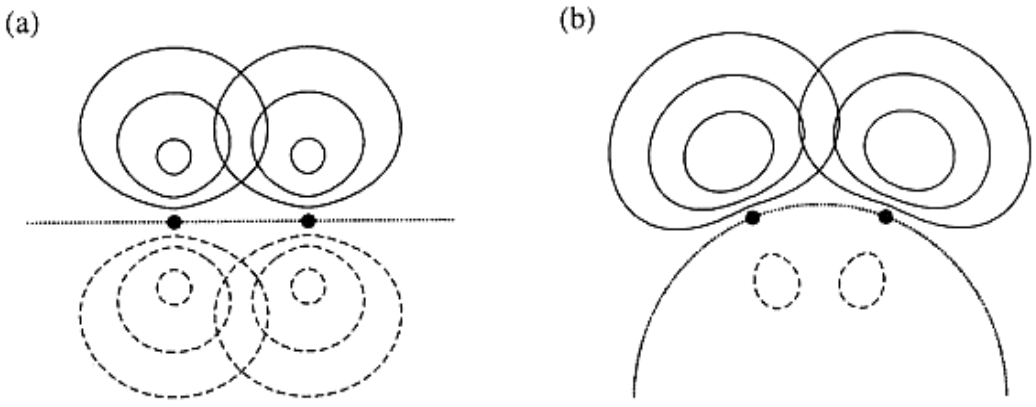

Figure 2-7: *a) The π orbitals of graphene, b) Rearrangement of π orbitals in C_{20}* [22].

Figure 2-8: *Rehybridization of a carbon nanotube* [30]**.**

2.1.2 Defects and Disorder in Carbon nanotubes

Thermodynamically, it is impossible that defects density goes to zero for each material structure. As it has been discussed, ideal orbital configuration in graphene sheet is sp^2 but disorders in the CNT play their own role. Disorders, edges, defects and topological perturbations enjoy orbital configuration of sp^3 completely. Figure 2-9 shows scanning tunneling microscope (STM) view of a point defect in the CNT structure. [31,32]

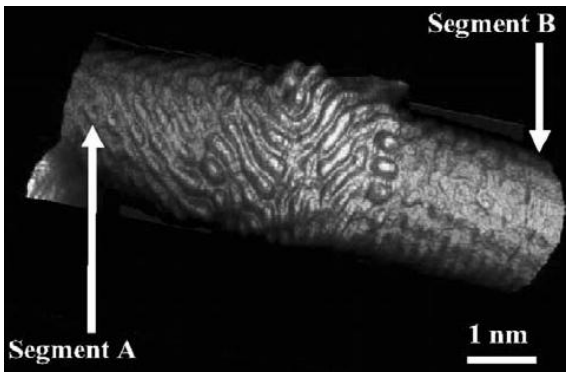

Figure 2-9: *STM view of the point defect between two chirally-distinct segments on the CNT* [32].

- **Classification of Intrinsic Defect and Disorder in the CNT**

1. Vacancies: The most common defects in the lattices of crystalline materials are point vacancies. In the reticular lattice of graphene, vacancies are created by breaking three strong C=C bonds and spending close 7.8 eV energy. Vacancy defects in the CNTs are produced post-synthesis by knock-on phenomena such as high energy electron, ion, or neutron radiations. Figure 2-10 represents different vacancy defects in the graphene lattice. [32]

2. Interstitials defects: Interstitials defects are considered as second important types of defects commonly. In the graphene lattice, bonding an extra atom and missing long order of graphene lattice leads to these defects. [32]

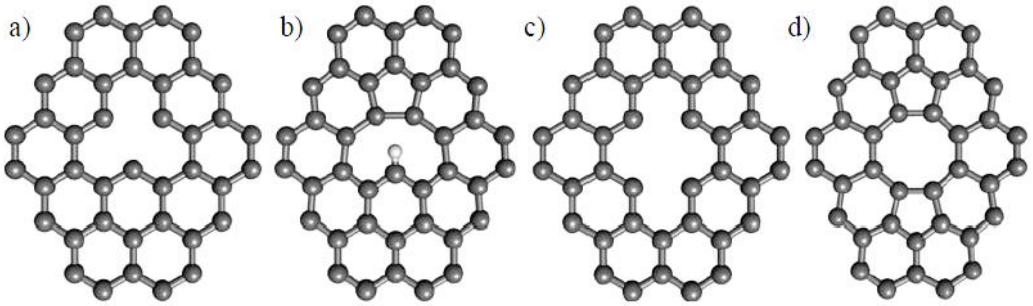

Figure 2-10: *Vacancy defects in the graphene lattice: Mono-vacancy (a) before and (b) after reconstruction. Di-vacancy (c) before and (d) after reconstruction* [32].

3. Stone-Wales Defects and non-hexagonal rings:

The **Stone-Wales (SW)** defects are most important disorders in the CNT structure. This defect affects mechanical and functional properties of CNT significantly. When CNT is exposed to stress and experiences local strain, the covenant bonds between carbons atoms are stretched. It leads to increase the overall energy of the lattice. Maximum bond rotation without distribution of graphene lattice and changing in the orbital configuration is about 3.5 eV (Require energy for converting sp^2 to sp^3 hybridization). But if rotation of carbon bond would be around 90º, it results in converting four adjacent hexagons into two pentagons and two seven-sided heptagons. This 5-7-7-5 configuration is known as Stone-Wales (SW) defect. The Stone-Wales transformation (Figure 2-11) is created when CNT lattice experiences more than 5% tensile deformation. [32–35]

The other defect in this class includes a single “5-7” couple that is created by replacing a pentagon adjacent to a heptagon instead two hexagons. The single 5-7 defect destroys rotational symmetry and changes the orientation of graphene lattice. Actually, SW defect is a pair of 5-7 defects without separation. Pentagonal rings are considered as regions which enjoy high electron density. Figure 2-12 introduces these defects. [32,34]

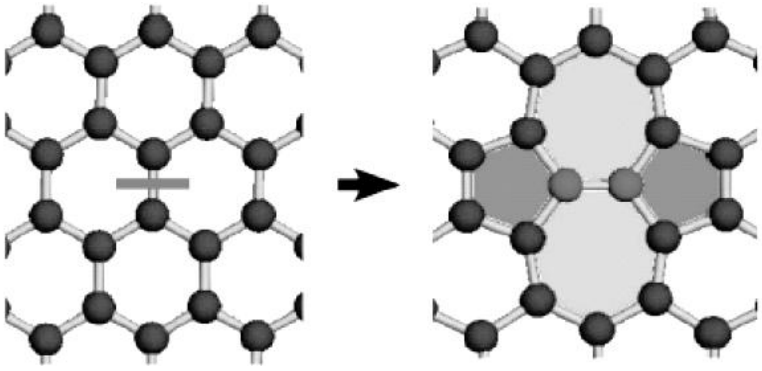

Figure 2-11: *The Stone-Wales transformation in the graphene lattice* [35].

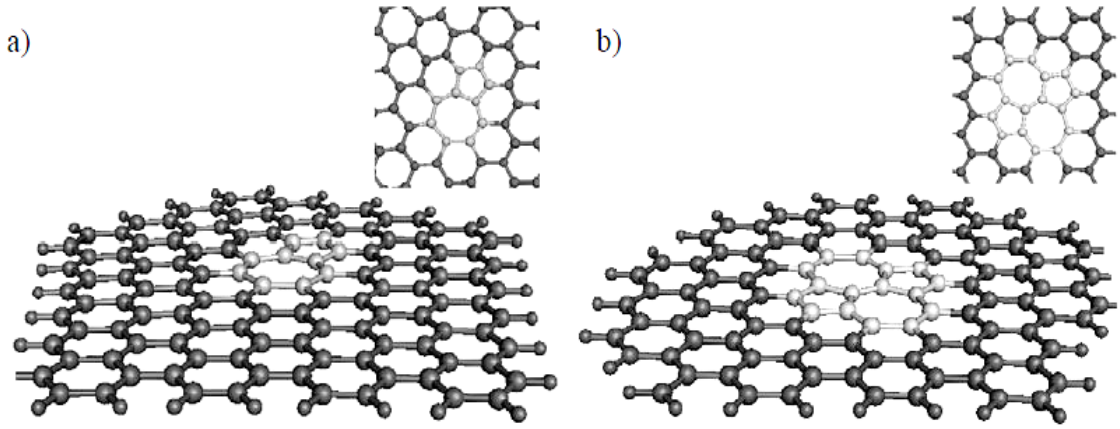

Figure 2-12: *(a) A single 5-7 defect and (b) a 5-7-7-5 Stone-Wales defect* [32].

2.1.3 Reactivity of Carbon Nanotubes

The ability to react with the surroundings is subjected while the reactivity of a material is studied. Hence, for the better understanding of reaction tendency and the fuctionalization of CNTs, study of reactivity is vital. [22]

Graphene is low-reactive chemically, because of the planar sp^2 hybridized carbon lattice. But story for carbon nanotubes is different. CNTs are bent in one dimension, and it results in creating more chemical activity for curved carbonaceous materials. So on, due to three dimensional bending, fullerene enjoys more reactivity than graphene and CNT as figure 2-13 shows. [21]

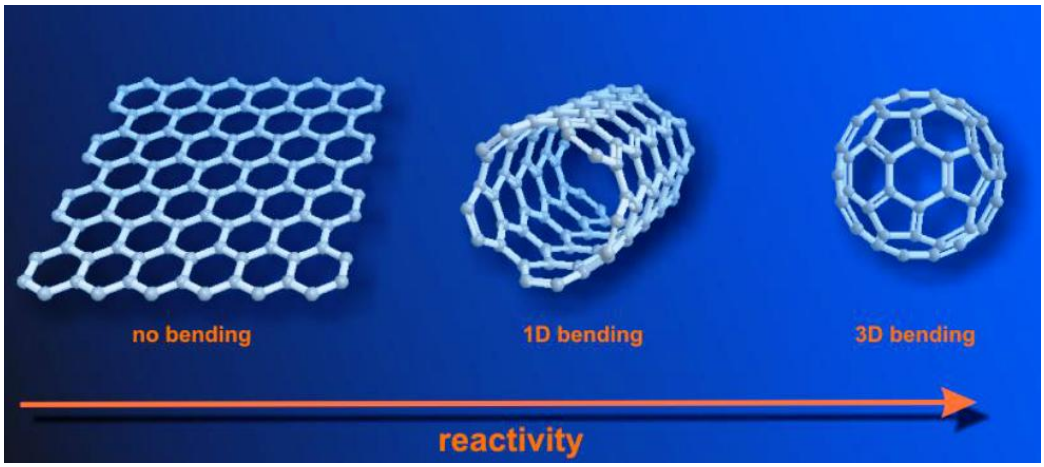

Figure 2-13: *Relationship between bending degree and chemical reactivity for graphene sheet, CNT and fullerene* [21].

Curvature in the materials with aromatic carbon lattice determines rehybridization degree. Hence, bending is in relationship with reactivity tightly and increasing the reactivity of CNT just by bending is possible. **Pyramidalization angle (θ_P)** which shows local reactivity index is defined by:

$$\theta_P = (\theta_{\sigma\pi} - 90)^\circ , \qquad (2\text{-}1)$$

where $\theta_{\sigma\pi}$ is angle between σ and π orbitals. This parameter for trigonal sp^2-orbital and tetrahedral sp^3-orbital is equal to 0 and 19.47 respectively according to figure 2-14. Also, the more curvature leads to higher pyramidalization angle. [22,36]

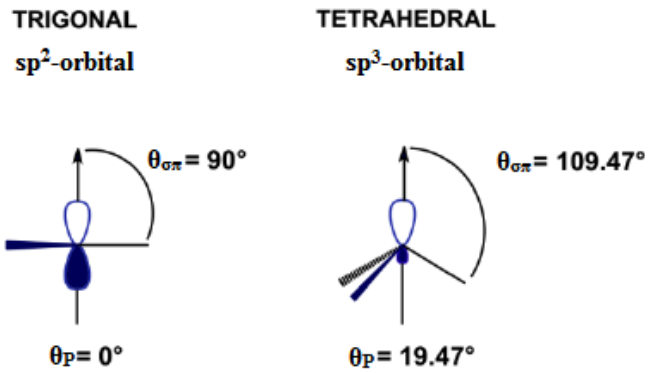

Figure 2-14: *Pyramidalization angle for sp^2 and sp^3 orbitals* [21,36].

In the CNTs, dependent on the local mixture of sp^2- and sp^3-orbitals, this parameter is variable. Chirality is most effective parameter on the pyramidalization angle. Generally, the chirality, which leads to the larger pyramidalization angle, results in the more reactivity. Based on what is claimed, it is clear that most reactive parts of carbon nanotube are the end caps of tubes which have maximum curvature (Figure 2-15). [21,22,36,37]

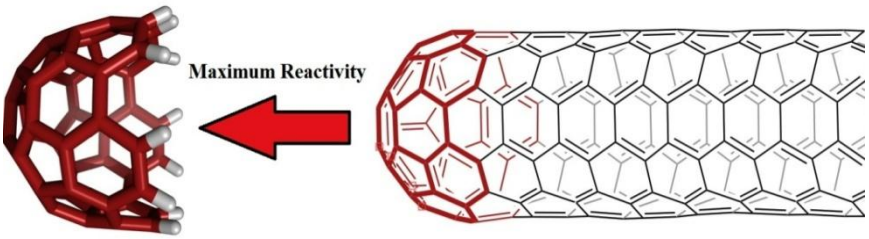

Figure 2-15: *The end cap of tube, maximum curvature, maximum reactivity* [38].

π-orbital misalignment is nominated as other effective concept on the activity of CNT. While CNT structure enjoys mixture of sp^2 and sp^3 orbitals, this state contains unsaturated orbitals. The bonding of a tetravalent sp^3 orbital to a trivalent sp^2 orbital leads to create one unattached hybrid orbital and free for bonding. This phenomenon is known as π-orbital misalignment. The higher ratio of sp^3 orbitals in the structure means the more free bonds and the higher reactivity. [22]

As discussed in the previous paragraphs, different parts of carbon tube have different orbital state. Distinctly, edges, disorders, imperfections and defects, open ends terminated and functional groups locations enjoy different electron density than basal part. Disorders are the centers of association of unpaired electrons. This situation leads to show strong tendency to chemisorption of chemical species. Hence these sites are known as **active sites** (Figures 2-16 and 2-17). [5,39]

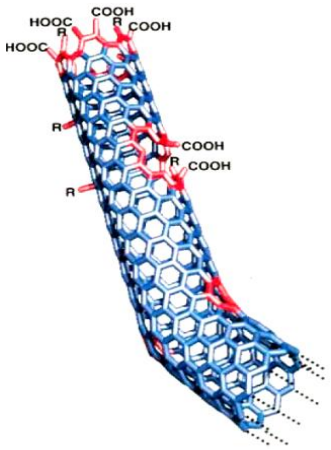

Figure 2-16: *sp^3- hybridized defects related to open ends terminated and functional groups* [13].

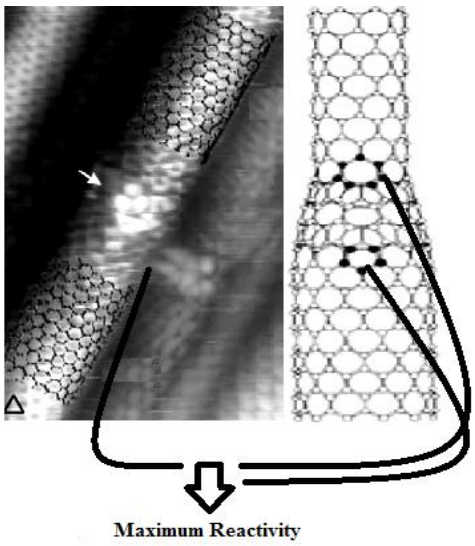

Figure 2-17: *Defects act as active sites.*

Also mechanical damaging like bending of the tube increases reactivity. So every external stress can act as an agent which increases the chemical reactivity of CNT. Figure 2-17 shows that chemical reactivity (hydrogenation energy) is changed by increasing bending angle of tubes. [37]

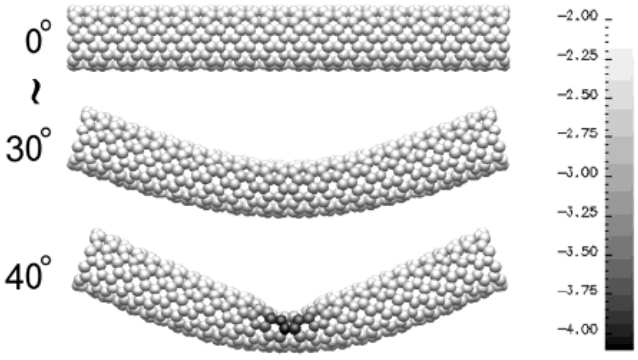

Figure 2-18: *Changing chemical activity as function of bending angle* [37].

2.1.4 Functional Groups on the CNT

Functional groups are a part of inherent identity of CNTs. Even on the surface of pristine CNTs, some functional groups are located. Although, existing functional groups disturbs some functional properties but sometimes they are essential for many applications. Organic chemical species such as dyes, proteins or nucleic acids can be coupled with functionalized nanotubes for sensor technology. In the composite industries, side wall functional groups can react with polymers and improve the mechanical properties of nanocomposites structure. [4]

According to figure 2-19, functionalization possibilities for carbon nanotubes can be including defect-group functionalization, covalent sidewall functionalization, non-covalent exohedral functionalization with surfactants, non-covalent exohedral functionalization with polymers and endohedral functionalization. [8,13]

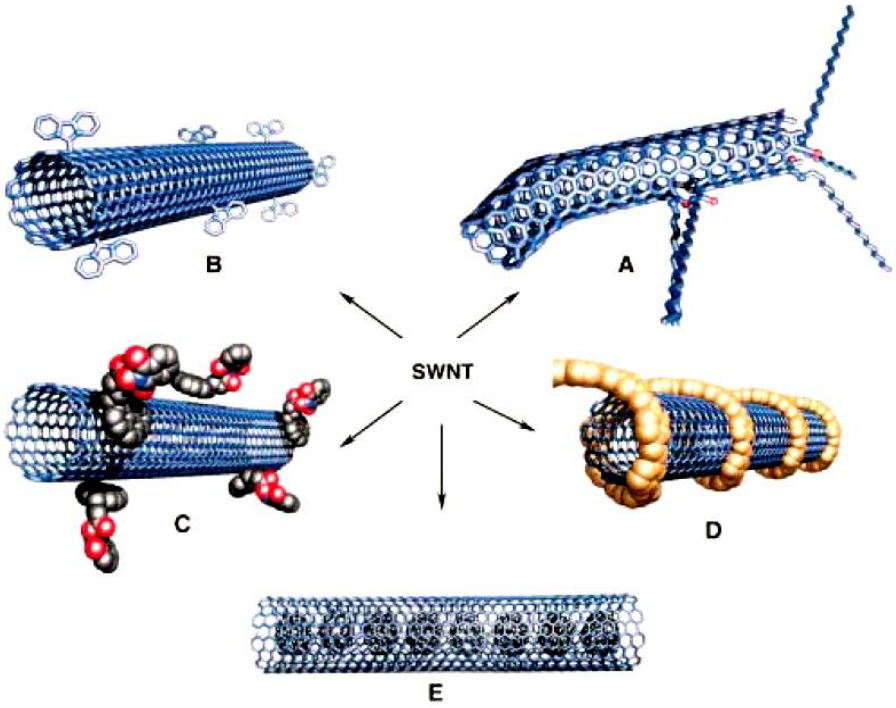

***Figure 2-19**: Functionalization possibilities for CNTs: A) defect-group functionalization, B)covalent sidewall functionalization, C) non-covalent exohedral functionalization with surfactants, D) non-covalent exohedral functionalization with polymers and E) endohedral functionalization* [13].

Generally, functional groups located on the CNT surface, based on the kind of attachment, can be categorized to non-covalent and covalent. **Non-covalent functionalization** which is based on van der Waals, hydrophobic or π-π interaction, involves weak forces. As example, while CNTs are suspended, some molecules can be replaced by solvent. **Covalent functionalization** is based on strong covalent bonds which are not reversible. The sidewall, defects, and disorders are favorable locations for this kind of functionalization. Different and various approaches are available for achieving to this kind of functionalization. [40,41]

Functional groups affect wettability and solubility of CNTs. The surface of pristine CNT is hydrophobic but functional groups make it more hydrophilic. It provides adsorption light molecules and polar compounds. Functionalization increases oxygen content but leads to decrease surface area and adsorption of nonpolar components. [42]

2.2 Ultrasonic Dispersion of Carbon Nanotubes

Controlling the dispersion of CNTs in a suspension or a composite matrix is considered as a vital and challenging process for achieving to the desirable properties of final product. The dispersion of nanoparticles in the suspension is considered as one of the applications of ultrasonic technology. Van der Waals forces and surface tension of liquid are known as motive forces for creating **agglomerates** in the suspension. Agglomeration tendency is stronger for higher viscosity suspensions like resins. Deagglomeration phenomenon will be achieved by overcoming to attraction forces. **Sonication process** by using ultrasonic waves is one of the most important strategies for achieving to this matter. [6,7]

Ultrasonic waves which happen at frequencies above 20 kHz are known as a subcategory of sound waves. So they show all the characteristics properties of sound waves. During sonication process, sound waves which propagate in the suspension make alternating high-pressure and low-pressure cycles. Rate of the creation of these cycles is depended on frequency. High intensity ultrasonic waves create vacuum bubbles in the liquid during the low-pressure cycle. When the bubbles achieve to maximum possible volume, during a high pressure cycle, they will collapse. This phenomenon is called **cavitation**. Cavitation phenomenon includes formation, growth, and implosive collapse of bubbles in a liquid (Figure 2-20). Figure 2-21 represents ultrasonic dispersion process. [6,43]

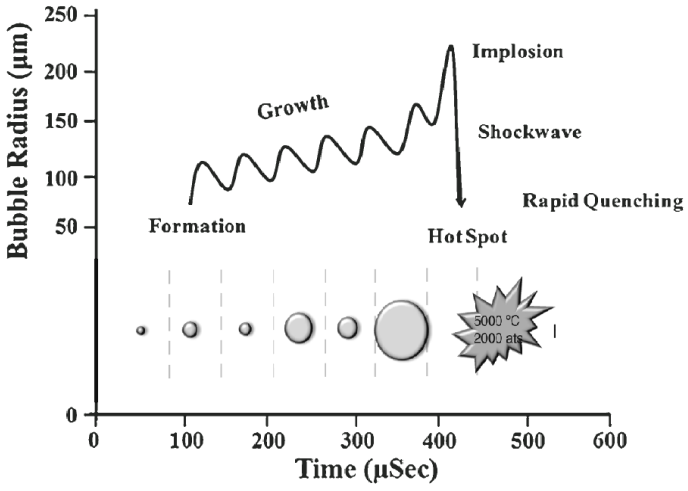

Figure 2-20: *Cavitation phenomenon by ultrasonic waves* [44].

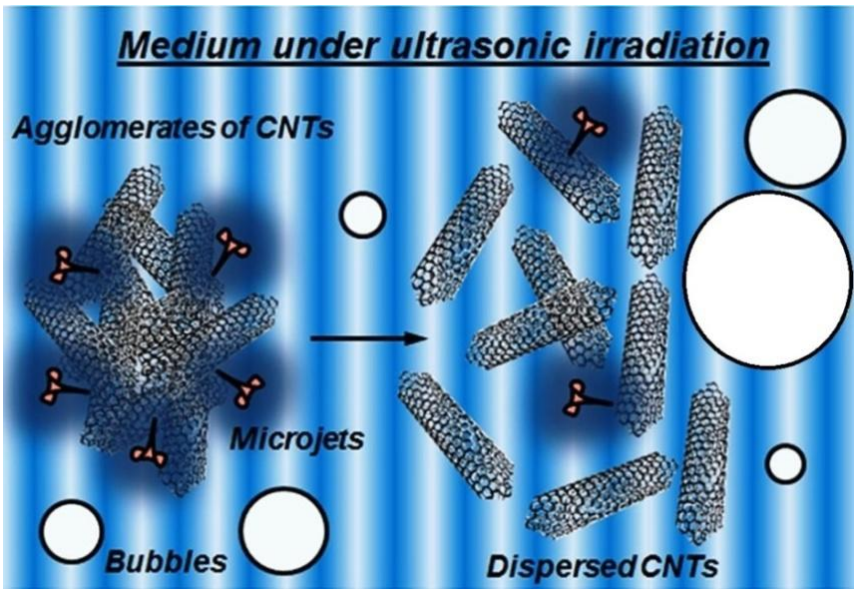

Figure 2-21: *Ultrasonic dispersion process* [15].

In the sonication process, each micro-bubble acts as a micro-reactor. During sonication, different reactive species are produced in different **reaction zones**. According to figure 2-22, hot spot, interfacial region and bulk region form three reaction zones during sonication process. [43]

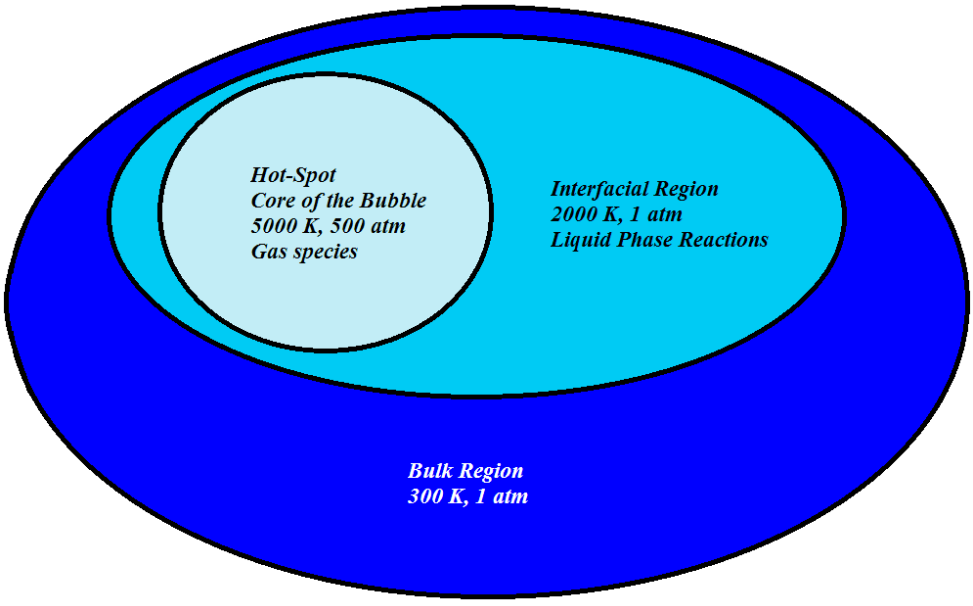

Figure 2-22: *Reaction zones during ultrasonication process.*

First zone is hot spot which is the core of bubbles with local temperature of 5000 k and pressure of 500 atm during final collapse of cavitation. Absolutely, in this region, chemical species are in gas phase. Second zone is interfacial region between the cavitational bubble and bulk liquid. In this region, reactions occur in liquid phase at 2000 k. Finally, bulk region forms third zone which enjoys room temperature because cavitation is an

adiabatic process. Study of thermodynamic situation of these regions is vital subject while chemical reactions which occurred during sonication are matter. [43]

Most effective factor in transformation of energy in the cavitation is the intensity of acceleration. The Higher acceleration results in increase of the probability of the creation of vacuum bubbles. Amplitude of the oscillation is used for describing intensity of the acceleration. Hence it can be claimed that the higher amplitude leads to the more creation of cavitation. The high power or low frequency ultrasound enjoys the high amplitudes. In addition to the intensity and amplitude, sonication processing is depended on some other parameters such as pressure, temperature, viscosity, and concentration. [6]

The total amount of energy (E) which is delivered to a suspension is in relationship with amount of deagglomeration directly. According to equation 2-2,

$$E = P.t\ , \tag{2-2}$$

this energy is depended on either applied power (P) or time (t) of sonication. [45]

Some side effects come with sonication during dispersion process. It may create defects and damaging, functionalization reactions on the CNT sidewalls, and even in extreme situations, CNTs will be fragmented into smaller pieces. [8]

2.3 Optical Spectroscopy Methods

For the first time, the term of **'spectroscopy'** was explained in 1666 by Sir Isaac Newton. In the Spectroscopy methods, analyzing the interactions between radiation and material provides quantitative and qualitative studies. [46]

2.3.1 Fundamental Concepts of Optical Spectroscopy

Spectroscopy is the study of interaction between matter and radiation as a function of wavelength or frequency. Hence the base of optical spectroscopy methods is the study of interaction between electromagnetic waves and material. Collected data which is obtained by spectroscopy methods forms **spectrum**. Spectrum is a plot of radiation intensity as a function of wavelength or frequency. [47,48]

Figure 2-23 shows simple form of a **spectrometer** schematically. In this system, source produces electromagnetic waves, then monochromator selects specific wavelength. Further, interaction between sample and light will be detected by detector at the end. [46]

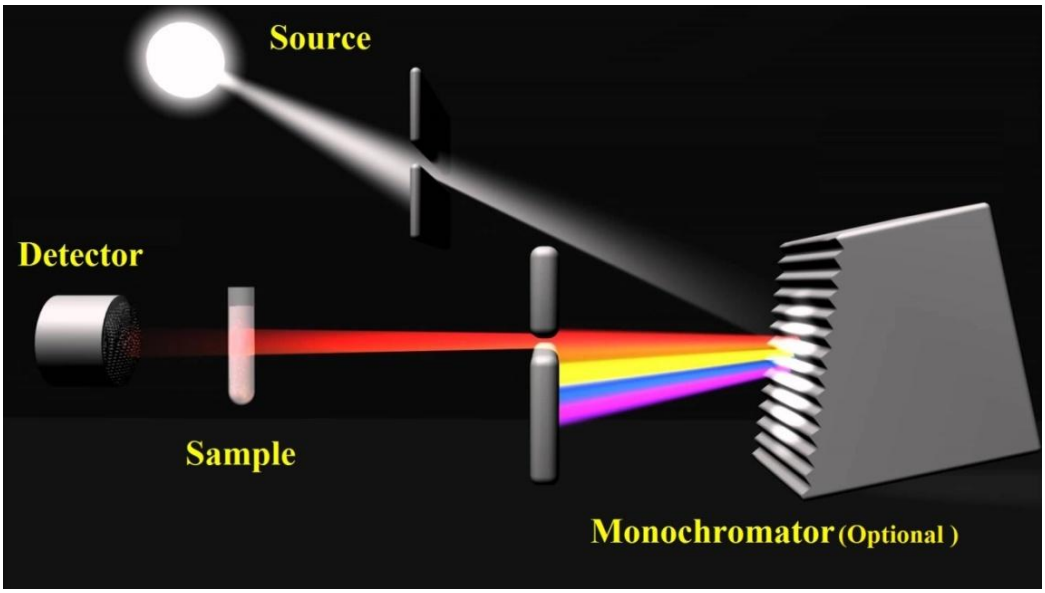

Figure 2-23: *Simple form of a spectrometer.*

- **Electromagnetic Radiation**

In addition to region of visible radiation, radiowave, microwave, infrared, ultraviolet, X-ray and γ-ray form the different regions of electromagnetic radiation. Figure 2-24 represents these regions along molecular effects which are resulted from the interaction of radiation with material. [49]

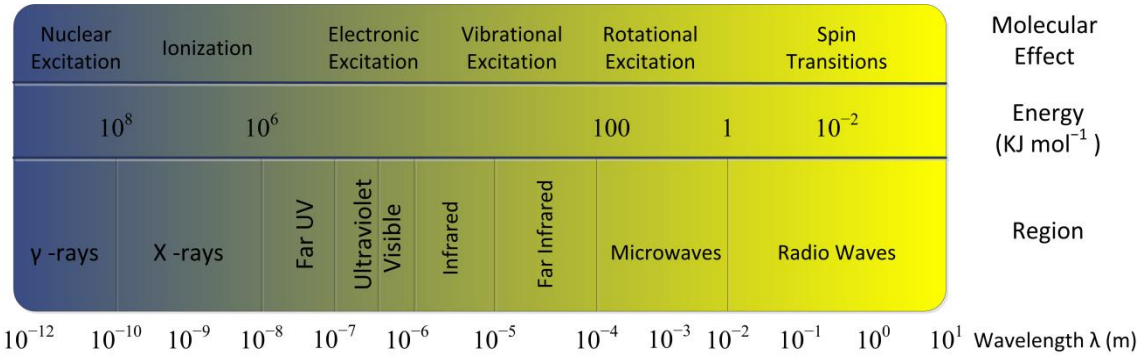

Figure 2-24: *Electromagnetic radiation regions and molecular effects.*

The German Physicist, Max Planck (1858-1947), explained an equation between energy (E) of a charged atomic oscillator and the frequency (ν) of its associated electromagnetic wave according to:

$$E = h\nu, \tag{2-3}$$

which was Published in 1900. In this equation, (h = 6.626 × 10^{-34} J s) is known as Planck constant. [50]

Five years later, Albert Einstein described that the value of E represents the minimum amount of energy which is necessary to form an electromagnetic field (a **'quantum'**).

The quanta point of view formed **photon concept**, when described the radiation behavior with considering an independent unit (particle) instead of an electromagnetic wave. [50]

Hence, equation 2-3 is called **Planck–Einstein relation** when explains the energy of each photon in terms of the photon's frequency. Regarding that speed of light (c) relates wavelength (λ) to frequency (ν) according to:

$$c = \nu\lambda, \tag{2-4}$$

Planck–Einstein relation can be explained following to:

$$E = \frac{hc}{\lambda} \tag{2-5}[15]$$

- **Classification of Optical Spectroscopy Methods**

Optical spectroscopy methods can be classified based on several outlooks. As explained in the figure 2-24, they can be classified based on molecular effects resulted from the amount of radiation energy. Furthermore, they can be classified based on photon-matter interactions, and also unit of material (atom or molecule) studied in spectroscopy process. [47–49]

Most important photon-matter interactions which can be as base of a scientific classification for optical spectroscopy methods include absorption, emission, photon elastic scattering, and photon inelastic scattering. What follows is a short description of each interaction. [48]

1. **Absorption** phenomenon happens when energy from radiative source will be absorbed by the atoms or molecules of material. [48]

2. **Emission** phenomenon occurs when radiative energy will be released by material. [48]

3. **Photon elastic scattering** phenomenon is a collision which incident and target particles remain intact without missing energy. The photon elastic scattering by atoms is one of the significant types of interaction of radiation with matter. [51]

4. **Photon inelastic scattering** phenomenon is an interaction between a particle and a photon that kinetic energy of the incident particle is not conserved. In this process, some of the energy of incident particle will be decreased or increased. The collision between photon and particle that leads to inelastic scattering is called Raman scattering. In this phenomenon, frequency of the photon will be shifted after incident. (In further sections, Raman scattering will be discussed extendedly). [52]

In addition, spectroscopy methods can be divided based on the unit of material (atom or molecule) studied according to:

1. **Atomic spectroscopy**

Generally, atomic absorption spectroscopy (AAS) and atomic emission spectroscopy (AES) are two types of atomic spectroscopy that use visible and ultraviolet light. These absorptions and emissions are created by electronic transitions. The base of atomic spectroscopy is configuration of electrons. Atomic spectral lines are the output of this kind of spectroscopy method. [48,53]

2. **Molecular spectroscopy**

In molecular spectroscopy, vibrational, rotational and electronic energy transitions of molecules play most important role. **Born-Oppenheimer approximation** explains that energy of a molecule can be estimated by sum of electronic energy (E_{el}), vibrational energy (E_{vib}) and rotational energy (E_{rot}) following to:

$$E = E_{el} + E_{vib} + E_{rot} \tag{2-6}$$

Actually, spectral lines in molecular spectroscopy explain the changes of molecule energy after absorption, emission, and scattering interactions. The molecular spectra are so more complex than atomic spectra due to the combination of vibrational, rotational and electronic transitions to form spectrum. Molecular spectroscopy provides a lot of useful information about molecules such as molecular structure, chemical bond strength, dipole and quadrupole moments, and molecular degrees of freedom. [53]

As the most important molecular spectroscopy methods can mention to infrared and Raman spectroscopy. In these techniques which are also categorized as vibrational spectroscopy methods, changes in vibration and rotation at molecular level are evaluated. Furthermore, it should be considered that infrared spectroscopy is based on IR light absorbed, but Raman spectroscopy is based on inelastic scattered photons. Further, Fourier transform infrared spectroscopy (FTIR) and Raman spectroscopy techniques (The methods which are applied in this thesis) will be discussed by details. [46]

2.3.2 Fourier Transform Infrared (FTIR) Spectroscopy

At the first time, Sir William Herschel discovered infrared radiation in year 1800. After that, first IR spectra were published by Coblentz in 1905 but **Infrared spectroscopy** is used commercially since 1940s. [49,54]

IR spectroscopy is a molecular spectroscopy based on absorption. In this method, absorption of **infrared (IR) light** causes changes in the vibrational motions of the molecules. Each specific bond vibrates in unique and quantized frequencies. Regarding that

IR beam is not monochromatic and enjoys a large number of frequencies, when the frequency of vibrational mode of a molecule matches with the frequency of IR beam, the IR light will be absorbed. At the end, absorbed frequencies are detectible by detector. [55]

A basic IR spectrum is formed by the percent of light absorbance or transmittance on the vertical axis against wavenumbers ($\bar{\upsilon}$) on the horizontal axis. In other worlds, IR spectrum explains that different molecules absorb different sets of energies. Hence, different molecules have distinguishable IR spectra and each molecule structure enjoys especial infrared spectrum. **Wavenumber** is presented according to:

$$\bar{\nu} = \frac{1}{\lambda} \tag{2-7}$$

so based on equations 2-5, it can be claimed that:

$$E \sim \bar{\nu} \tag{2-8}$$

Commonly, the unit of wavenumber ($\bar{\upsilon}$) is reported cm^{-1}. [49]

Infrared wave enjoys the longer wavelength and lower frequency than visible light (Frequencies: 0.003 - 4×10^{14} Hz, Wavelengths: 1 mm - 750 nm). The infrared spectrum is divided into three regions. These regions include **far, mid and near infrared** with wavenumber of (10 – 400), (400 – 4000), and (4000 – 14000) cm^{-1} respectively. The region of mid-infrared is most important region for interpretation of chemical groups usually. [49]

Interpreting the measured signal, which is called **interferogram,** is not possible directly. For Interpreting of the signal, decoding of individual frequencies is required. **Fourier transform** which is a mathematical method performs this process. The Fourier transform decomposes a function of time of the signal into own constitutive frequencies. [51,56]

Main advantage of the FTIR spectroscopy is collecting high spectral resolution data over a wide spectral range simultaneously. Using Fourier transform system for infrared spectroscopy leads to higher signal to noise ratios, higher resolution, and superior wavelength accuracy. FTIR can be used for analysis of solid, liquid or gas samples. [57,58]

- **Basic Principles**

Molecular vibration obeys quantum mechanics rules. The vibrational motion is a quantized function, so only certain transitions are allowed by atoms, according to:

$$E_n = \left(n + \frac{1}{2}\right) h\nu \tag{2-9}$$

where ν is the frequency of vibration, and n is the quantum number (0, 1, 2, 3, …..). $E_0 = \frac{1}{2}h\nu$ is the lowest energy level, then $E_1 = \frac{3}{2}h\nu$ is the next lowest and so on. After interacting between molecule and radiation beam, a quantum of energy is either emitted or absorbed that is fitted with the energy gap (ΔE) is equal to:

$$\Delta E = h\nu \tag{2-10}$$

Figure 2-25 represents these quantized vibrations. [59]

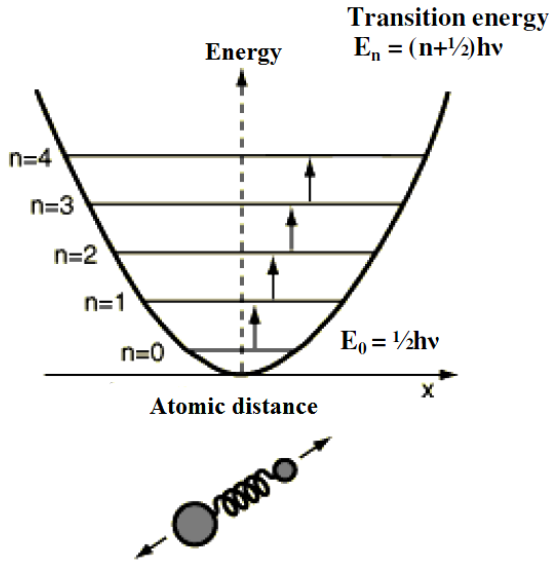

Figure 2-25: *Quantized vibrations of atoms* [59].

Determining intensity of the light before and after interaction with sample (I/I_0) as function of frequency of the light (ν) is basic principle of IR spectroscopy. Infrared spectrum is reported based on transmittance, reflectance, or absorbance. Equation 2-11 explains the transmittance concept based on the light intensities ratio. [58]

$$T_\nu = \left(\frac{I_t}{I_0}\right)_\nu \tag{2-11}$$

In this equation, parameter T_ν is transmittance at frequency ν, I_t is intensity of transmitted light, and I_0 is intensity of light before interacting. Equation 2-12 explains reflectance (R_ν) concept, where I_r presents intensity light reflected from the surface of specimen. [58]

$$R_\nu = \left(\frac{I_r}{I_0}\right)_\nu \tag{2-12}$$

Absorbance which is the third phenomenon is explained by **Beer-Lambert Law** following:

$$A_\nu = -\log T_\nu = \varepsilon_\nu c l\,, \tag{2-13}$$

where *c* is concentration of chemical bonds which absorb infrared radiation, *l* presents path length, and ε_ν is frequency-dependent absorptivity constant. [58]

As mentioned, molecules absorb specific frequencies. This basic principle notices the structure of molecules. These absorptions are corresponding resonant frequencies. It means just the photons with specified energies excite molecular vibrations. The resonant frequencies are depended to the strength of bond and the mass of atoms. The higher vibrational frequencies come from lighter atoms and stronger bonds. [60]

The vibrational frequencies for diatomic molecules are calculated by:

$$\nu = \frac{1}{2\pi}\left(\frac{f}{\mu}\right)^{\frac{1}{2}}, \tag{2-14}$$

where f is force constant (Nm^{-1}) and μ shows reduced mass per molecule (Kg) that will be defined by equation 2-15 as:

$$\mu = \frac{m_1\ m_2}{m_1 + m_2}, \tag{2-15}$$

where m_1 and m_2 are masses of individual atoms.

With regarding to

$$\bar{\nu} = \frac{1}{\lambda} = \frac{\nu}{c},$$

so:

$$\bar{\nu} = \frac{1}{2\pi c}\left(\frac{f}{\mu}\right)^{\frac{1}{2}} \tag{2-16}[49]$$

All kinds of molecules cannot show infrared absorptions. Just when **electric dipole moment (μ)** of the molecule is changed, during the vibration, it is considered as **'infrared-active'** molecule. Dipole is defined as a charge dislocated through the distance. This physical concept is a vector quantity and explained as:

$$\mu = q.r\ , \tag{2-17}$$

where q is electrical charge and r is distance between the charges. Physical unit of dipole is coulomb-meter (Cm). If even total charge of a molecule would be zero, positive and negative charges of chemical bonds will be not completely overlap. This situation leads to dipole moment. The dipole moment notices that charge separation in a molecule is occurred. Figure 2-26 shows changes in the dipole moment for a heteronuclear diatomic molecule. This molecule is an IR-active molecule. [49,61]

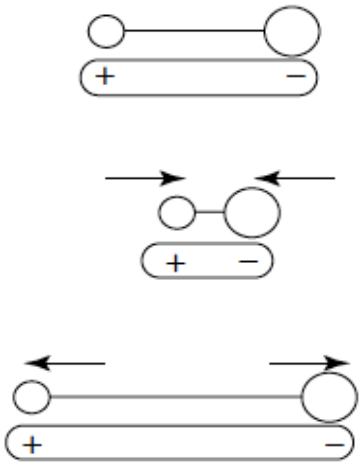

Figure 2-26: *Change in the dipole moment of a heteronuclear diatomic molecule* [49].

In contrast, a homonuclear diatomic molecule is considered as an **'infrared-inactive'** molecule because its dipole moment remains zero. Molecular symmetry is considered as an important concept when infrared activity is discussed. (It will be discussed during section '2.3.3. Raman Spectroscopy' by details), but in a nutshell, for diatomic molecules, it can be claimed that symmetrical diatomic molecules which have single bond and one vibrational mode, like N_2, are not observed in the infrared spectrum, while asymmetrical diatomic molecules, like CO, are observed in the IR spectrum. [49]

A molecule can vibrate in several ways which are called **vibrational modes**. Vibrational modes explain vibrational degrees of freedom in a molecule. The number of vibrational modes, in linear molecules, is 3N-5 and, 3N-6 for nonlinear molecules, where N is number of atoms. [22]

Vibrations can lead to either change in bond length **(stretching)** or bond angle **(bending)** as figure 2-27 shows.

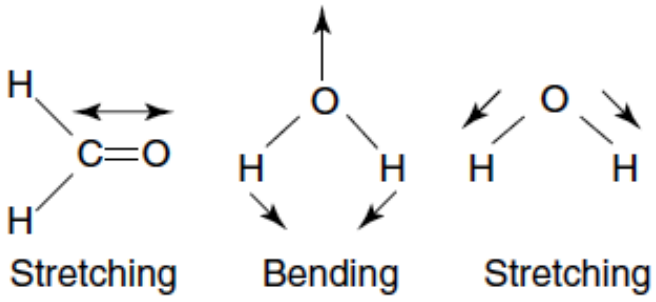

Figure 2-27: *Stretching and bending vibration modes* [49].

According to figure 2-28, term of symmetrical stretching is used when bonds can stretch in-phase and term of asymmetric stretching is used for out-of-phase stretching. [49]

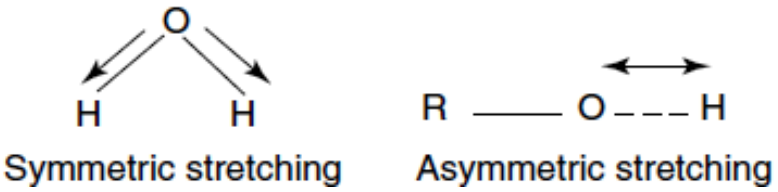

***Figure 2-28**: Symmetric and asymmetric stretching vibrations* [49].

Different kinds of bending vibration modes can also contribute to infrared spectrum. Figure 2-29 shows these bending vibration modes that are known as deformation, rocking, wagging and twisting. [49]

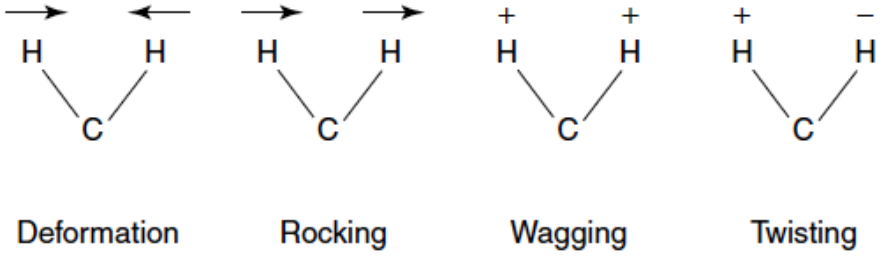

***Figure 2-29:** Different types of bending vibration modes* [49].

For more complex molecules, two other bending vibrations types are existed. These bending vibration modes are known as ‘in-plane’ and ‘out-of-plane’ bending according to figure 2-30. [49]

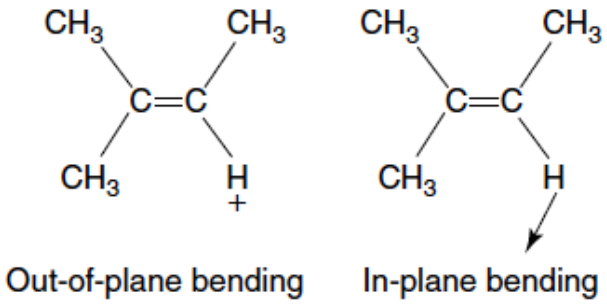

***Figure 2-30:** Out-of-plane and in-plane bending vibration modes* [49].

This section tried to explain basic concepts related to IR spectroscopy in summary. What follows is an explanation of FTIR instrument.

- **Instrumentation**

In this section, FTIR spectrometer will be discussed. **FTIR spectrometer** is consisted by a source, interferometer, sample compartment, detector, amplifier, A/D convertor, and a computer. IR radiation after passing through sample will be detected by detector. It is simplest explanation for this spectrometer. Figure 2-31 represents different parts of the FTIR spectrometer and explains how it works. According to figure2-31, after radiation source, an interferometer which is known as **Michelson interferometer** is set. In-

terferometer is an optical device which produces special type of signal includes infrared frequencies. [56,57]

The Michelson interferometer enjoys special part which is called **beamsplitter**. Duty of the beamsplitter is dividing incoming infrared beam to two beams. These beams will have different destinations. One beam will be reflected by a flat mirror which is fixed and on the other side; the other beam will be reflected by a flat mirror which can have movement in so short distance. After reflecting beams by their respective mirrors, they recombine at beamsplitter again. It is clear that the infrared signal is the result of these beams interfering with each other that is known as **interferogram.** [56,57]

The interferogram has especial and unique properties which is function of the movable mirror position. In the detector which is set after sample compartment, the difference of the intensities of these beams is measured as a function of paths difference. [56,57]

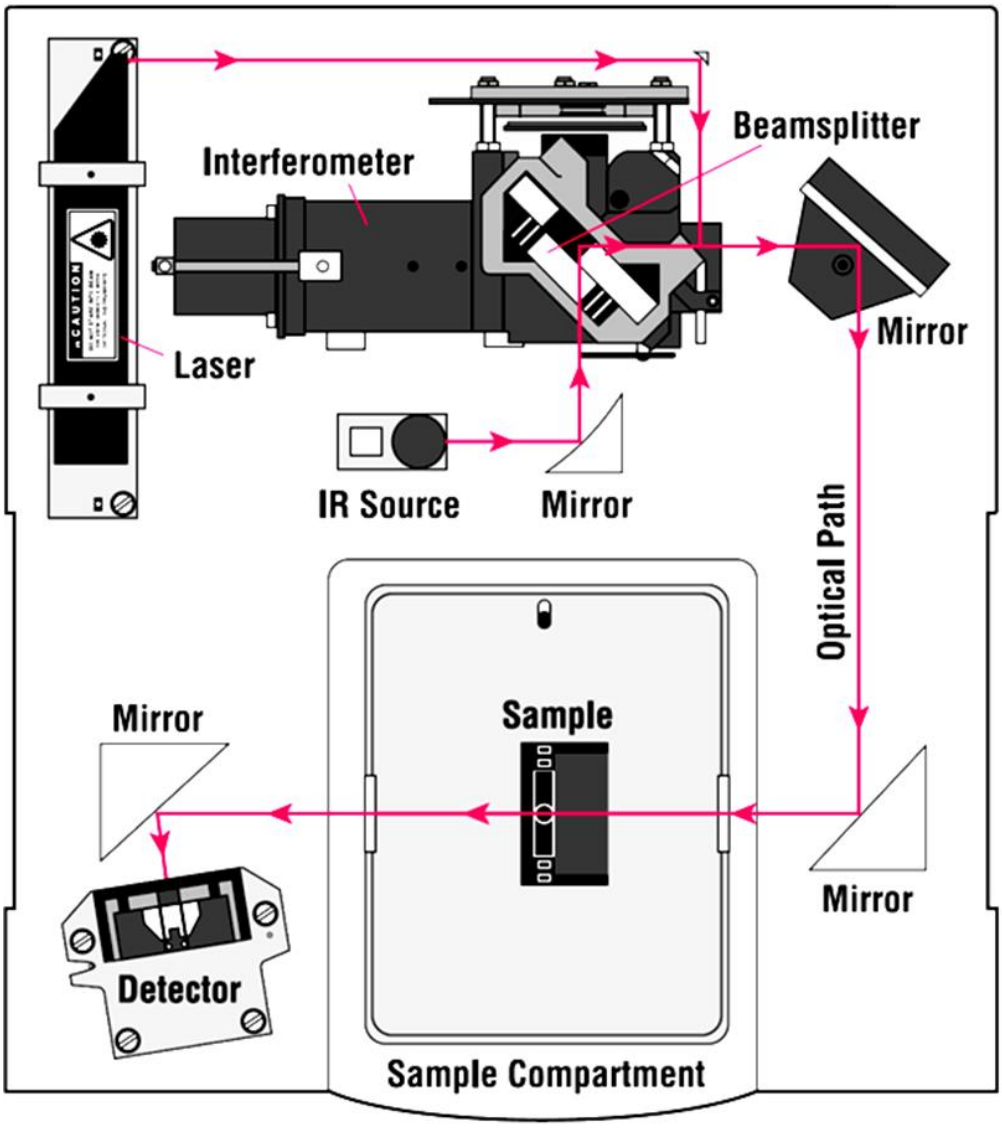

Figure 2-31: *Structure of FTIR spectrometer* [56].

Displacement of movable mirror plays important role in the FTIR spectrometer. If distances between two mirrors and the beamsplitter would be the same, consequently, traveled distance by two beams will be the same, and this situation is defined as **zero path difference (ZPD).** [57,62]

In case, movable mirror would be moved away from the beamsplitter, the light which hits to this mirror should travel longer distance. The distance which the movable mirror moves away from the ZPD is called as mirror displacement (Δ) and amount of extra distance travelled by the light is equal 2Δ. Based on these distances, equation 2-18 defines **optical path difference (OPD)** concept which is shown by (δ) following:

$$\delta = 2\Delta \qquad (2\text{-}18)[57,62]$$

The optical path difference (OPD) is the multiples of wavelength. Equations 2-19 and 2-20 present this relationship, by considering constructive and destructive interferences of the waves respectively.

$$\delta = n\lambda \qquad (2\text{-}19)$$

$$\delta = \left(n + \frac{1}{2}\right)\lambda \qquad (2\text{-}20)$$

with n = 0,1,2,3...

Accordingly, detector can detect maximum and minimum intensity of signal by constructive interference and destructive interference respectively. Hence, back and forth movement of the mirror leads to increase and decrease of the signal intensity. It gives rise to a cosine wave and the created plot is called as interferogram. The interferogram is a plot of the signal intensity versus OPD. [57,62]

The interferogram is a signal which is function of the time. **Fourier transform** converts this signal to spectrum which is the functional of frequency. This mathematical operation makes the signal interpretable as figure 2-32 shows. [57]

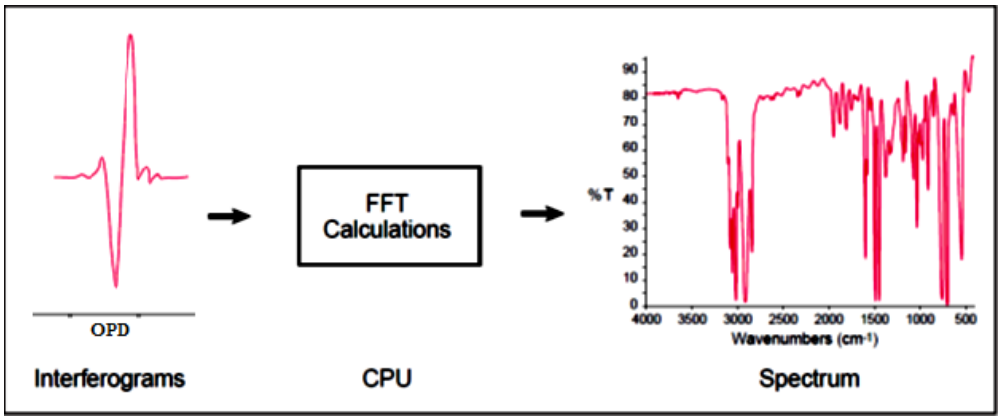

Figure 2-32: *Converting interferogram to spectrum by the Fourier transform operation* [56].

The motivation for the Fourier transform comes from the analysis of Fourier series in the sense that their application is restricted to periodic functions. By Fourier series, complex but periodic functions are written as the sum of simple waves that are mathematically modeled by sines and cosines. The Fourier Transform is an extension of the Fourier series that can be applied to continuous and periodic functions. In general, the Fourier transform shows how to break the signal waveform components into the sum of sinusoidal function which is an alternate representation. Equation 2-21 represents this mathematical operation which is applied in FTIR method,

$$A(r) = \sum X(k)\exp(-2\pi \frac{irk}{N}) \,, \tag{2-21}$$

where A(r) and X(k) present frequency domain and time domain points respectively, for a spectrum of N points. After Fourier transformation operation, the created spectrum can be viewed as the inversion of OPD. The unit of OPD is centimeter, so the inversion of OPD which is known as wave number has the unit of cm^{-1}. [57,62,63]

Attenuated Total Reflection (ATR)

In **reflection spectroscopy** methods, the absorption properties of a specimen can be extracted from the reflected light. The reflection spectroscopy methods are divided into two major categories, internal and external reflection. **Attenuated total reflection (ATR)** is belonged to internal reflection spectroscopy techniques. ATR is applied in conjunction with IR spectroscopy device. Because in current thesis, FTIR-ATR device is used for IR managements, The ATR technique will be discussed by details. [64]

In the ATR method, IR beam is directed into a crystal which enjoys relatively higher refractive index. Reflecting the IR beam from internal surface of the crystal leads to create an **evanescent wave**. 'Evanescent' means 'tending to vanish'. It is suitable name for these waves, because the intensity of evanescent waves decays exponentially, with increasing distance from the interface which they are formed. The evanescent waves are formed when sinusoidal waves are reflected internally in the interface. Figure 2-33 shows formation of evanescent waves. Some of the energy of evanescent wave is absorbed by sample and then reflected radiation goes toward detector. Figure 2-34 represents ATR technique schematically. [65,66]

This reflection occurs at an angle which is bigger than the critical angle, so that total internal reflection happens. The **critical angle ($\boldsymbol{\theta_c}$)** is defined by ratio of refractive indices of crystal and sample according to equation 2-22,

$$\theta_c = \sin^{-1}\left(\frac{n_s}{n_c}\right) \tag{2-22}$$

where n_s is the refractive index of sample and n_c is the refractive index of crystal. [66]

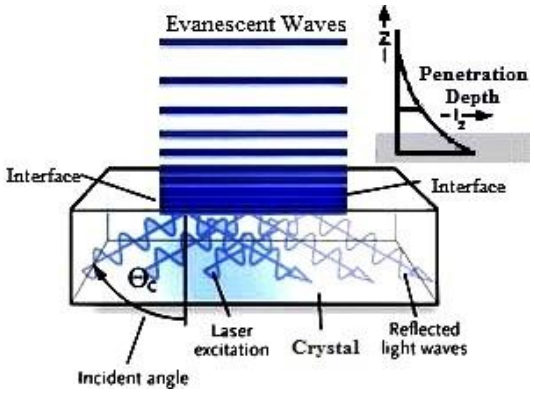

Figure 2-33: *Formation of evanescent waves.*

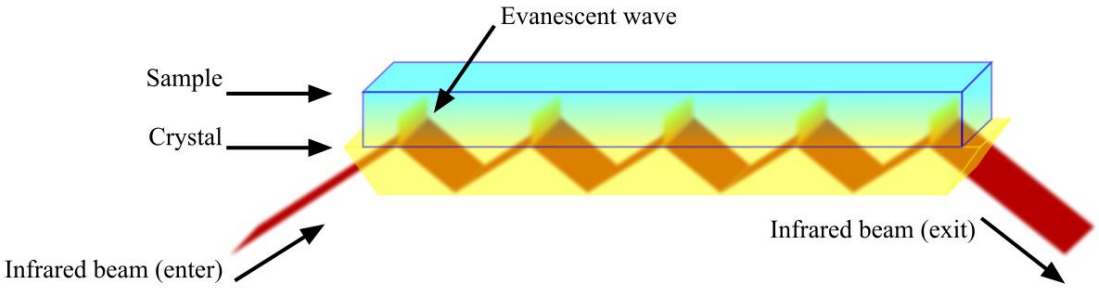

Figure 2-34: *Attenuated total reflection (ATR) technique* [67].

Another key concept for ATR analysis is **depth of penetration (d_p)** of the infrared beam into specimen. This concept is defined as the distance required for the electric field amplitude to fall to e^{-1} of its value at the surface. Equation 2-23 explains this concept as:

$$d_p = \frac{\lambda}{2\pi(n_c{}^2 sin^2\theta - n_s{}^2)^{1/2}} , \tag{2-23}$$

where λ presents the wavelength of light and θ is the angle at which the light strikes the surface of the crystal. [66]

For comparison of specimen absorbance in the ATR measurement with that of a transmission measurement, calculation of the evanescent wave volume is necessary. The effective penetration of the IR beam which is shown by (d_e) explains volume of evanescent wave. The effective penetration (d_e), is specific for parallel polarization ($d_{e\parallel}$) and perpendicular polarization ($d_{e\perp}$) following equations 2-24 and 2-25.

$$d_{e\perp} = \frac{n_c{}^2 n_s \cos\theta}{n_c{}^2 - n_s{}^2} \cdot \frac{\lambda}{\pi\sqrt{n_c{}^2 sin^2\theta - n_s{}^2}} \tag{2-24}$$

$$d_{e\parallel} = \frac{n_c{}^2 n_s \cos\theta}{n_c{}^2 - n_s{}^2} \cdot \frac{2n_c{}^2 sin^2\theta - n_s{}^2}{(n_c{}^2 - n_s{}^2) sin^2\theta - n_s{}^2} \cdot \frac{\lambda}{\pi\sqrt{n_c{}^2 sin^2\theta - n_s{}^2}} \tag{2-25}$$

The effective penetration (d_e) for an unpolarized IR beam is explained by equation 2-26.

$$d_e = \frac{d_{e\perp} + d_{e\parallel}}{2} \tag{2-26}$$

Increase of **effective path length (EPL)** also is possible by increasing number of reflections (N) within the ATR crystal as following equation:

$$EPL = d_e \times N \tag{2-27}$$

Generally, according to above equations, for selecting suitable ATR crystal to enjoy favorable effective path length (EPL), the refractive indices of crystal and sample should be considered. Common ATR crystals include germanium, silicon, zinc selenide and diamond. [66]

The ATR method makes possible that sample be examined directly without preparation. It is suitable for samples in either solid or liquid state. The important advantage of ATR method is related to thin sampling path length. In traditional FTIR sampling, sample should be diluted with IR transparent salt, pressed into a pellet or pressed to a thin film. For transmission-based tests like FTIR, the high thickness of specimen is not favorable, because most of the IR radiation will be absorbed. The ATR sampling method provides so thin sampling path length. Most important result of this matter is improving signal-to-noise ratio by using ATR. [66]

- **Interpretation of Spectrum**

By FTIR spectroscopy either qualitative analysis based on wavenumber of peak, or qualitative analysis based on intensity of peak are possible. Further both of them will be explained.

Qualitative Analysis

Position and wavenumber of each peak is helpful for qualitative analysis. As it mentioned before each special bond and chemical functional group displays the peaks at unique and specific frequencies in IR spectrum. In other words, IR spectrum provides a fingerprint for chemical groups. Figure 2-35 shows an IR spectrum along the positions of important bonds. [58]

Quantitative Analysis

The Beer-Lambert law (Equation 2-13),

$$A = log\frac{I_0}{I} = \varepsilon cl,$$

is base of the quantitative analysis of IR spectrum. The parameters I_0 and I can be obtained by **tangential baseline method** according to figure 2-36.

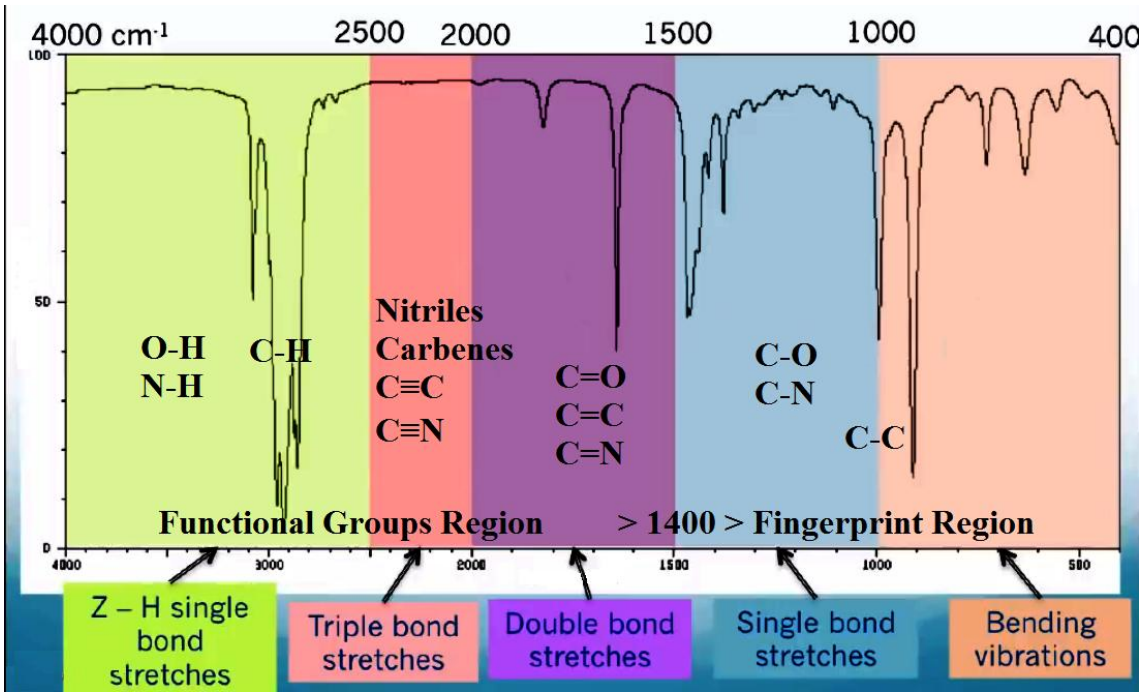

Figure 2-35: *Major functional groups and bonds along IR absorption frequency regions.*

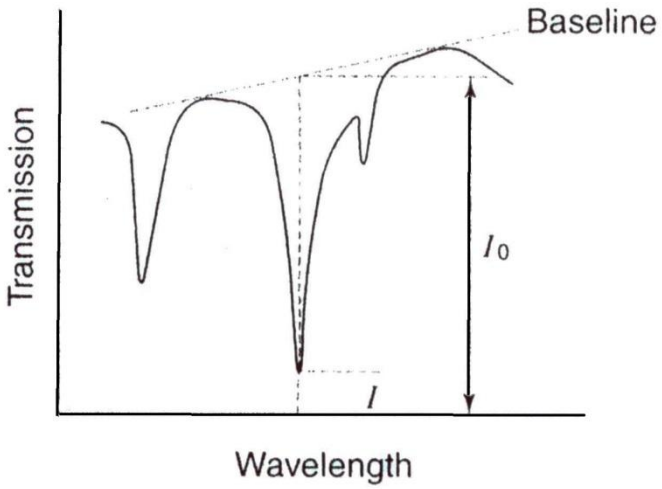

Figure 2-36: *Tangent baseline measurement* [68].

Finally, quantitative measurements are possible via comparing the magnitude of absorption (A_u) of unknown concentration (c_u) with absorption (A_s) of a standard solution enjoyed known concentration (c_s). Below equations explain this method according to:

$$A_s = \varepsilon c_s l \,,$$

$$A_u = \varepsilon c_u l \,,$$

therefore

$$\frac{A_s}{c_s} = \frac{A_u}{c_u} = \varepsilon l$$

Hence the concentration of unknown sample is

$$c_u = \frac{c_s A_u}{A_s} \tag{2-28}$$

This method is usable just when relationship of absorption/concentration is liner. Using calibration graph can solve this problem. The calibration graph makes it possible that any unknown concentration can be determined by using some standard points even for nonlinear absorption/concentration situation, according to figure 2-37. [68]

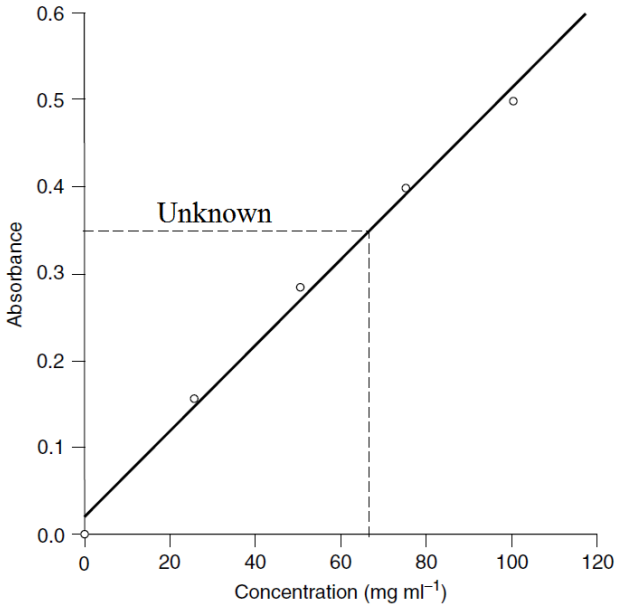

Figure 2-37: *Calibration graph for determination of unknown concentration* [68].

2.3.3 Raman Spectroscopy

Raman Effect was discovered by C. V. Raman in 1928. Surprisingly, during 1930s Raman measurements were used more than infrared measurements because direct recording was possible by using a photographic plate in Raman measurements but for infrared measurements, it had to be recorded manually. [68]

Raman spectroscopy is based on the inelastic scattering of monochromatic light. This method same as FTIR, is suitable for characterization of solid, liquid and gaseous samples. In the Raman spectroscopy method, in the first step, monochromatic light produced by laser source interacts with sample. Then, electric field of the radiation distorts electron clouds which are making chemical bonds in sample. When the electric field reverses while wave traverses, the deformed electron clouds can be relaxed and then the

stored energy is reemitted. Frequency of the reradiated beam is shifted than the original monochromatic frequency. This shifting is known as Raman Effect. It informs us about vibrational and rotational transitions in the atoms and molecules. [69,70]

- **Basic Principles**

Laser light which is a monochromatic beam stimulates molecules and transforms them into oscillating dipoles. Figure 2-38 explains three different frequencies of **Raman transitions**. In this figure, frequency of vibration of molecules is $\upsilon_{m,}$ and on the other side, frequency of laser light is considered υ_0. [70,71]

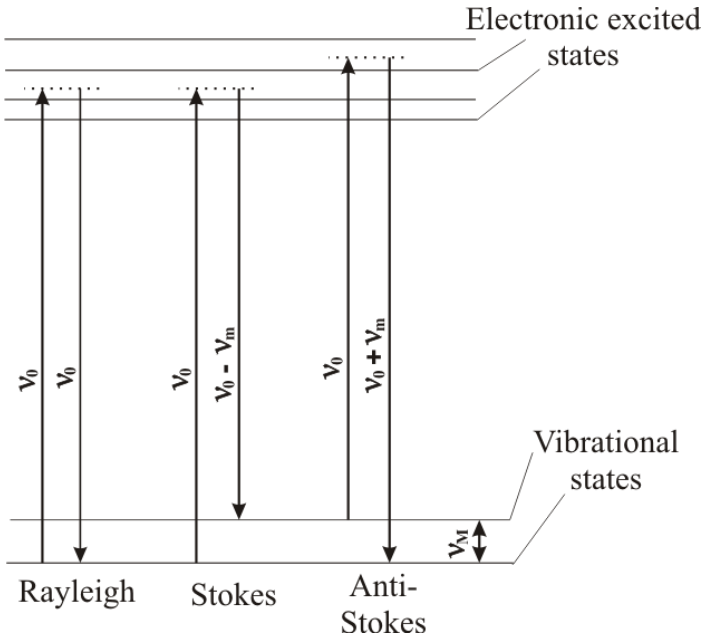

Figure 2-38: *Different frequencies of Raman transitions* [72].

According to figure 2-38, three different Raman transitions can be considered:

1. Elastic Rayleigh: In this transition, a molecule absorbs a photon with the frequency υ_0 and then the excited molecule comes back to basic vibrational state with radiating electromagnetic wave which enjoys same frequency ν_0 like excitation beam. These kinds of molecules are called "**No Raman-active molecules**". [70,71]

2. Stokes: In this type of transition, a photon which is belonged laser beam with frequency υ_0 is absorbed by **Raman-active molecule** which is in basic vibrational state. The energy of phonon transfers to the molecule with frequency ν_m. In this situation, frequency of scattered electromagnetic wave is reduced to $\nu_0 - \nu_m$. [70,71]

3. Anti- Stokes: In this mode, a **Raman-active molecule** which is already in the excited vibrational state absorbs a photon with frequency ν_0. In this situation, molecule comes back to basic vibrational state and frequency of scattered electromagnetic wave is $\nu_0 + \nu_m$. [70,71]

Figure 2-39 compares possible transitions in Raman spectroscopy with optical process which occurs in the IR spectroscopy. In absorption process (IR spectroscopy), energy is absorbed and then dissipated. But in Rayleigh transition, an elastic collision is happen so there is along with no change in energy. In contrast Rayleigh process, in the Raman stokes and Raman anti- stocks, energy of the photon is transferred in molecule. [73]

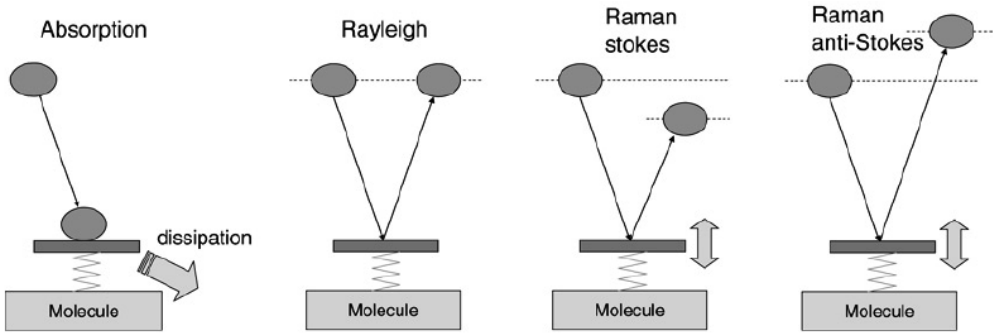

Figure 2-39: *Possible optical processes in IR and Raman Spectroscopy* [73].

The difference in frequency between new frequencies (Raman bands) and the original frequency is specific for each molecule and also it is equal with vibrational and rotational frequencies of the molecule numerically. Raman shift ($\bar{\nu}$) is in relationship with force constant (f) and reduced mass (μ) according to same expression in equation 2-16 for infrared spectroscopy [68]:

$$\bar{\nu} = \frac{1}{2\pi c}\left(\frac{f}{\mu}\right)^{\frac{1}{2}} \tag{2-29}$$

Figure 2-40 shows a pattern for Raman spectrum. Each Raman transition is distinguishable in this figure. The Raman shift ($\bar{\nu}$)(cm^{-1}) forms horizontal axes and Raman intensity which its unit is reported usually 'counts per second (cps)'makes vertical axes. Stokes scattering is formed in positive wavenumbers and anti-stocks scattering is placed in negative wavenumbers. Most of the research are based on stokes scattering but also anti- stocks scattering can be used in few studies. [69,74]

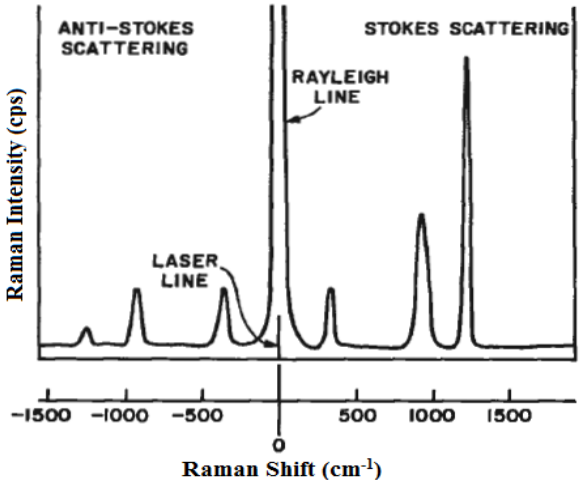

Figure 2-40:*Place of different Raman transitions in Raman spectrum* [69].

About 99.999% of all photons in Raman spectroscopy will be scattered as elastic Rayleigh scattering. So just about 0.001% of emission signals are including inelastic Raman signal with frequencies $v_0 \pm v_m$. Regarding explained situation, some instruments like filters are applied in Raman spectrometer for increasing quality of signals. [70]

Raman scattering has root in the vibrations which cause change in the **polarizability (α)** of the electron cloud of molecule. The polarizability of a molecule is capability of the molecule to be polarized under the influence of an electron field E. Polarizability is in relationship with dipole moment (μ) according to equation 2-30 [68]:

$$\mu = \alpha E \tag{2-30}$$

IR and Raman spectroscopy methods can to be complementary in the studies of molecules due to their difference in **selection rules** for activity. Whereas change in dipole moment during vibration provides to be IR-active, but for being Raman-active, change in polarizability should happen. [71]

The **symmetric vibrations** cause the weak or no dipole change but largest changes in polarizability and therefore Raman scattering. In contrast, **asymmetric vibrations** lead to larger change in dipole moment and most intense IR absorption. [71]

Figure 2-41 shows different vibration modes of carbon dioxide (CO_2) and observation of each vibration mode in IR or Raman spectroscopy.

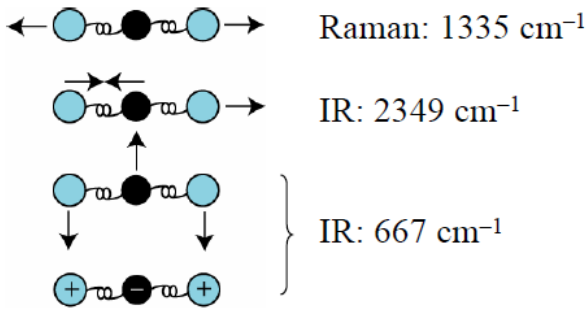

Figure 2-41: *symmetric and asymmetric vibration modes of CO_2 molecule* [75].

For detection of a molecule by IR or Raman spectroscopy methods, it is not necessary all vibration modes of a molecule be active for each method. It is possible for a specific molecule, a vibration mode would be active for IR method, and another would be active for Raman method. This situation can result in different patterns for a molecule which is active in either IR or Raman methods. Figure 2-42 illustrates IR and Raman spectra of carbon disulphide (CS_2) molecule. This figure is a good example for proving what is explained above. [71]

In this figure V_s, V_{as} and δ represent symmetrical stretching vibration, asymmetrical stretching vibration, and bending vibration respectively. According to figure 2-42, the vibration modes which enjoy changes in polarizability,

$$(\frac{\partial \alpha}{\partial Q} \neq 0),$$

are appeared in the Raman spectrum and in contrast when

$$(\frac{\partial \mu}{\partial Q} \neq 0),$$

changes in dipole moment lead to IR absorption (Parameter Q will be presented in future). Regarding figure 2-42 and what is claimed above, the changes in dipole moment or polarizability can be occurred without happening another. Further, for deeper understanding and more clarification, relationship between dipole moment and polarizability (equation 2-30) will be discussed by using more details. [71,76]

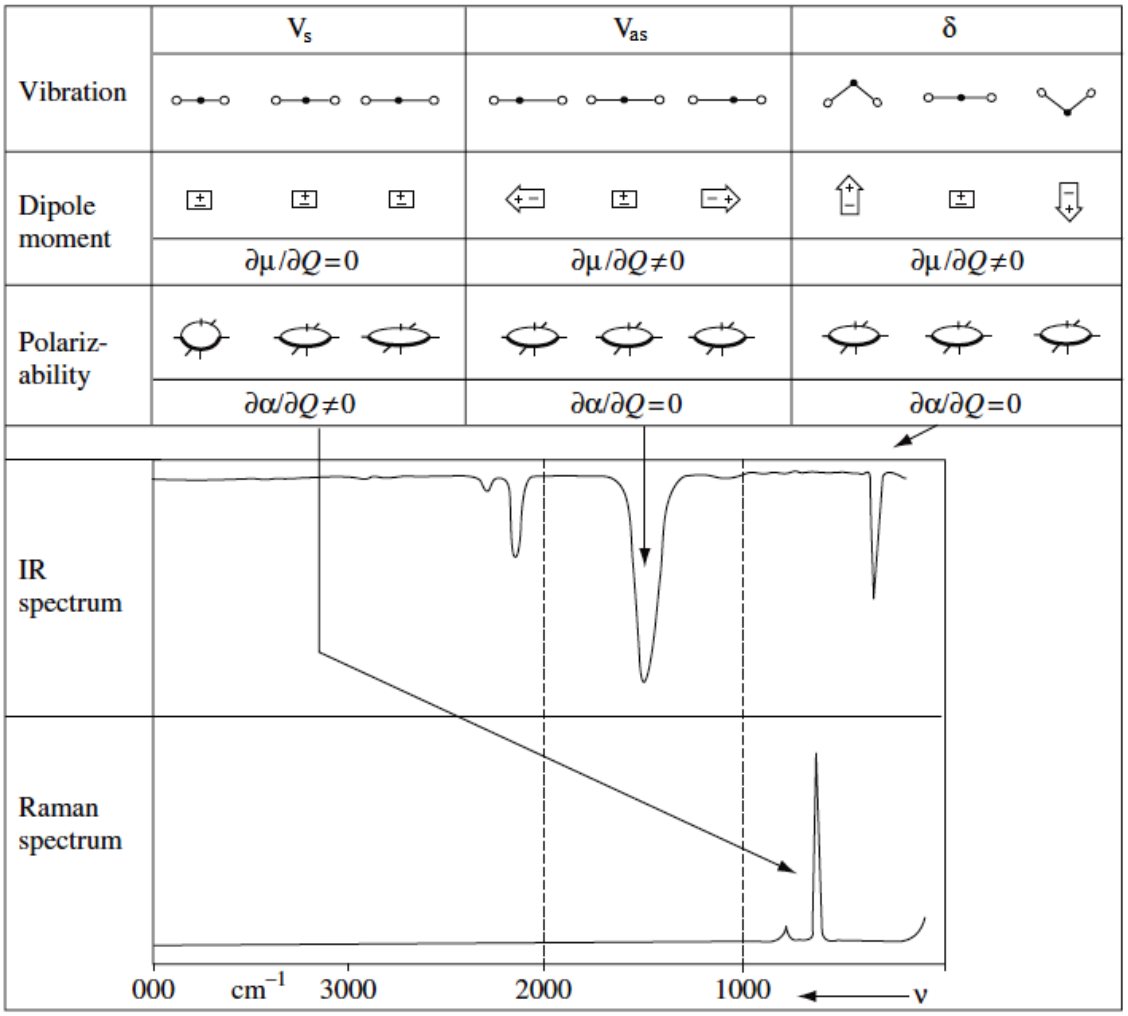

***Figure 2-42**: Possible molecular vibrations of carbon disulphide(CS_2) along their IR and Raman peaks* [77].

Basic relationship between polarizability and dipole moment as explained in equation 2-30 is written as:

$$\mu = \alpha E$$

The parameters μ and E are vectors, and α is a tensor. Polarizability tensor is usually symmetric. Dipole moment can be explained in term of Cartesian components, so it can be written as:

$$\begin{bmatrix}\mu_x\\ \mu_y\\ \mu_z\end{bmatrix}=\begin{bmatrix}\alpha_{xx} & \alpha_{xy} & \alpha_{xz}\\ \alpha_{yx} & \alpha_{yy} & \alpha_{yz}\\ \alpha_{zx} & \alpha_{zy} & \alpha_{zz}\end{bmatrix}\begin{bmatrix}E_x\\ E_y\\ E_z\end{bmatrix} \tag{2-31}$$

and hence:

$$\begin{cases}\mu_x = \alpha_{xx}E_x + \alpha_{xy}E_y + \alpha_{xz}E_z\\ \mu_y = \alpha_{yx}E_x + \alpha_{yy}E_y + \alpha_{yz}E_z\\ \mu_z = \alpha_{zx}E_x + \alpha_{zy}E_y + \alpha_{zz}E_z\end{cases}$$

and so:

$$\alpha_{xy} = \alpha_{yx};\ \alpha_{yz} = \alpha_{zy};\ \alpha_{xz} = \alpha_{zx} \tag{2-32}$$

On the other hand, polarizability and dipole moment are function of time and amplitude of vibration according to following equations (2-33 and 2-34), whereas:

$$E = E_0 \cos 2\pi\nu_0 t \tag{2-33}$$

Equation 2-33 shows parameter E is function with time (t) and electron field (E_0) of incident electromagnetic wave. Also in this equation, ν_0 represents frequency of laser beam (electromagnetic wave). [78,79]

As mentioned, amplitude of molecular vibration plays own role in polarizability and dipole moment according to below Fourier series:

$$\alpha = \alpha_0 + \left(\frac{\partial\alpha}{\partial Q_k}\right)_0 Q_k + \cdots \tag{2-34}$$

where Q_k is normal mode of vibration in molecule at frequency ν_k with amplitude Q_k^0 according to:

$$Q_k = Q_k^0 \cos 2\pi\nu_k t \tag{2-35}$$

Finally, relationship between polarizability and dipole moment can be written as:

$$\mu = \alpha_0 E + \left(\frac{\partial\alpha}{\partial Q_k}\right)_0 Q_k E \tag{2-36}$$

According to explained equations and relations, and regarding vectorial concept of dipole moment and polarizability which is a matrix, relationship between changes in μ and α is complicated specially for anisotropic materials. [78,79]

Another rule discussed in Raman activity is **mutual exclusion rule.** For a specific type of molecules, a specific selection rule is proposed. In a **centrosymmetric molecule**, no band can be active in both methods (IR and Raman spectroscopy). It is called the mutual exclusion rule. For all molecules with a center of symmetry, transitions which are permitted in Raman spectrum are forbidden in IR spectrum and vice versa. Hence if a molecule would have peaks at same frequencies in IR and Raman spectrum, this molecule cannot be centrosymmetric. [68]

- **Instrumentation**

Laser beam is used as excitation radiation in Raman spectroscopy because it is a monochromatic beam. Lasers beam used is Raman method is obtained at special wavelength in blue or the infrared regions. Because Raman scattering is so weak, laser beam should be well focused on the specimen and also scattered radiation must be collected efficiently. One of the most important subjects for achieving to this matter is configuration of device. Most suitable angles between incident laser beam and sample are 90° or 180° (the back scattered). Figure 2-43 shows major parts of a Raman spectrometer. [80]

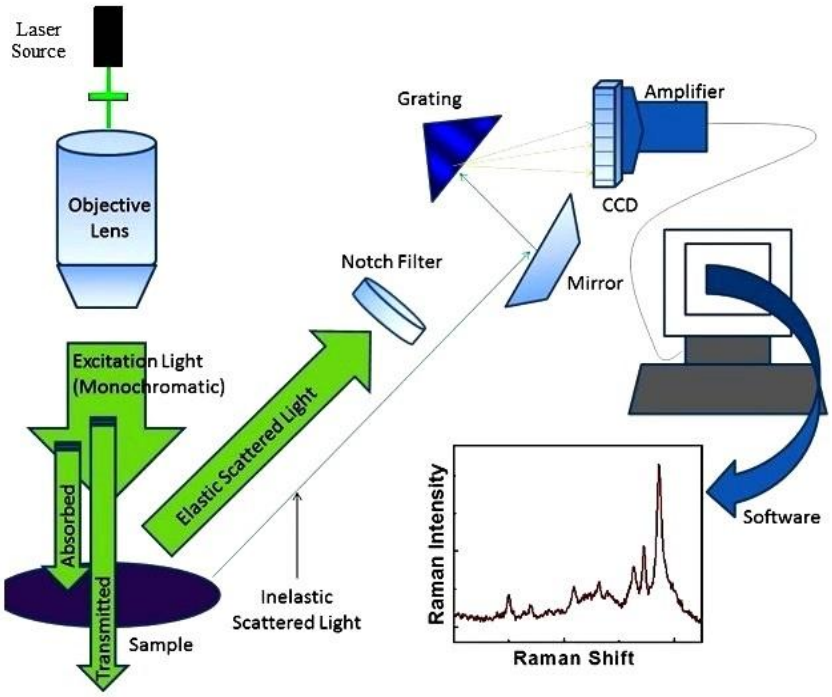

Figure 2-43:*Major parts of Raman spectrometer* [81].

After incident of the laser beam to sample and scattering phenomenon, a filter is put that filters the elastic scattered light. It is known as **notch filter**. Then, for obtaining the Raman spectrum, separation of the scattered inelastic radiation to its composite wave-

lengths is required. **Diffraction grating** performs this task. Also, the diffraction grating plays most important role in spectral resolution. [80,82]

Gratings are designed for achieving to optimum resolution over narrow wavelength range. So for selecting most suitable grating for Raman spectrometer, favorable resolution and the wavelength of used laser must be considered. [80,82]

After grating, diffracted beams are directed to **charge-coupled devices (CCDs)** which are silicon-based semiconductors. The CCDs perform role of detector device for Raman spectrometer system. Surface of the CCD is formed by an array of photosensitive elements. These photosensitive elements are known as pixels. Each pixel performs role of an individual detector. Hence each diffracted wavelength is detected by an individual pixel. [82]

- **Interpretation of Spectrum**

Raman spectroscopy provides to obtain useful information including: composition of material, stress/strain state, crystal symmetry and orientation, quality of crystal and amount of material. Similar to FTIR spectroscopy, each special vibration mode or chemical bond enjoys unique frequency. This matter makes base of qualitative analysis in Raman spectroscopy. The intensity of Raman peaks is directly proportional to concentration or amount of species. [83,84]

Table 2-1 compares characterization of some impotent functional groups or bonds by Raman and IR spectroscopy along own vibration frequencies. In this table δ shows bending vibration and υ represents stretching vibration.

Table 2-1: *Comparison of Raman and IR spectroscopy for characterization of some functional groups or vibration modes along own vibration frequency [85].*

Functional Group / Vibration	Region (cm^{-1})	Raman	IR
δ (CC) aliphatic	250-400	strong	weak
ν (O-O)	845-900	strong	weak
ν (C-O-C)	800-970	medium	weak
ν (C-O-C) asym	1060-1150	weak	strong
ν (CC) alicyclic, aliphatic	600-1300	medium	medium
ν (CC) aromatic ring chain vibrations	1580, 1600 1450, 1500 1000	strong medium strong/medium	medium medium weak

Table 2-1: *Comparison of Raman and IR spectroscopy for characterization of some functional groups or vibration modes along own vibration frequency [85]*

Functional Group / Vibration	Region (cm^{-1})	Raman	IR
δ (CH_3)	1380	medium	strong
δ (CH_2) δ(CH3) asym	1400-1470	medium	medium
ν (C-(NO_2)	1340-1380	strong	medium
ν (C-(NO_2) asym	1530-1590	medium	strong
ν (N=N) aromatic	1410-1440	medium	-
ν (N=N) aliphatic	1550-1580	medium	-
δ (H_2O)	~1640	weak broad	strong
ν (C=N)	1610-1680	strong	medium
ν (C=C)	1500-1900	strong	weak
ν (C=O)	1680-1820	medium	strong
ν (C≅C)	2100-2250	strong	weak
ν (C≅N)	2220-2255	medium	strong
ν (C-H)	2800-3000	strong	strong
ν (=(C-H))	3000-3100	strong	medium
ν (≅(C-H))	3300	weak	strong
ν (N-H)	3300-3500	medium	medium
ν (O-H)	3100-3650	weak	strong

As mentioned, Raman spectrum can explain a lot of information like crystallographic features of sample. Table 2-2 shows how this information can be obtained according to feature of Raman peak.

Table 2-2: *Information obtained according to feature of Raman peak [84].*

Feature of Peak		Information
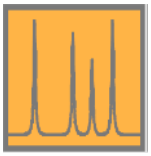	Characteristic Raman frequencies	Composition of material

Table 2-2: *Information obtained according to feature of Raman peak [84].*

Feature of Peak		Information
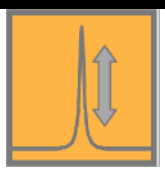	Intensity of Raman peak	Amount of material
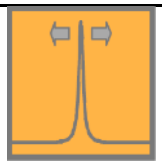	Changes in frequency of Raman peak	Stress/strain state
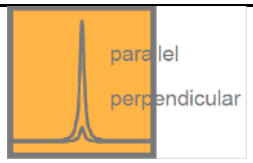	Polarization of Raman peak	Crystal symmetry and orientation
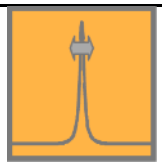	Width of Raman peak	Quality of crystal

As explained a lot of information is hidden in Raman spectrum. In future, interpretation of Raman spectrum of CNT will be discussed by details.

2.4 Study of Carbon Nanotubes Surface by Optical Spectroscopy

For characterization and analysis of carbon materials surface, using more than one method is necessary. In other words, single analytical method cannot be successful to explain all of the surface chemical properties. Some properties of carbon like capability of this material in high absorption of radiation create some challenges in characterization of functional groups located on surface. During this thesis, for studying functional groups located on the CNT surface and defects, FTIR method and Raman spectroscopy is used respectively. [5]

2.4.1 Characterization of Functional Groups on the Carbon Nanotubes by FTIR Spectroscopy

In this section, some experimental research and studies on the characterization of functional groups located on CNTs by FTIR spectroscopy will be surveyed. FTIR spectroscopy is most popular method for analyzing functional groups on the surface of coals, carbon blacks, carbon fibers, carbon films and carbon nanotubes (CNTs). [5]

Favorable **signal-to-noise (S/N)** ratio, in the FTIR spectroscopy, plays important role in the characterization of functional groups located on carbon materials surface. Actually

opacity of carbon materials leads to decrease of energy throughput, and also reduce spectral S/N ratio. The major problem of FTIR analysis of carbon materials is black body absorption of carbon. High opacity of carbon leads to creation problems for direct transmission analysis in the mid-infrared spectral region. [5]

Common solution for decreasing effect of this problem is diluting carbon materials with favorable **transparent medium materials** like KBr for intensifying signals. Also as other challenge, particle light-scattering leads to not only radiation loss but also reflection form surface. This phenomenon creates shifting of spectrum, specially, in high frequency region. [5]

Analyzing carbon materials by IR spectroscopy is difficult traditionally, because of the opacity of carbon. With regarding to noise problem in the analysis of carbon materials, using FTIR-ATR method is recommended. Most challenge during using FTIR-ATR is selecting suitable prism. Selecting diamond prism, while carbon martial are studied, makes more problems in the ATR analysis.

According to equation 2-23,

$$d_p = \frac{\lambda}{2\pi(n_c{}^2 sin^2\theta - n_s{}^2)^{1/2}},$$

which is discussed in previous sections, if the reflection index of sample would be so close to that of the prism, the ratio of indexes is almost 1, the square root of term is negative and there is no ATR effect. For solving this problem using germanium ATR crystal instead diamond for measuring ATR spectrum of carbon samples is recommended. [12]

A lot of studies are done about characterization of functional groups on the carbon materials by IR spectroscopy. Table 2-3 represents IR absorption bands and peaks for some oxygenated functional groups on the carbon materials surface. [5]

Table 2-3: *IR absorption frequencies for oxygenated functional groups on the carbon materials surface [5].*

Functional Group	Wavenumber (cm^{-1})		
	1000-1500	**1500-2050**	**2050-3700**
C-O stretch of ethers	1000-1300	-	-
Ether bridge between rings	1230-1250	-	-
Cyclic ethers containing COCOC groups	1025-1141	-	-
Alcohols	1049-1276	-	3200-3640
Phenolic groups: C-O stretch O-H bend/stretch	 1000-1220 1160-1200	 - -	 - 2500-3620

Table 2-3: *IR absorption frequencies for oxygenated functional groups on the carbon materials surface [5].*

Functional Group	Wavenumber (cm^{-1})		
	1000-1500	1500-2050	2050-3700
Carbonates; carboxyl-carbonates	1000-1500	1590-1600	-
Aromatic C=C stretching	-	1585-1600	-
Quinones	-	1550-1680	-
Carboxylic acids	1120-1200	1665-1760	2500-3300
Lactones	1160-1370	1675-1790	-
Anhydrides	980-1300	1740-1880	-
Ketenes (C=C=O)	-	-	2080-2200
C-H stretch	-	-	2600-3000

Also, nitrogen functional groups on the carbon have been characterized by FTIR spectroscopy. Table 2-4 represents wavenumbers regions related to these functional groups in IR spectrum. [86]

Table 2-4: *IR absorption frequencies for nitrogen functional groups on the carbon materials surface [86].*

Functional Group	Wavenumber (cm^{-1})
C-N (aliphatic), N-H	1020-1150
C-N (in C_3N_4), CC, C=N	1220-1265
sp^2 carbon, C-N, C=N	1300-1350
CH_3, CC, C=N	1360-1380
sp^3 CH_x	1450
C-N, C=N, C=C	1500-1510
C=N	1550-1570
C=N, C=C	1600
C=C, C=N, NH_3	1620-1650

Functionalization of CNTs by acidic agents is most popular and important way to achieve functionalized surface. Laszlo Vanyoreka et al. (2014) [87] have done one of the most recent and comprehensive research in this field. They have studied on the CNTs oxidized with HNO_3, H_2SO_4/HNO_3, $HClO_4$ and H_2O_2 by FTIR spectroscopy. Figure 2-44 shows FTIR spectra related to this study. According to these spectra, concentration of OH groups is following order: $H_2O_2 < HClO_4 < HNO_3 < H_2SO_4/HNO_3$. [87]

2.4.2 Characterization of Carbon Nanotubes by Raman Spectroscopy

Raman spectroscopy is most sensitive method for the analysis of materials with high symmetric covalent bonds along negligible or no natural dipole moment. The carbon-carbon (C-C) bonds have this situation. In addition, Raman spectroscopy is sensitive to even little changes in structure and changes in orientation of C-C bonds. These mentioned points make Raman spectroscopy as a unique method for characterization of carbon materials. [88]

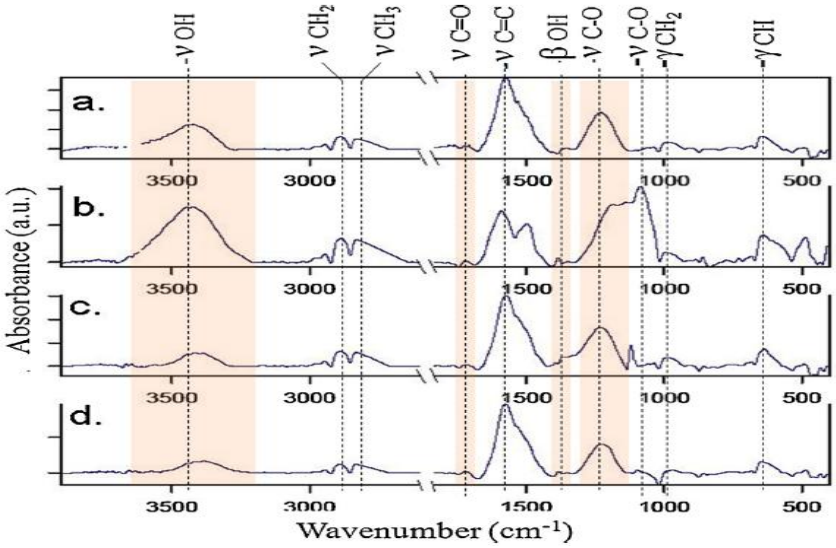

Figure 2-44: *FT-IR spectra of CNTs oxidized with (a) HNO_3, (b) H_2SO_4/HNO_3, (c) $HClO_4$ and (d) H_2O_2* [87].

- **Raman Spectroscopy of Graphene**

As mentioned, Raman spectroscopy is one of the best characterization methods for analysis of carbon materials such as graphene. Figure 2-45 shows Raman spectrum of graphene with considering important peaks. These peaks are known by special names. Characters **G, D and 2D (or G') bands** are applied exclusively for Raman spectrum of graphene in the special wavenumbers. [89,90]

The **G peak** which is related to $\mathbf{E_{2g}}$ **phonon** at central zone of **Brillouin zone**, lies at 1580 cm^{-1}. In the first step for explaining concept of Brillouin zone, attention to honeycomb lattice of graphene is vital. In graphene structure, carbon atoms are settled in the honeycomb lattice. Figure 2-46 (a) shows a small segment of this lattice in a unit cell. In this figure, vectors $\vec{a}$ and $\vec{b}$ along vectors $\overrightarrow{G_1}$ and $\overrightarrow{G_2}$ of the reciprocal lattice are presented. Figure 2-46 (b) presents central part of the reciprocal lattice of graphene and the first Brillouin zone. The corners of the Brillouin zone are points K_i which are explained by:

$$\overrightarrow{k_1} = (\overrightarrow{G_2} - \overrightarrow{G_1})/3,\ \overrightarrow{k_2} = (2\overrightarrow{G_2} + \overrightarrow{G_1})/3, \overrightarrow{k_3} = (2\overrightarrow{G_1} + \overrightarrow{G_2})/3,\ \textit{etc.} \qquad (2\text{-}37)\ [90,92]$$

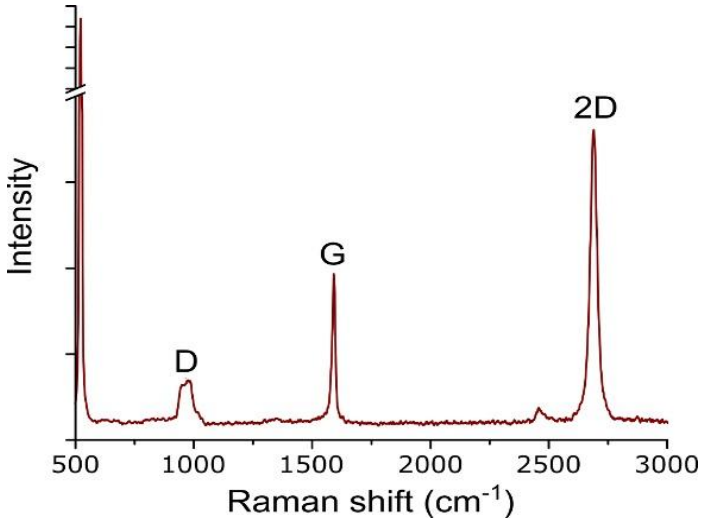

Figure 2-45: *Raman Spectrum of Graphene* [91].

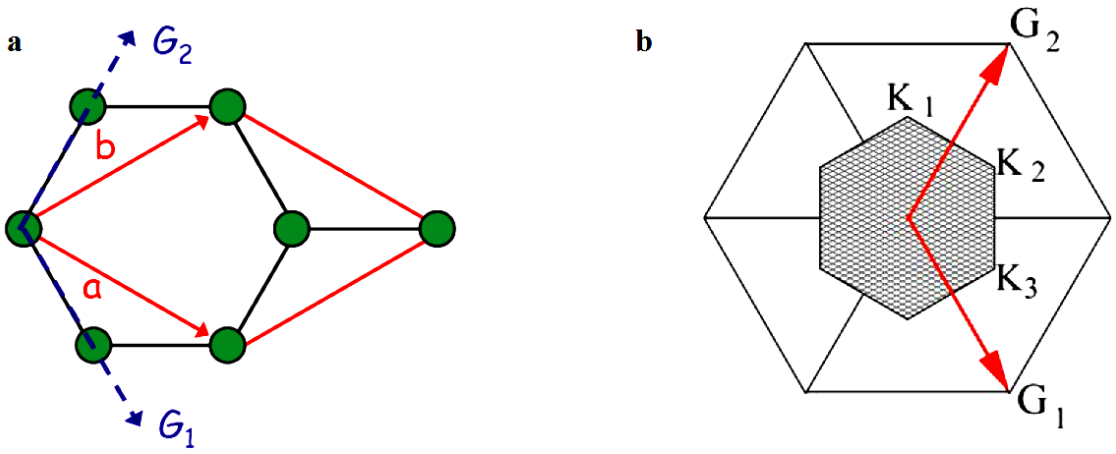

Figure 2-46: *Brillouin zone in graphene lattice* [92].

The E_{2g} phonon consists of in-plane displacement of the carbon atoms. If υ be considered as frequency of phonon, based on equation 2-3,

$$E = h\nu,$$

E_{2g} is 196.0 meV. Figure 2-47 shows displacement pattern corresponding to the E_{2g} phonon. [93,94]

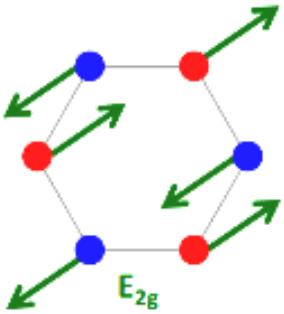

Figure 2-47: *The displacement pattern corresponding to the E_{2g} phonon* [94].

The G peak is most important fingerprint for characterization of graphene in Raman spectroscopy but consider that the position of the G peak will be changed when doped graphene is analyzed. [90]

Other peak which is shown in figure 2-45 is **D band**. This peak represents defects. The D band is a breathing mode for sp^2 atoms. Different **layer-breathing modes (LBMs)** are related to the displacement of graphene layers. In the breathing mode, the top and bottom of graphene layers fluctuate in the directions which make a scheme like a breather. Figure 2-48 schematically represents this phenomenon. The D band is appeared at defects and edges of flakes. [89,90,95,96]

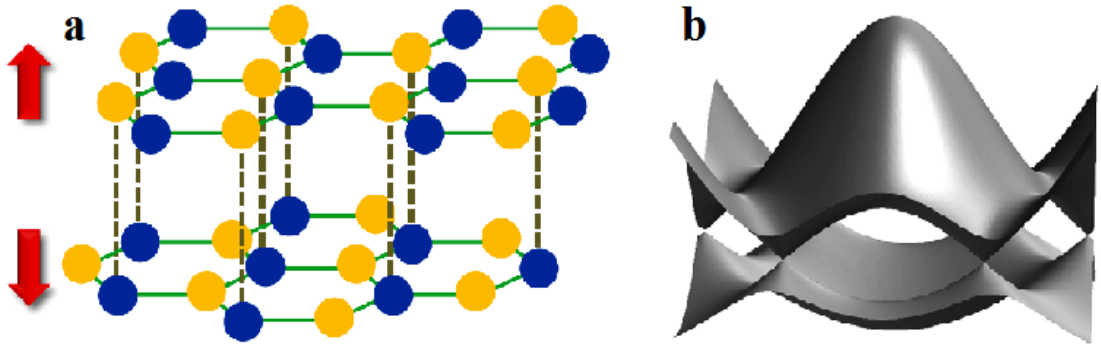

Figure 2-48: *Breathing mode for bilayer graphene* [97,98].

According to figure 2-45, the second order of the D peak which is known as **2D peak** happens at 2700 cm^{-1}. The intensity of this peak informs about the number of graphene layers. Sharp 2D peak represents monolayer graphene and, on the other side, for the more layers, broader 2D peak is expected. [89,90]

- **Raman Spectroscopy of Carbon Nanotubes**

As mentioned in previous sections, carbon nanotubes are rolled up of graphene sheets. Single-wall carbon nanotubes (SWCNTs) are cylindrical tubes with a single graphene wall, and double-wall carbon nanotubes (DWCNTs) enjoy second layer of graphene.

It is not a big surprise, if it would be claimed that the Raman spectrum of SWCNT is similar to graphene. Figure 2-49 shows Raman spectrum of the SWCNT with G, D, and G'(or 2D) bands. In addition, in this spectrum, a series of bands at low frequencies are presented. They are known as **Radial Breathing Mode (RBM) bands**. The RBM bands exclusively will be appeared in SWCNTs spectrum. The RBM peaks are corresponding to expansion and contraction of the tubes. [88]

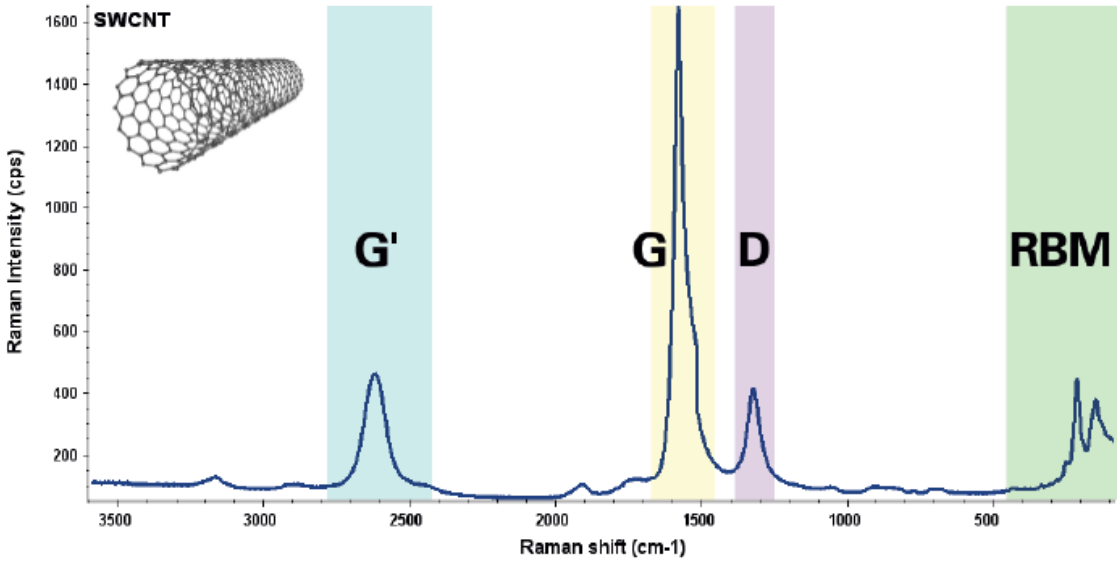

Figure 2-49: *Raman spectrum of SWCNT with important bands* [88].

Figure 2-50 represents Raman spectra of multi walls carbon nanotubes (MWCNTs) compare to SWCNTs. According to graphs, three important differences are obvious. Absence of RBM modes, more prominent D bands, and more 2D (G') bands in the MWCNTs spectrum consist these differences. [88]

In the Raman spectrum of MWCNT, the peaks which are corresponding the RBM modes are absent because the outer tubes delimit breathing mode. The more prominent D band in the MWCNTs spectrum explains more disorder in the structure of analyzed sample. As discussed, G' band in MWCNT spectrum is increased due to extra layers. [88]

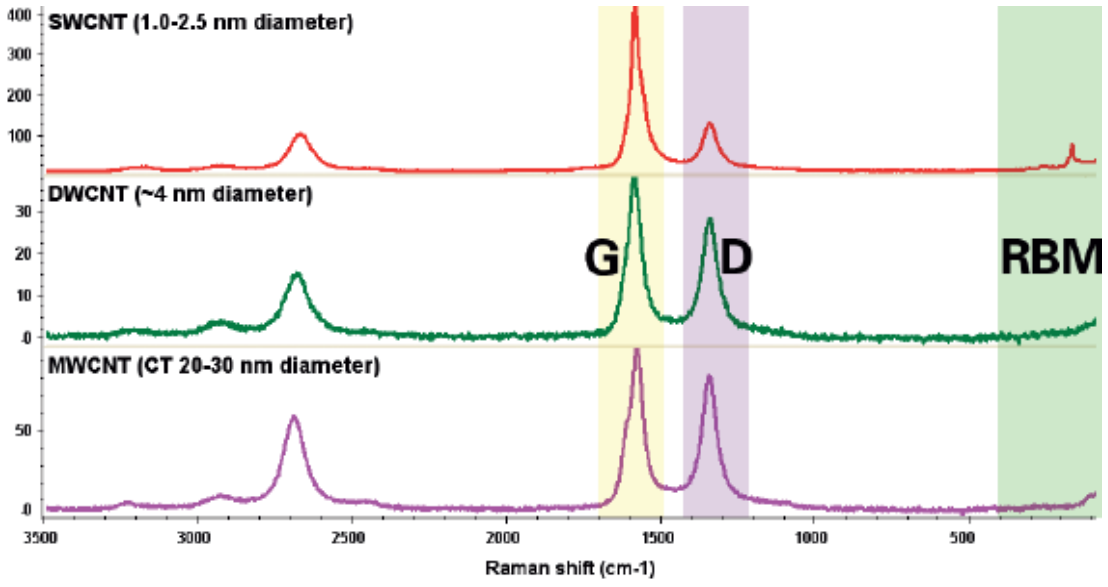

Figure 2-50: *Comparison of the Raman spectra related to SWCNT, DWCNT, and MWCNT* [88].

- **Raman Map of CNT**

Raman map provides to study of the homogeneity of sample by screening specimen surface. Figure 2-51 shows Raman map images of a CNT sample. Most important features (RBM, G band and D band) in the Raman spectrum of CNT are distinguishable in these maps. They explain distribution of these features in studied area. This distribution is distinguishable by different colors which show Raman intensity. [99–101]

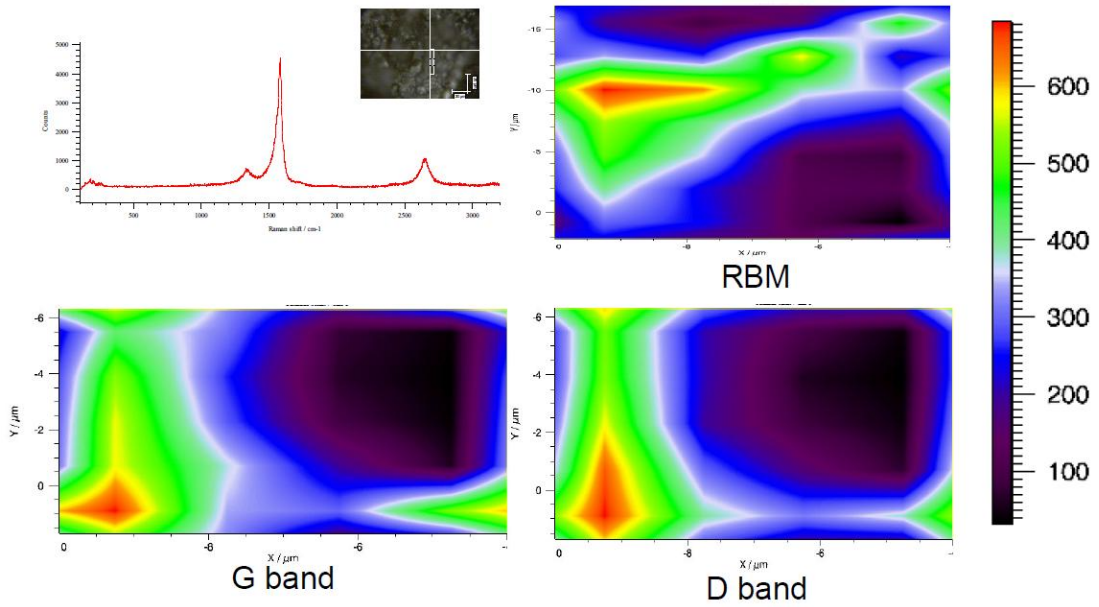

Figure 2-51: *Raman map images of a CNT sample, and distribution of RBM, G band and D band* [101].

- **Characterization of Disorders and Defects on the CNTs by Raman Spectroscopy**

A lot of studies and research are done for characterization disorders, defects and effect of functionalization on the surface of CNTs by Raman spectroscopy. Majority of these studies have been done while CNTs are affected by HCl, HNO_3, H_2SO_4, $NH_4(OH)$, and hydrogen peroxide (H_2O_2) solutions. [102–104]

As example, C. Galiotis et al. (2008) [102] have studied on effect of oxidation on the MWCNT surface, through acidic and basic agents. Figure 2-52 shows Raman spectra which are related to this study.

Intensities of D and G peaks play vital role in analyzing Raman spectrum of CNT while study of defects and disorders be subjected. **I_G/I_D ratio** is used as a suitable tool for studying changes in the surface of CNTs. In the figure 2-52, changes in the intensities of G and D bands, in different CNT samples functionalized in different mediums compare to pristine CNT is observable. [102]

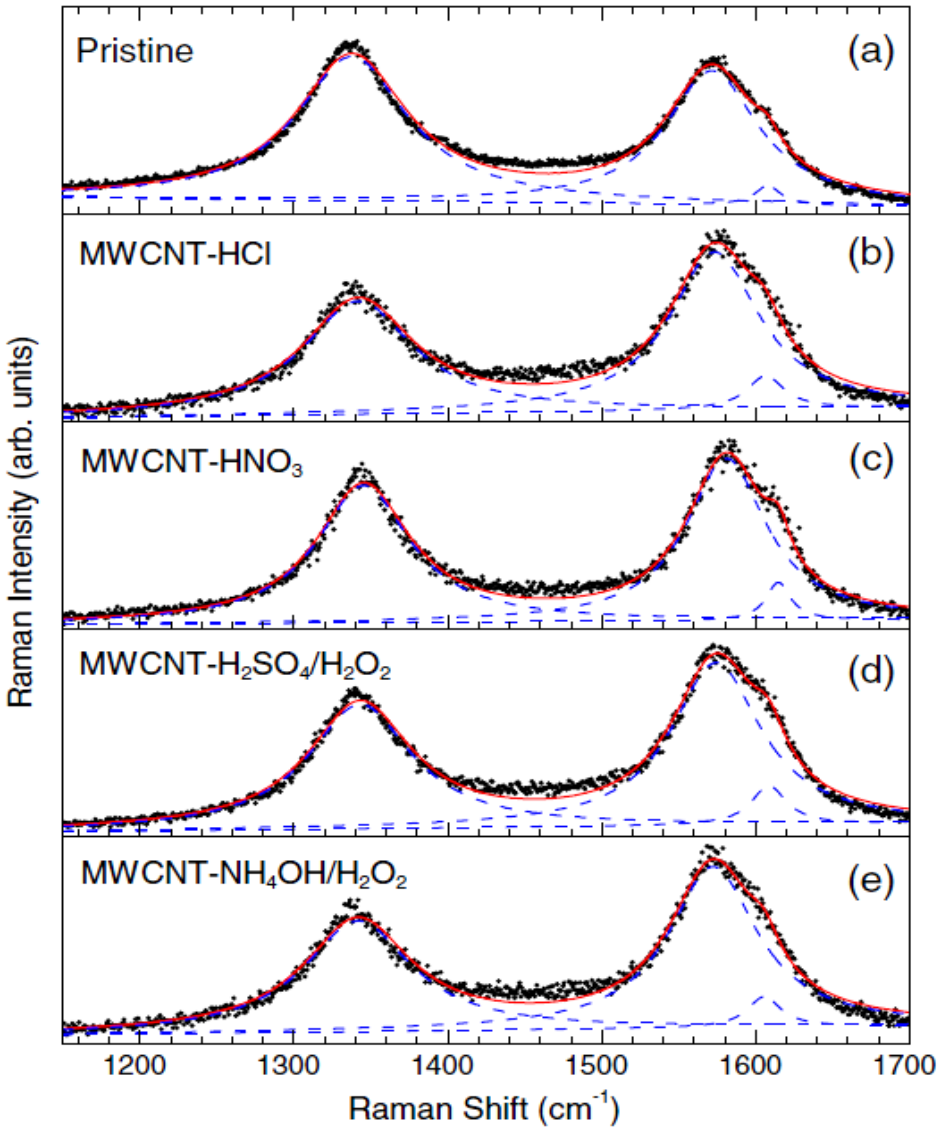

Figure 2-52: *Raman spectra of MWCNT samples after treatment with different agents* [102].

Another study, which has been done by E. Borowiak-Palen et al. (2009) [103], completes the results of previous mentioned study. In this study, MWCNT batches were exposure in H_2SO_4, HNO_3 and HCl solution between 0.17 h and 720 h. Figure 2-53 shows Raman spectra related to the MWCNT samples after acid treatment. According to this figure, the G and D bands are shifted clearly. This shift is depended on the type of acid. In addition, acid treatment time is directly influencing on the intensity of peaks. [103]

The I_G/I_D ratio in the Raman spectrum presents relative sample purity. Figure 2-54 represents I_G/I_D ratios versus acid treatment time related to E. Borowiak-Palen et al. (2009) [103] research. The I_G/I_D ratio gives information about the amount of defects on CNTs surface. Practically, D band located around 1300 cm^{-1} represents sp^3 carbons (orbital configuration of defects and disorders) and G band settled around 1600 cm^{-1} shows sp^2 carbons. [103,105]

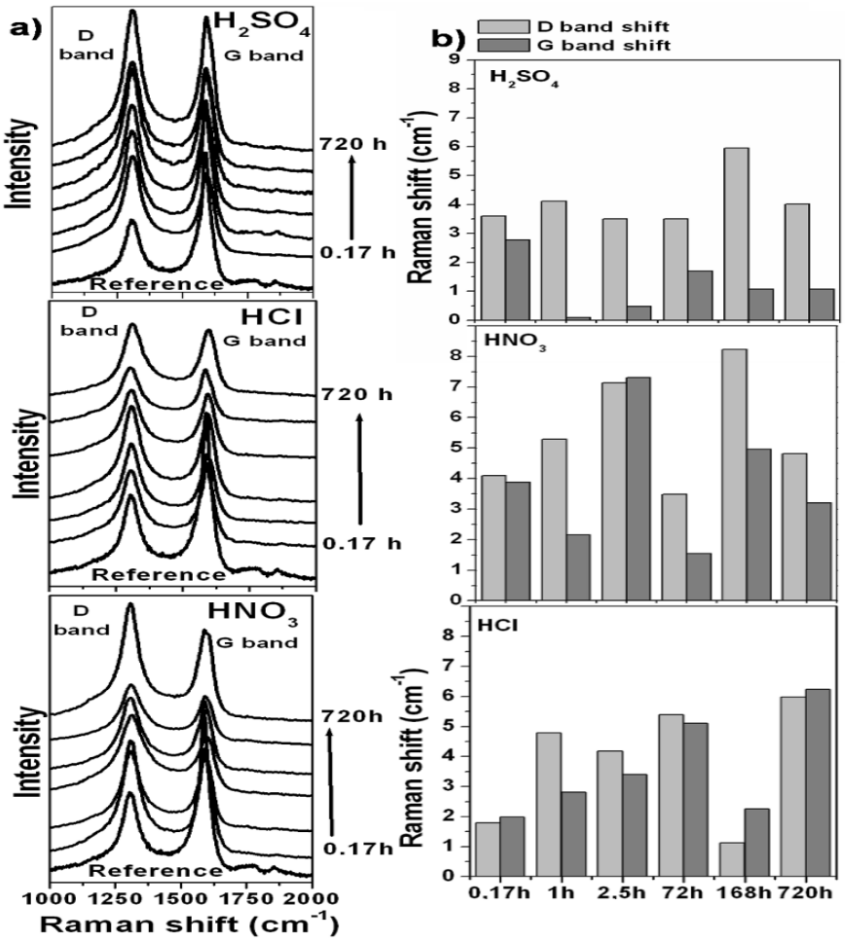

Figure 2-53: *Raman spectra of the MWCNT treated by H_2SO_4, HNO_3 and HCl acids* [103].

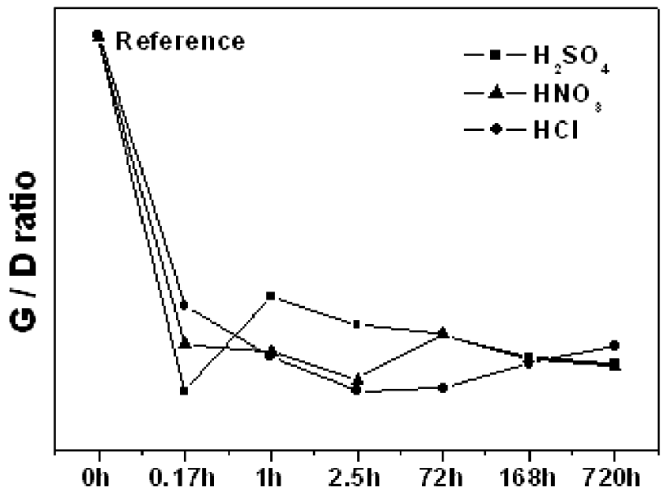

Figure 2-54: *The I_G/I_D ratios of different CNTs functionalized in different mediums and acid treatment times* [103].

3. EXPERIMENTAL

This chapter introduces experimental work related to current thesis in three main sections. They are including materials, processing and characterization. Figure 3-1 presents whole structure of this chapter schematically.

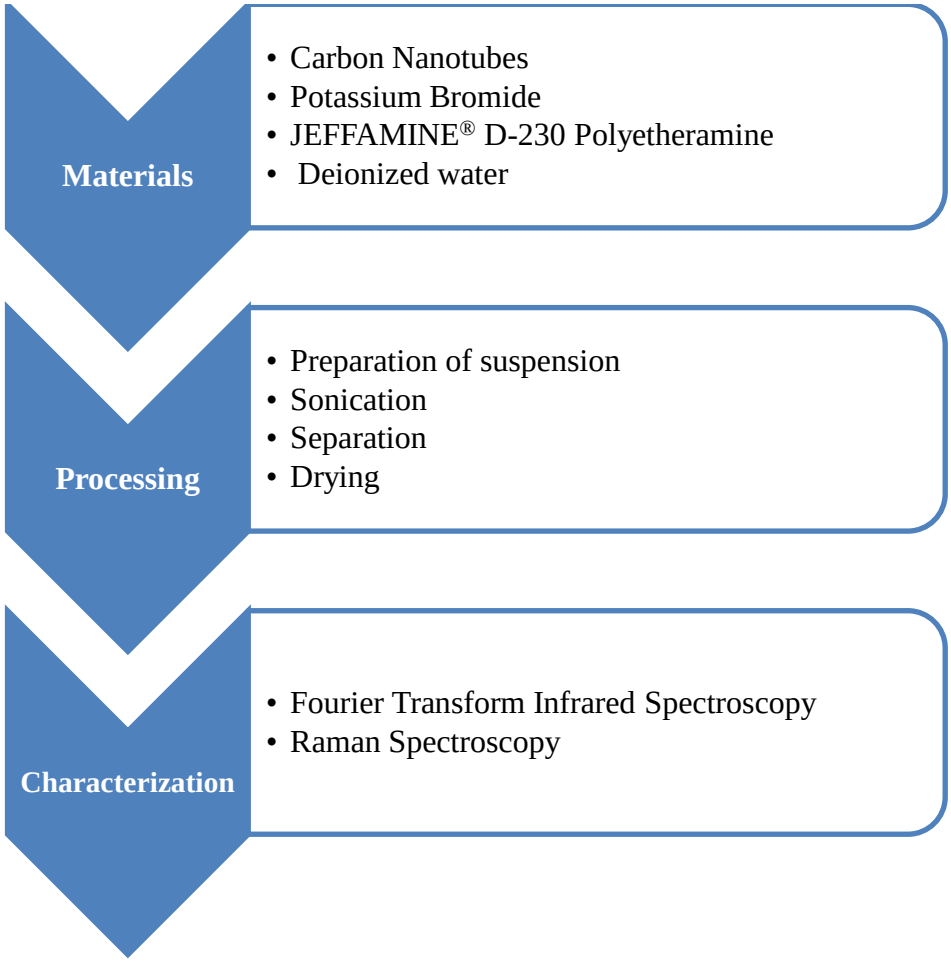

Figure 3-1: *The whole structure of experimental chapter.*

The first section explains different raw materials which are used in practical work. The second section describes whole process and instruments which are involved in each step. Finally, last section which is most important section, describes characterization methods and devices that are used in the current study.

3.1 Materials

In this section, different raw materials which are used during current study are discussed. Chemical formula and structure, properties, and commercial brand of used raw materials are explained during this section.

- **Carbon Nanotube**

In the current study, NANOCYL™ NC7000 carbon nanotubes (CNTs) are used. They are thin multi-wall carbon nanotubes produced by catalytic carbon vapor deposition (CCVD) process. Figure 3-2 shows NC7000 by naked eye and transmission electron microscope (TEM) view. Also table 3-1 explains properties of NC7000 CNTs [106].

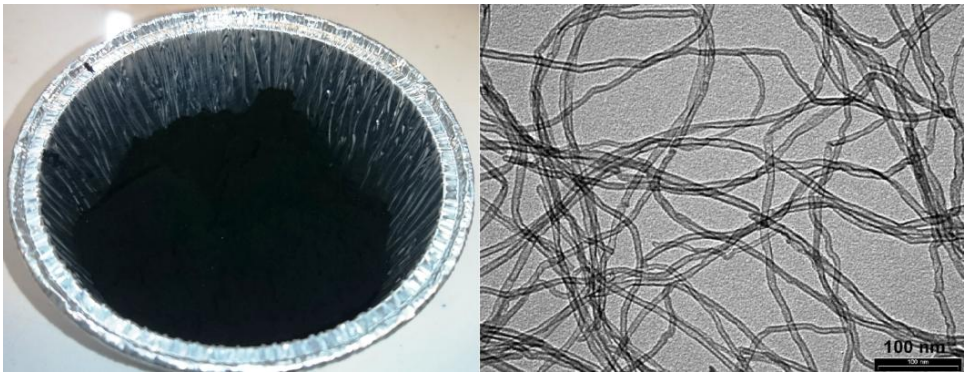

Figure 3-2: *NC7000 CNT, naked eye and TEM view.*

Table 3-1: *Important chemical and physical properties of NC7000 [106].*

Property	Value	Unit
Average Diameter	9.5	nanometers
Average Length	1.5	micron
Surface Area	250-300	m^2/g
Carbon Purity	90	%
Metal Oxide	10	%

- **Potassium Bromide**

In this research, Uvasol® potassium bromide (KBr) is used. It is produced by Merck Co. for using in IR spectroscopy specifically. Potassium bromide (KBr) is not IR-active and it is used as a transparent material in IR spectroscopy. Figure 3-3 presents chemical structure and naked eye view of this component.

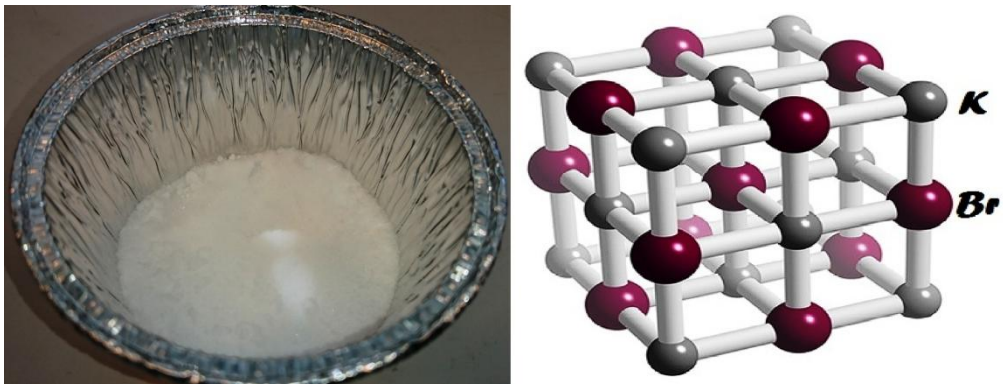

Figure 3-3: *Uvasol® potassium bromide, chemical structure and naked eye view.*

- **Jeffamine® D-230 Polyetheramine**

Jeffamine D-230 polyetheramine is known by repeating oxypropylene units in the backbone. As figure 3-4 represents, Jeffamine D-230 polyetheramine (JD230) is a difunctional, primary amine with an average molecular weight of about 230. The primary amine groups are located on secondary carbon atoms at the end of the aliphatic polyether chain. Table 3-2 also describes some properties of this organic liquid. [107]

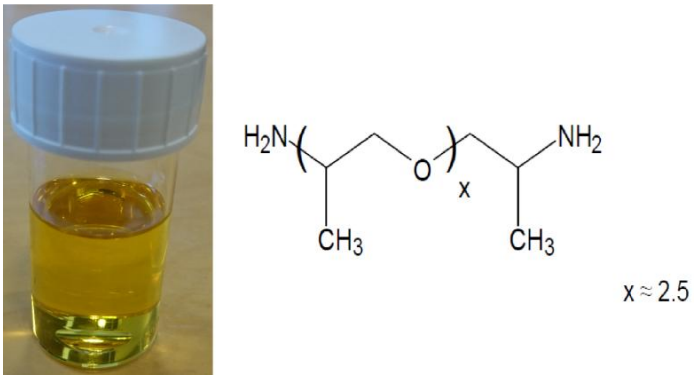

Figure 3-4: *Jeffamine D-230 Polyetheramine, chemical structure and naked eye view.*

Table 3-2: *Chemical and physical properties of JD230 [107].*

Property	Value	Unit
Chemical Analysis		
Primary amine, % total amine	97 (Min)	%
Total acetylatables	8.3 – 9.1	meq/g
Total amine	8.1 – 8.7	meq/g
Total amine, % acetylatables	94 min	%
Water	0.20 max	wt%
AHEW (Amine hydrogen equivalent wt.)	60	g/eq
Equivalent wt. with isocyanates	120	g/eq

Table 3-2: *Chemical and physical properties of JD230 [107].*

Property	Value	Unit
Viscosity (25˚C)	9.5	cSt
Density (25˚C)	0.948	g/ml
Flash point	121	°C
pH	11.7	-
Refractive index	1.4466	-

3.2 Processing

In this project, at the first place, 10 suspensions of JD230-CNT and 11 suspensions of DIW-CNT with constant ratio are prepared. In the second step, each sample is sonicated for specific time and by unique energy. In the third step sonicated CNTs are separated from liquid phase by helping Büchner funnel, filter paper, and vacuum pump. At the end, remained powder is dried by drier. After this process, samples are ready for characterization.

3.2.1 Preparation of suspension

As mentioned 10 suspensions of JD230-CNT and 11 suspensions of DIW-CNT with constant ratio of 0.25 % for sonication step are prepared. Figure 3-5 shows these suspensions. Also tables 3-3 and 3-4 show information related to JD230-CNT and DIW-CNT suspension respectively. In these tables, JD230-CNT samples are named as J_n. This symbol presents JD230-CNT sample sonicated by n KJ energy. For DIW-CNT samples, naming is based on the time of sonication where W_n symbol presents DIW-CNT sample sonicated for n min.

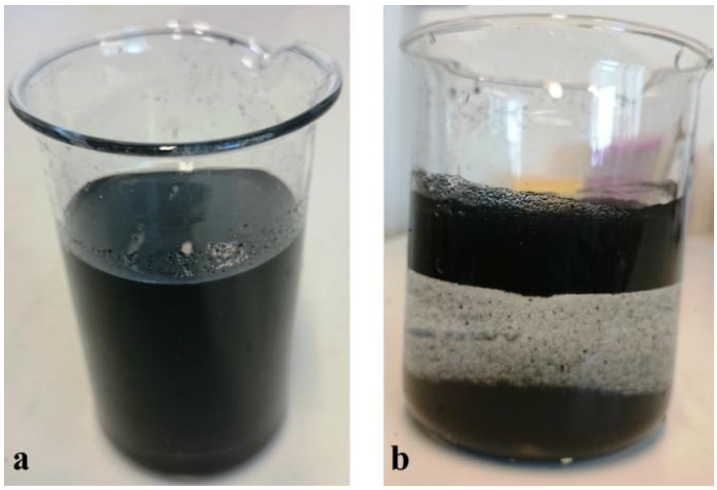

Figure 3-5: *JD230-CNT (a) and DIW-CNT(b) suspensions.*

Table 3-3: *Information related to suspension preparation of JD230-CNT samples.*

Sample Name	Volume of JD230 (ml)	Mass of JD230 (gr)	Mass of CNT (gr)	$(m_{CNT}/m_{JD230})\%$
J_0	80	71.098	0.177	0.25
J_{10}	80	71.043	0.177	0.25
J_{20}	80	71.055	0.177	0.25
J_{30}	80	71.076	0.177	0.25
J_{40}	80	71.070	0.177	0.25
J_{50}	80	71.081	0.177	0.25
J_{60}	80	71.121	0.177	0.25
J_{70}	80	71.114	0.177	0.25
J_{80}	80	71.079	0.177	0.25
J_{90}	80	71.052	0.177	0.25

Table 3-4: *Information related to suspension preparation of DIW-CNT samples.*

Sample Name	Volume of DIW (ml)	Mass of DIW (gr)	Mass of CNT (gr)	$(m_{CNT}/m_{DIW})\%$
W_0	200	200.55	0.5042	0.25
W_4	200	20023	0.5070	0.25
W_5	200	200.47	0.5058	0.25
W_6	200	200.35	0.5051	0.25
W_8	200	200.63	0.5042	0.25
W_{10}	200	200.58	0.5054	0.25
W_{15}	200	200.51	0.5031	0.25
W_{20}	200	200.26	0.5096	0.25
W_{25}	200	200.73	0.5021	0.25
W_{30}	200	200.33	0.5054	0.25
W_{35}	200	200.89	0.5012	0.25

After preparing suspensions, samples are ready for sonication process which will be explained further.

3.2.2 Sonication

After preparing of suspension, sonication process is started. JD230-CNT suspensions are sonicated via 10-90 KJ energy and DIW-CNT suspensions are sonicated for 4-35 min according to tables 3-5 and 3-6 respectively. Also table 3-7 presents other parameters related to sonication that are fixed for all of the samples. Device used in current project for sonication process is 'QSonica- Q700' which is shown in figure 3-6.

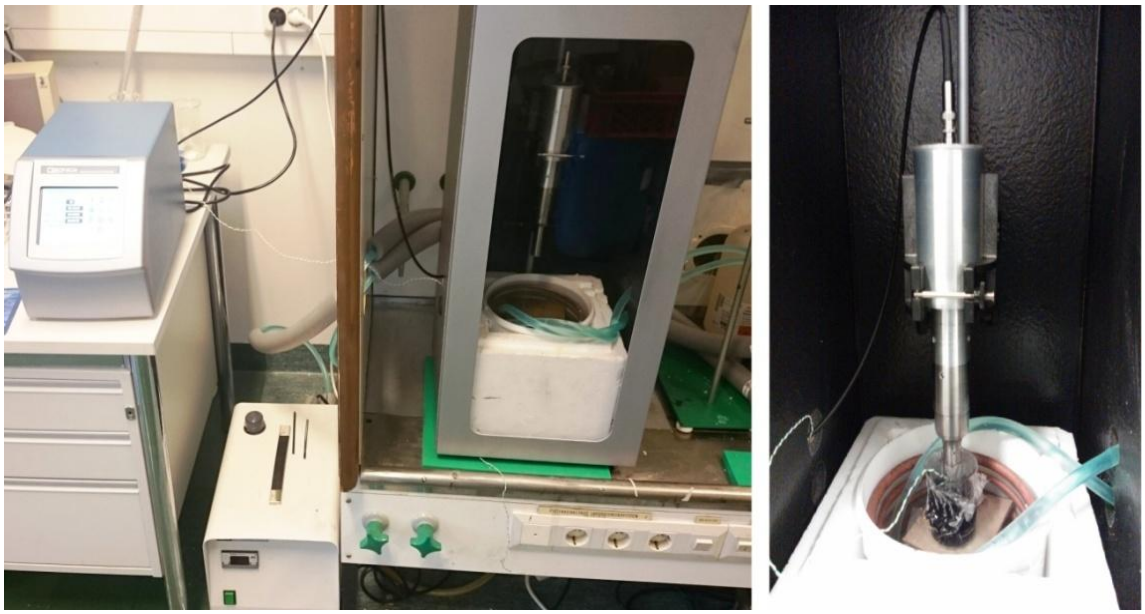

Figure 3-6: *QSonica- Q700 device.*

Table 3-5: *Information related to sonication of JD230-CNT samples.*

Sample Name	Sonication Energy (KJ)	Elapsed Time (min)	Sample Name	Sonication Energy (KJ)	Elapsed Time (min)
J_0	0	0	J_{50}	50.251	08:30
J_{10}	10.065	01:55	J_{60}	60.408	10:40
J_{20}	20.450	03:35	J_{70}	70.269	12:20
J_{30}	30.185	05:20	J_{80}	80.085	13:40
J_{40}	40.412	07:00	J_{90}	90.341	15:10

Table 3-6: *Information related to sonication of DIW-CNT samples.*

Sample Name	Sonication Energy (KJ)	Elapsed Time (min)	Sample Name	Sonication Energy (KJ)	Elapsed Time (min)
W_0	0	0	**W_{15}**	81.670	15
W_4	20.940	4	W_{20}	108.489	20
W_5	26.180	5	W_{25}	135.780	25
W_6	31.410	6	W_{30}	163.060	30
W_8	43.880	8	W_{35}	191.241	35
W_{10}	54.850	10			

Figures 3-7 and 3-8 show appearance of J_n and W_n series samples after sonication process.

Table 3-7: *Sonication parameters fixed for all of the samples.*

Amplitude	100
Temperature (Max)	70˚C (For J_n series samples)
	50˚C (For W_n series samples)
Pulse (t_1)	5 s
Pulse (t_2)	10 s

Figure 3-7: *Appearance of J_n series samples after sonication*

Figure 3-8: *Appearance of W_n series samples after sonication*

3.2.3 Separation

In the next step, CNT sonicated should be separated from liquid part. For achieving to this target, according to figure 3-9, a simple filtration system including Büchner funnel, porous plate, filter paper, Büchner flask, and vacuum pump (Vacuubrand-RE2) is used.

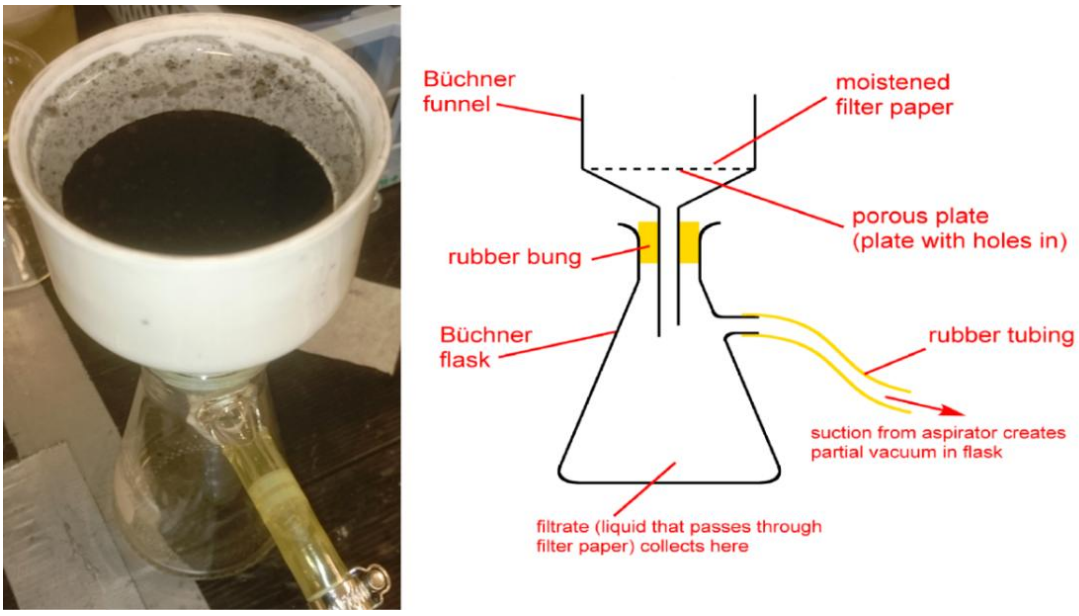

Figure 3-9: *Filtration system* [109].

For J_n series samples, after separation of liquid part, for removing JD230 completely, samples are washed by 500 cc water in the Büchner filtration system. Water can solve all of the JD230 remained in the sample according to following reaction [110].

$$RNH_2 + H_2O \longrightarrow RNH_3^+ + OH^-$$

Figure 3-10 shows samples sonicated after separation.

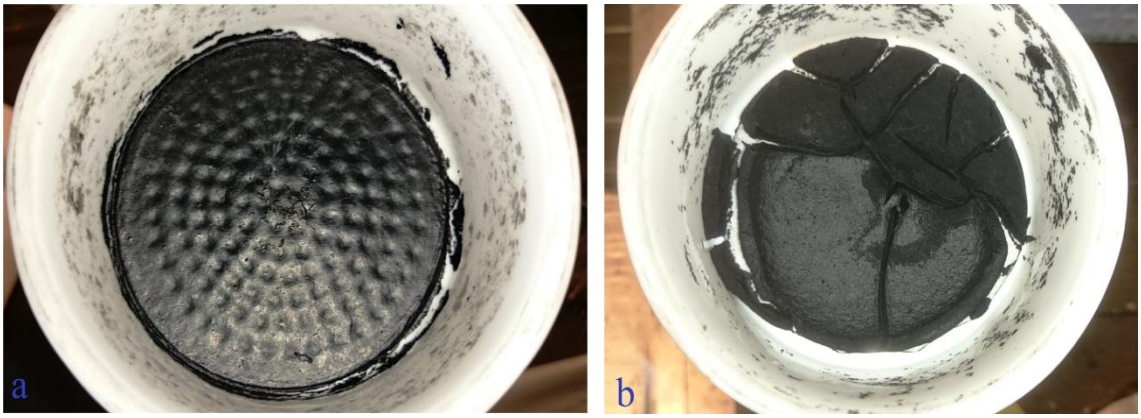

Figure 3-10: *Samples sonicated in the JD230 (a), and DIW (b), after separation step.*

3.2.4 Drying

Finally, at the last step of processing stage, for exiting non-bonded water, samples are dried at 50˚C for 4-5 hrs by 'Termaks - TS 8136' dryer (Figure 3-11). Also figure 3-12 shows samples after drying.

Figure 3-11: *Termaks - TS 8136 dryer.*

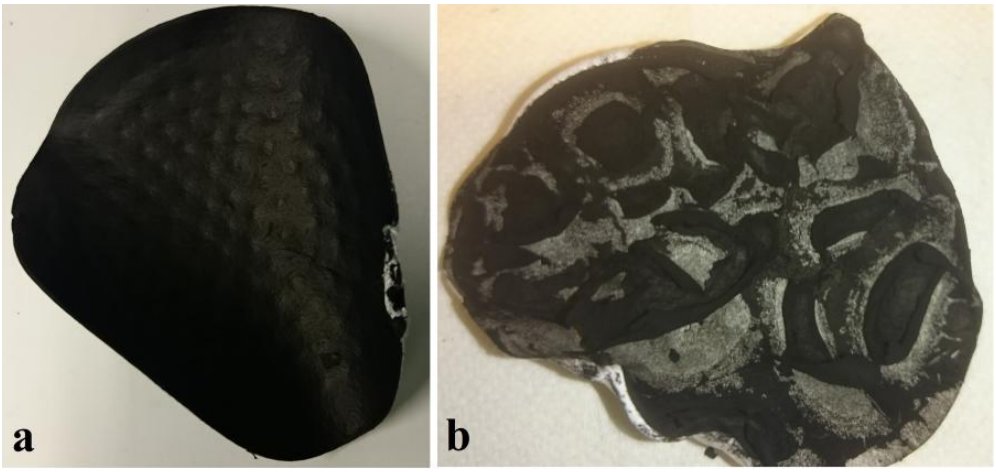

Figure 3-12: *CNTs sonicated in the JD230 (a), and DIW (b), after drying.*

3.3 Characterization

Current project studies functional groups formed on the surface of CNTs due to sonication process and relationship of amount of theses functional groups with sonication time. For achieving to this target, FTIR-ATR spectroscopy is used for characterization of functional groups on the CNTs. Also Raman Spectroscopy is used for studying effect of sonication on the surficial defects of the CNTs.

3.3.1 Characterization by Fourier Transform Infrared (FTIR) Spectroscopy

In this step, characterization of functional groups is defined as target. In the first place, JD230 and DIW are characterized by FTIR-ATR (BRUKER-TENSOR 27) device (Fig-

ure 3-13). Prism which is used for these measurements is diamond introduced in table 3-8. Also, table 3-9 presents spectroscopic parameters related to measurements by BRUKER-TENSOR 27 device.

Figure 3-13: *FTIR-ATR (BRUKER-TENSOR 27) device.*

Table 3-8: *Properties of diamond prism of BRUKER-TENSOR 27 device.*

Prism	Spectral Region (cm^{-1})	Refractive Index	Depth of Penetration at 45°, 1000 cm^{-1} (µm)
Diamond	45,000-10	2.42	1.66

Table 3-9: *Spectroscopic parameters of measurements by BRUKER-TENSOR 27.*

Number of Sample Scans	Resolution (cm^{-1})	Background Channel
64	4.0	Air, 64 scans

In the next step, for IR spectroscopy of CNT samples should be claimed that these measurements are not as easy as IR measurements of the liquids (JD230 and DIW). In the first place, mixture of the liquid (JD230) and pristine CNT without processing is selected for IR measurements by diamond-ATR (BRUKER-TENSOR 27) spectrometer. Table 3-10 shows combinations of this sample which is named JC (JD230-CNT).

Table 3-10: *Information of sample JC.*

12	Mass of Liquid (gr)	Mass of CNT (gr)	% CNT (wt)	Comments
JC	1.6 (JD230)	0.4	20	Non-processed

Figure 3-14 shows Diamond-ATR spectrum of sample JC by BRUKER-TENSOR 27 spectrometer. According to figure 3-14, high absorption of radiation by CNT and high noise-to-signal ratio (N/S) lead to produce an uninterpretable spectrum. For solving this problem, according to what was claimed in the previous chapter (Section 2.4.1), two strategies are fallowed. First, KBr powder as a transparent material is mixed with CNT

samples and second, diamond prism is changed to diamond - zinc selenide (Di/ZnSe) prism.

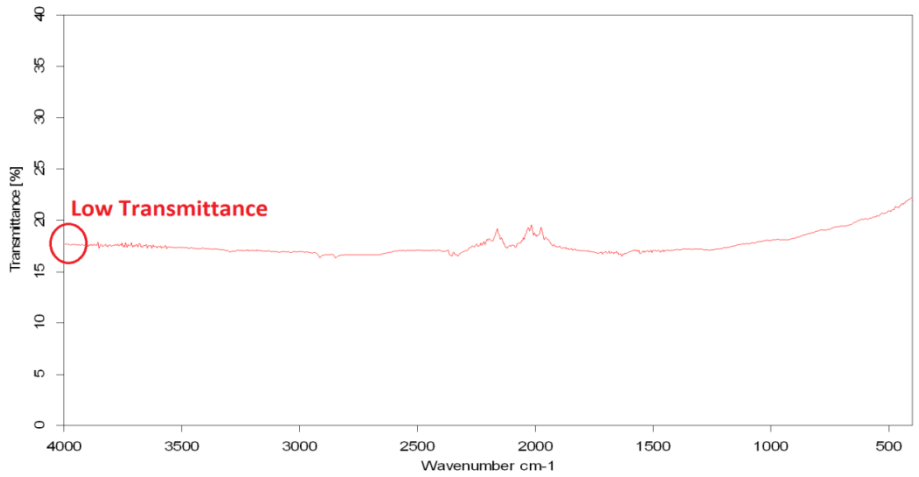

Figure 3-14: *Diamond-ATR spectrum of sample JC by BRUKER-TENSOR 27.*

As mentioned before, KBr is not IR active. So, for optimization of CNT/KBr ratio, different percentages of (m_{CNT}/m_{KBr}) according to figure 3-15 are tested.

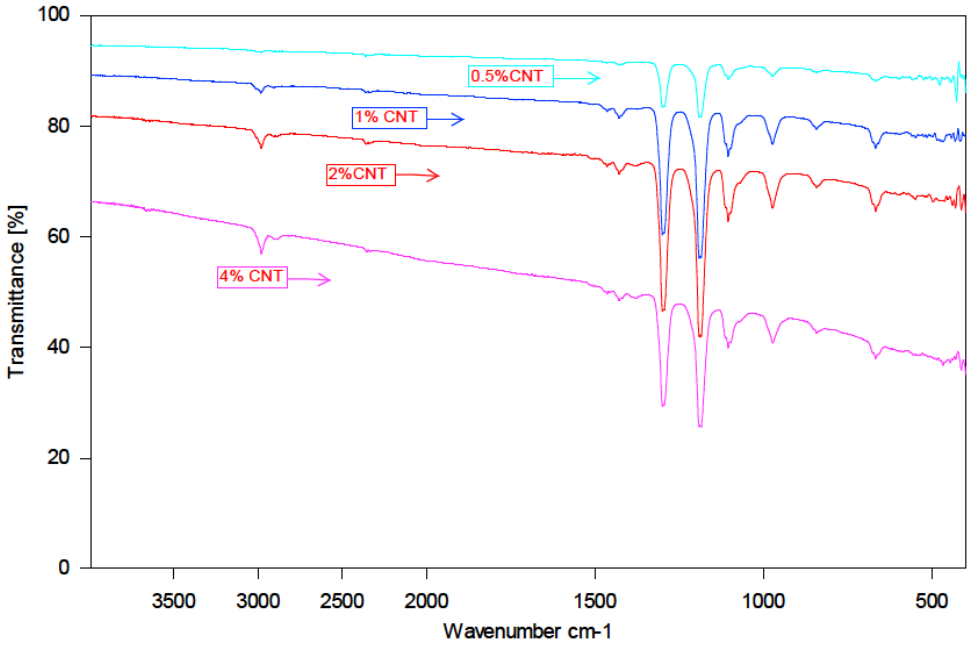

Figure 3-15: *IR spectra of the CNT/KBr samples with different ratios.*

With regarding to amount of absorption for different spectra in figure 3-15, percentage of (m_{CNT}/m_{KBr}) is optimized to 1%.

Also in continuation of improving S/N ratio strategy, for IR spectroscopy of CNT samples, Di/ZnSe-ATR (Perkin-Elmer Spectrum One) device (Figure 3-17 is used. Tables 3-11 and 3-15 represent properties of used Di/ZnSe prism and spectroscopic parameters of measurements respectively.

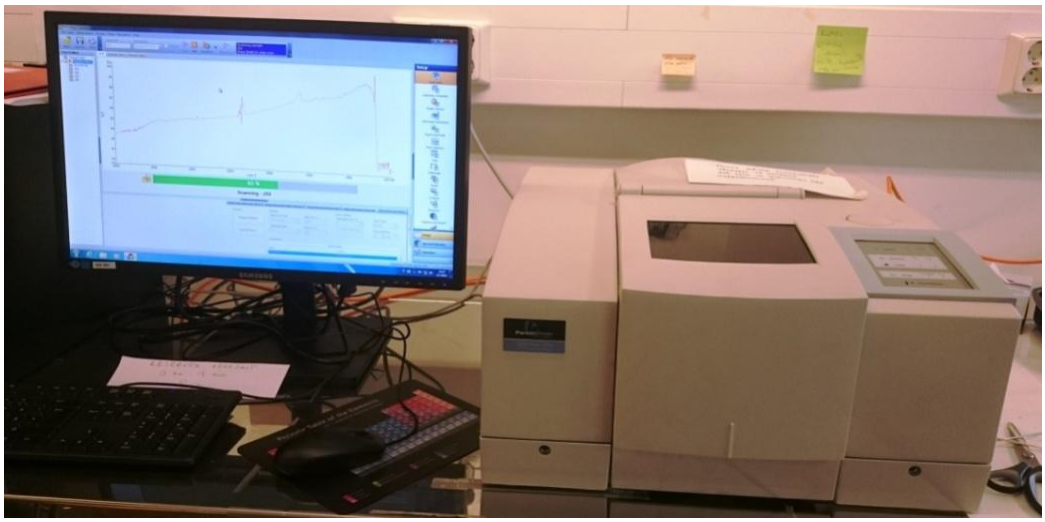

Figure 3-16: *FTIR-ATR (Perkin-Elmer Spectrum One) device*

Table 3-11: *Properties of Di/ZnSe prism of 'Perkin-Elmer Spectrum One' device.*

Prism	Refractive Index	Depth of Penetration at 45°, 1000 cm^{-1} (µm)
Di/ZnSe	2.4	2.0

Table 3-12: *Spectroscopic parameters of measurements by 'Perkin-Elmer Spectrum One' device.*

12	Resolution (cm^{-1})	Background Channel
64	4.0	Air, 64 scans

So based on the mentioned ratio, before IR measurements, sample preparation is done. In this stage, IR samples are prepared with considering 1% ratio for (m_{CNT}/m_{KBr}) according to tables 3-13 to 3-15. In sample preparation step most important point is uniformity of CNT/KBr mixture, because it affects on the IR absorption. Favorable uniformity is provided by crashing CNT samples/KBr mixture according to figure 3-17.

Figure 3-17: *IR-ATR sample preparation of functionalized CNT samples.*

Table 3-13: *Information of IR-ATR sample preparation for non-processed specimens.*

Sample Name	Mass of CNT (gr)	Mass of KBr (gr)	$(m_{CNT}/m_{KBr})\%$
Pristine CNT	0.0029	0.2933	1
JC	0.0080	0.8000	1

Table 3-14: *Information of IR-ATR sample preparation for the specimens sonicated in the JD230.*

Sample Name	Mass of CNT (gr)	Mass of KBr (gr)	$(m_{CNT}/m_{KBr})\%$
J_0	0.0039	0.3968	1
J_{10}	0.0056	0.5632	1
J_{20}	0.0038	0.3877	1
J_{30}	0.0033	0.3343	1
J_{40}	0.0038	0.3801	1
J_{50}	0.0034	0.3489	1
J_{60}	0.0039	0.3912	1
J_{70}	0.0048	0.4882	1
J_{80}	0.0037	0.3747	1
J_{90}	0.0030	0.3098	1

Table 3-15: *Information of IR-ATR sample preparation for the specimens sonicated in the DIW.*

Sample Name	Mass of CNT (gr)	Mass of KBr (gr)	$(m_{CNT}/m_{KBr})\%$
W_0	0.0048	0.4828	1
W_5	0.0030	0.3085	1
W_{10}	0.0045	0.4519	1
W_{15}	0.0035	0.3534	1
W_{20}	0.0033	0.3368	1
W_{25}	0.0040	0.4000	1
W_{30}	0.0045	0.4500	1
W_{35}	0.0036	0.3606	1

3.3.2 Characterization by Raman Spectroscopy

In the current study, Raman spectroscopy is used as a complementary test for justifying results obtained by IR spectroscopy. Relationship between sonication time, concentration of functional groups and defects which are created on the CNT suface would be significant point for this study. Hence Raman spectroscopy is employed for studding effect of sonication on the amount of defects on the surface of CNTs. For achieving to

this target, 5 samples (Sonicated and non-sonicated) are selected for Raman spectroscopy test. Table 3-16 represents features of the tests for samples W_0, W_4, W_6, W_8 and W_{10} by "RAMAN Imaging System WITEC alpha300R" device (Figure 3-18).

Table 3-16: *Features of the Raman spectroscopy tests.*

Laser Wavelength	Laser Power	Magnification of Objective Lens	Integration Time	Accumulations
532 nm	1 mW	20x	0.5 s	500

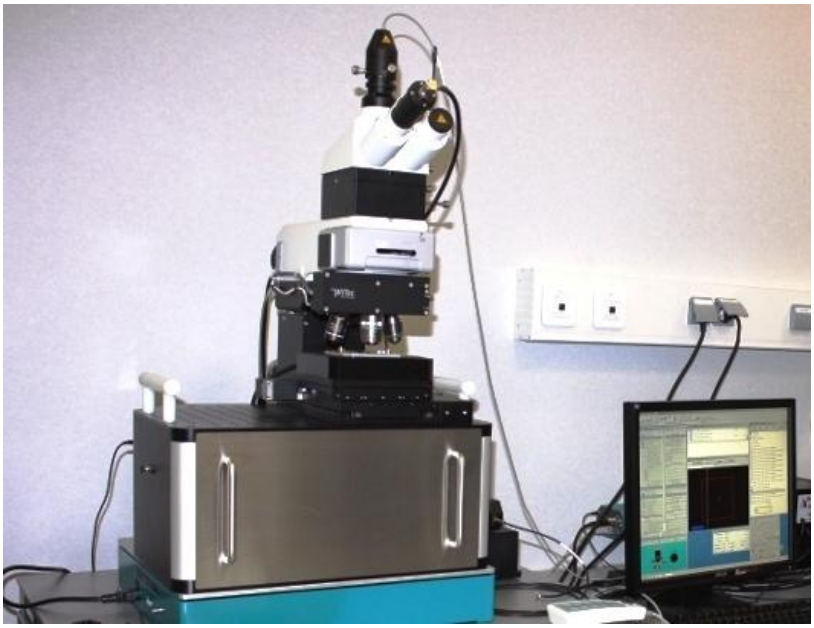

Figure 3-18: *RAMAN Imaging System WITEC alpha300R* [111].

4. RESULTS AND DISCUSSION

This chapter includes three sections. In the first section, raw materials are studied by FTIR. The second part considers study of CNTs sonicated in DIW. This part try to explain effect of sonication process on the surface chemistry of CNTs interacted with DIW by helping FTIR (Qualitative and quantitative analyses), and Raman spectroscopy. Third part follows same target but while medium in changed to JD230.

4.1 Study of Raw Materials

For characterization of functional groups formed on the CNTs due to sonication process, characterization of used raw materials and non-processed mixture of CNTs and liquid part is required. Figures 4-1 to 4-5 show IR spectra of these samples. Also tables 4-1 to 4-4 present qualitative analyses of these spectra (IR absorptions by frequency regions table is attached as 'Appendix A' [112]).

First spectrum (Figure 4-1) is belonged to KBr, the transparent material which all of the samples are including it. This graph shows used KBR enjoy high purity. Based on figure 4-1, it can be claimed that in the next spectra, all of the peaks come from just CNTs (Not KBr part).

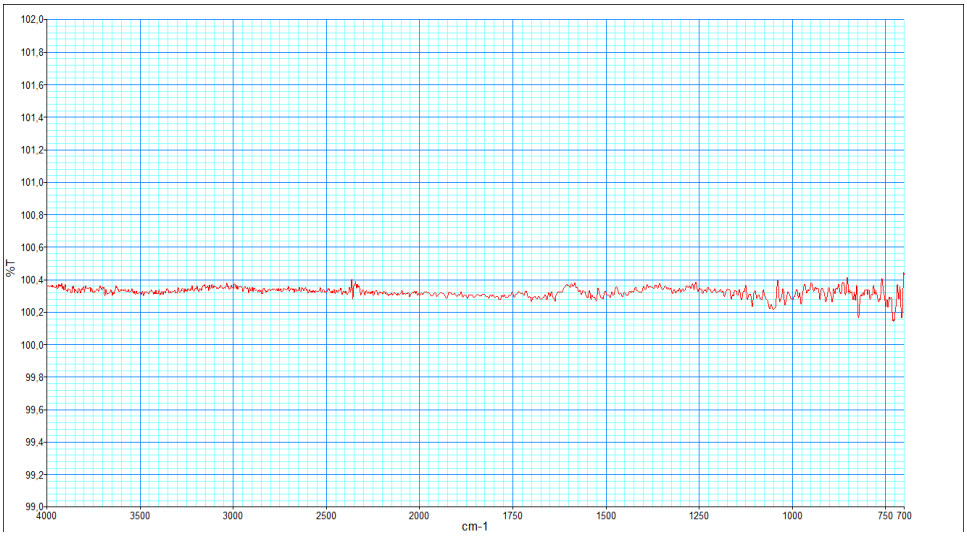

Figure 4-1: *IR spectrum of used KBr*

Figure 4-2 represents IR spectrum of pristine CNT. As it is cleared, Pristine CNT is also including some functional groups.

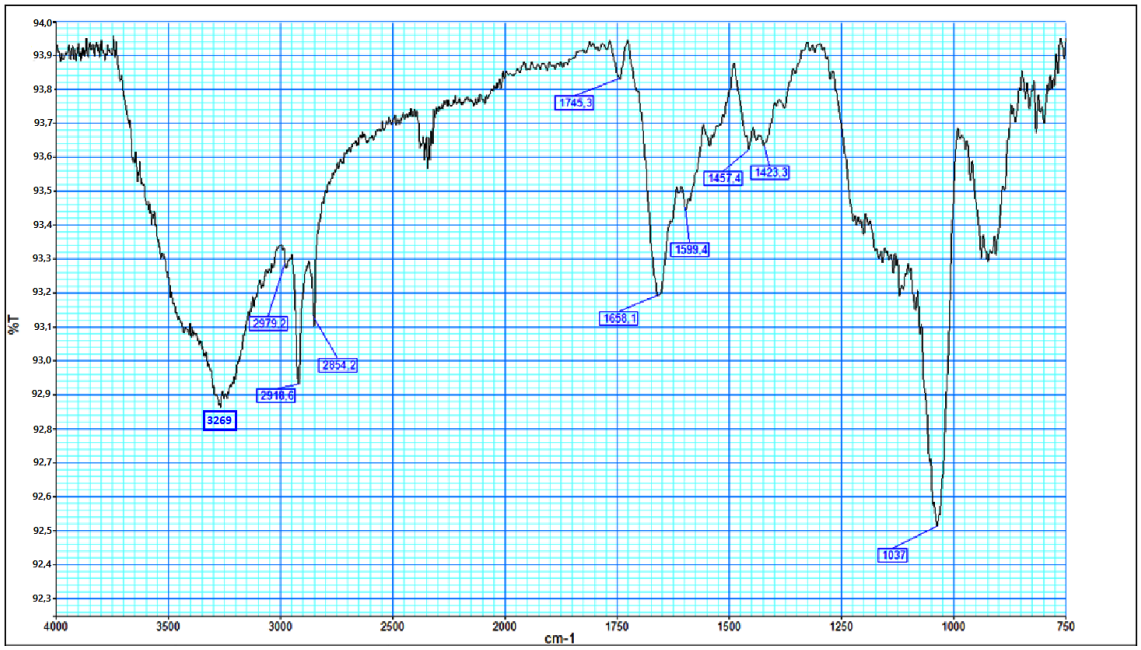

Figure 4-2: *IR spectrum of pristine CNT (NANOCYLTM NC7000).*

Table 4-1 represents qualitative analysis of IR spectrum of pristine CNT. This table shows each peak comes from which bond.

Table 4-1: *Qualitative analysis of IR spectrum of pristine CNT (NANOCYLTM NC7000).*

Wavenumber (cm^{-1})	Bond	Vibration Mode
3269	O-H	Stretching
2979	C-H	Stretching
2918	C-H	Stretching
2854	C-H	Stretching
2300-2400 (A group of peaks)	O=C=O Carbon dioxide	Related to atmosphere
1745	COOH	Stretching
1658	C=C	Stretching
1500-1340	C-H groups	Bending
1037	CO-O-CO Anhydrides	Stretching
928	C=C	Bending

The peaks which come from region 2300-2400 are related to CO_2 of atmosphere. This region will be not studied. Further, Figures 4-3 and 4-4 show IR spectra of two liquids which are used in current study. Also tables 4-2 and 4-3 determine different bonds of these liquids according to spectra.

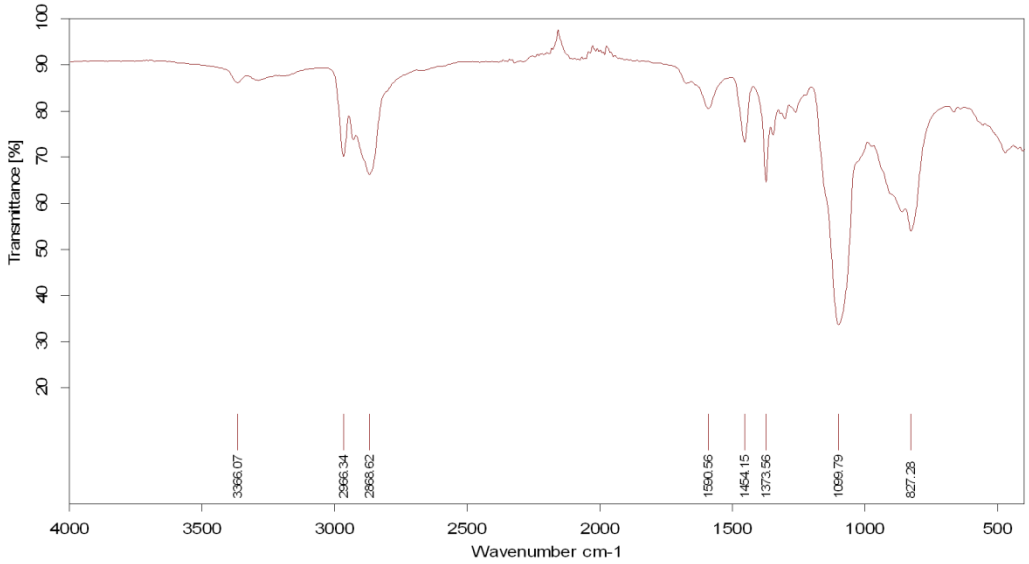

Figure 4-3: *IR spectrum of JD230.*

Table 4-2: *Qualitative analysis of IR spectrum of JD230.*

Wavenumber (cm^{-1})	Bond	Vibration Mode
3366	N-H	Stretching
2966	C-H	Stretching
2868	C-H	Stretching
1590	N-H	Bending
1454	C-H	Bending
1373	C-H	Bending
1099	C-O	Stretching
827	C-H	Bending

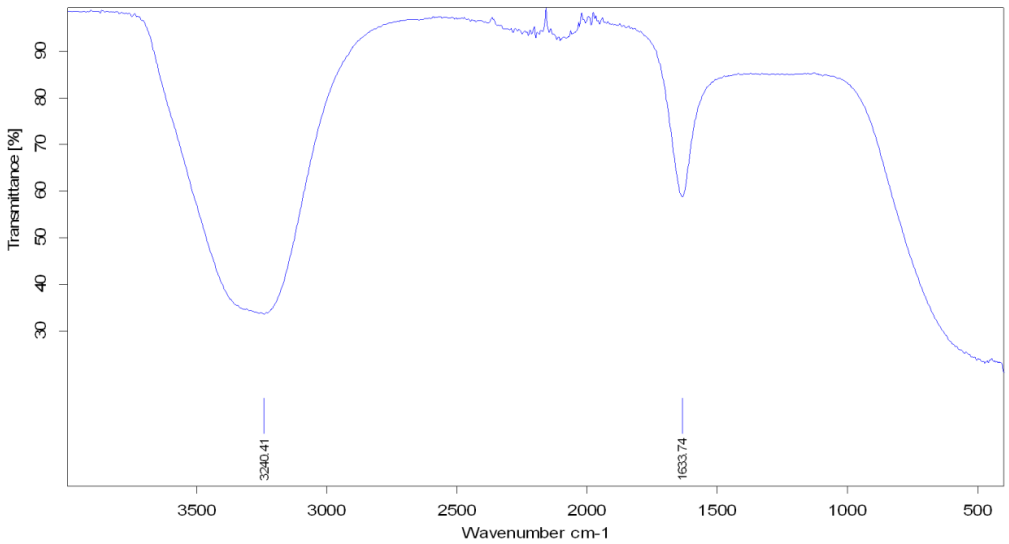

Figure 4-4: *IR spectrum of DIW.*

Table 4-3: *Qualitative analysis of IR spectrum of DIW.*

Wavenumber (cm^{-1})	Bond	Vibration Mode
3240	O-H	Stretching
1633	O-H	Bending

In continuation, what is important is study of bonds when CNTs and liquid (JD230) are mixed without sonication processing. Following figure shows spectrum of sample JC. As explained in the previous chapter, this sample is combination of pristine CNT and JD230 without sonication process (Ratio of mixing is available in the table 3-11).

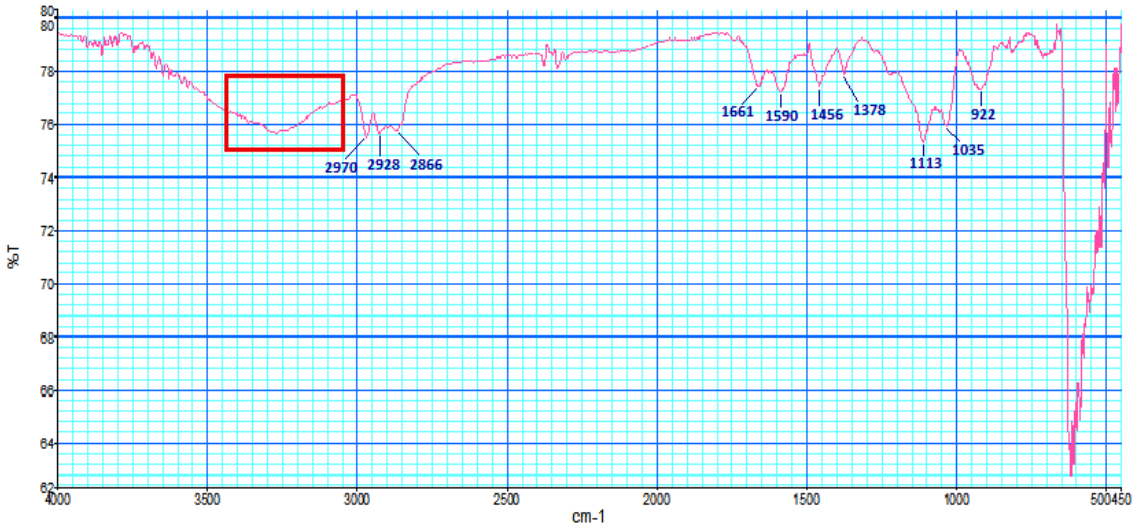

Figure 4-5: *IR spectrum of sample JC.*

Also table 4-4 represents qualitative analysis of JC spectrum which is presented by figure 4-5.

Table 4-4: *Qualitative analysis of IR spectrum of sample JC.*

Wavenumber (cm^{-1})	Bond	Vibration Mode
3400-3000	N-H and O-H groups	Stretching
2970	C-H	Stretching
2928	C-H	Stretching
2868	C-H	Stretching
1661	C=C	Stretching
1590	N-H	Bending
1456	C-H	Bending
1378	C-H	Bending
1113	C-O	Stretching
1035	CO-O-CO	Stretching
922	C=C	Bending
827	C-H	Bending

In the table 4-4, the peaks which come from JD230 are red and the peaks which come from pristine CNT are blue. Also in region 3000-3400, it may be an area resulted from overlapping different chemical groups including N-H and O-H bonds related to either CNTs surface or JD230.

4.2 Study of CNTs Sonicated in the DIW

This section makes most important discussion part of current study. In addition to discussion about interaction of water with CNTs, effect of sonication process on the structure and surface of CNTs will be explained by Raman spectroscopy results.

First of all, interaction of water with CNTs without soncation will be studied. Figure 4-6 shows spectrum of sample W_0. As mentioned in the "Experimental part", this sample passed all sample processing steps except sonication. So, sample W_0 is considered as reference sample for studying effect of sonication on W_n series samples.

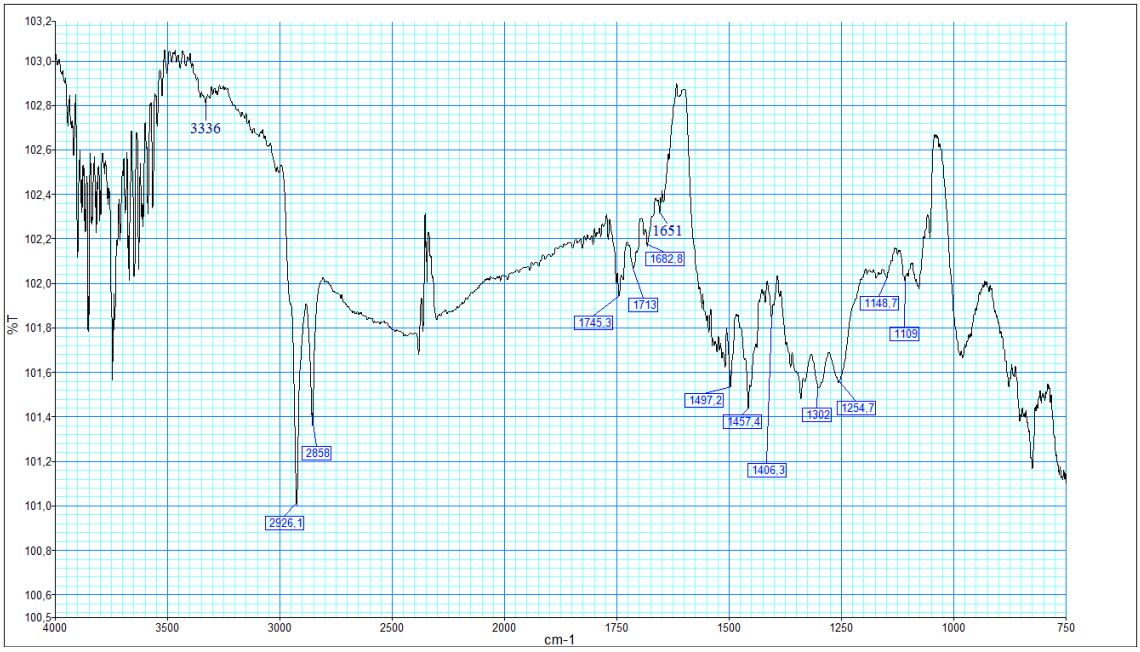

Figure 4-6: *IR spectrum of sample W_0.*

Comparison of spectrum related to sample W_0 with pristine CNT (Figure 4-2) reveals four important differences. Three new peaks are created and one strong peak is limited. Three new peaks located at 1713, 1651, and 1254 cm^{-1}, that are related to C=O, H-O-H and C-O bonds respectively, explain that mixing CNT and water leads to oxidation and hydration of CNT at room temperature (RT). Also the peak located at 1037 which is related to anhydrides is limited, because interaction of water with CNTs leads to solve anhydrides groups.

Table 4-5 represents qualitative analysis of spectrum of sample W_0.

Table 4-5: *Qualitative analysis of IR spectrum of sample W_0.*

Wavenumber (cm^{-1})	Bond	Vibration Mode
3336	O-H	Stretching
2926	C-H	Stretching
2858	C-H	Stretching
1745	COOH	Stretching
1713	C=O	Stretching
1651	H-O-H	Bending
1500-1340	C-H	Bending
1302	C-O	Stretching
1254	C-O	Stretching

So, oxidation and hydration are intrinsic effects of interaction of water with CNT. What follows is a study of effect of ultrasonic waves on this interaction. Figures 4-7 to 4-13 represent IR measurements of the CNT samples under sonication process between 5-35 min (or 21-191 KJ energy) in the water (DIW) medium.

According to these spectra, sonication of CNTs in DIW medium leads to two important events. At first, significant growth of the peak located around 1650 which is related to H-O-H (Bending mode) even by 5 min sonication, and in continuation, after 10 min sonication, a peak located around 1160 cm^{-1} which comes from C-O bond (Stretching mode) will be born and grown. These phenomena can be a symbol, the first sign for claiming that sonication leads to increase of oxidation and hydration on the CNTs surface.

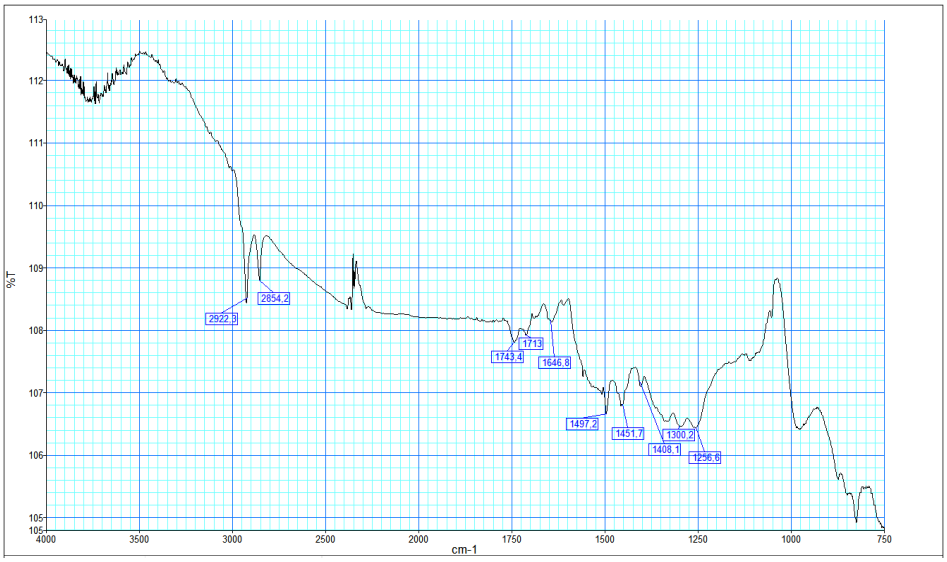

Figure 4-7: *IR spectrum of sample W_5.*

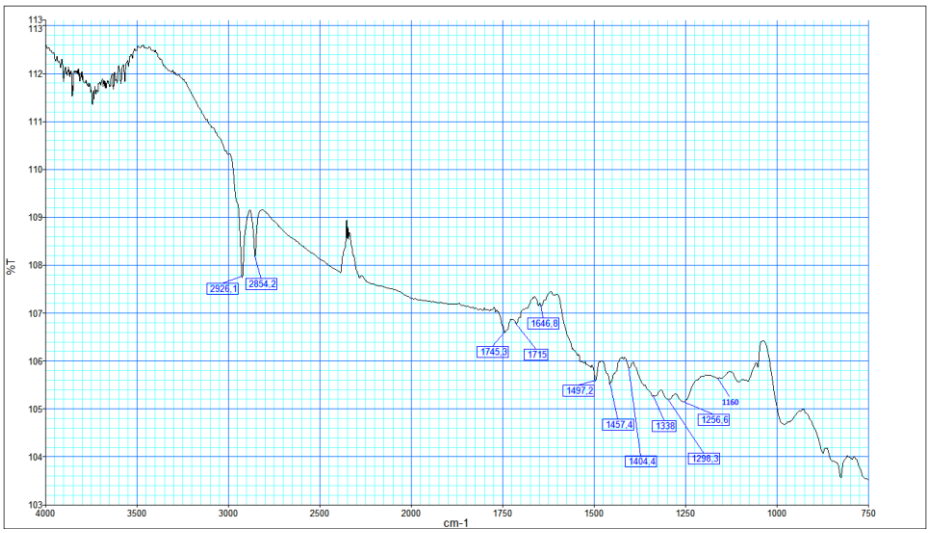

Figure 4-8: *IR spectrum of sample W_{10}.*

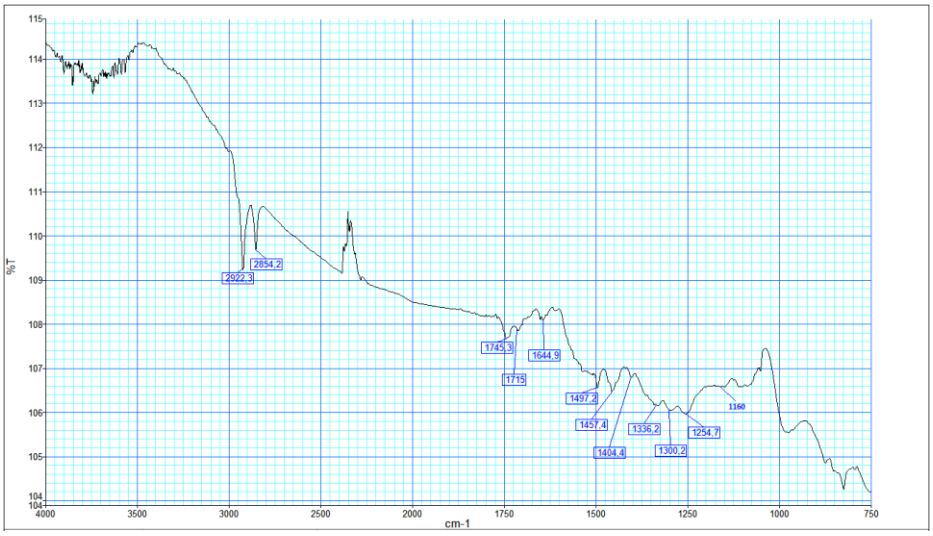

Figure 4-9: *IR spectrum of sample W_{15}.*

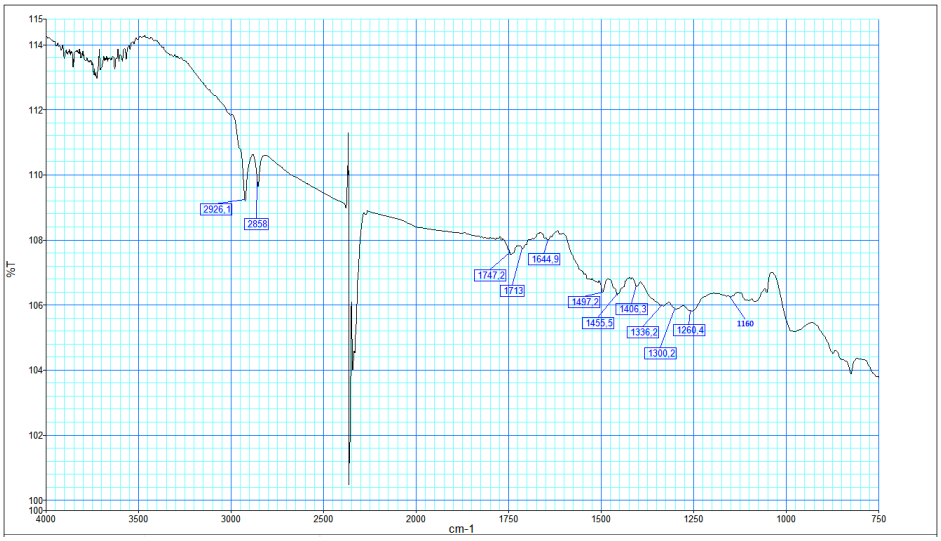

Figure 4-10: *IR spectrum of sample W_{20}.*

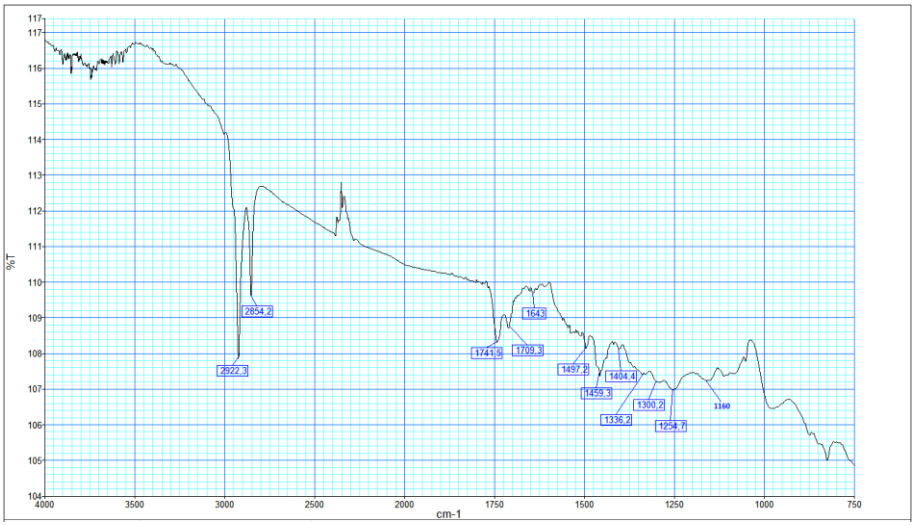

Figure 4-11: *IR spectrum of sample W_{25}.*

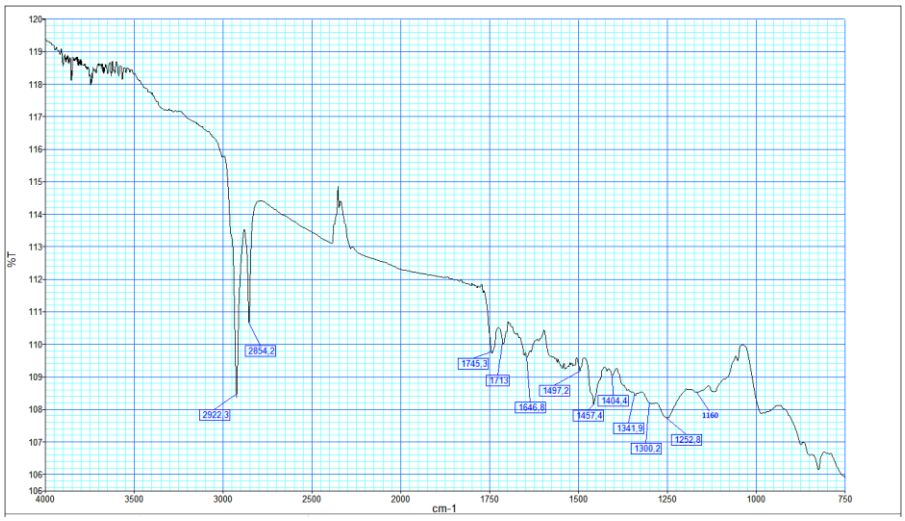

Figure 4-12: *IR spectrum of sample W_{30}.*

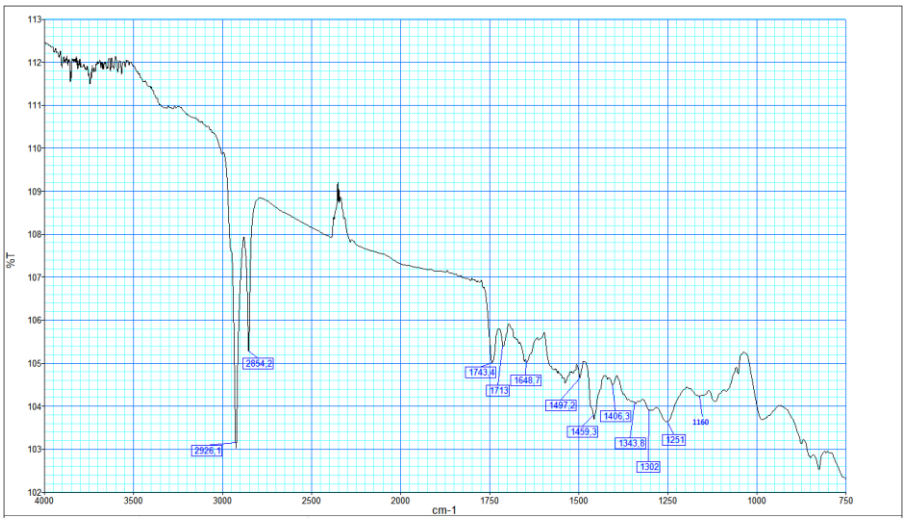

Figure 4-13: *IR spectrum of sample W_{35}.*

Table 4-6 compares IR investigations for three important samples W_0 (Non-sonicated), W_5 (Minimum sonication) and W_{35} (Maximum sonication).

Table 4-6: *Qualitative analysis of IR investigations related to samples W_0, W_5, and W_{35}*

Wavenumber (cm^{-1}) related to W_0	Wavenumber (cm^{-1}) related to W_5	Wavenumber (cm^{-1}) related to W_{35}	Bond	Vibration Mode
3336	3330	3330	O-H	Stretching
2926	2922	2926	C-H	Stretching
2858	2854	2858	C-H	Stretching
1745	1743	1743	COOH	Stretching
1713	1713	1713	C=O	Stretching
1651	1646	1648	H-O-H	Bending
1500-1340	1500-1340	1500-1340	C-H	Bending
1302	1300	1302	C-O	Stretching
1254	1256	1251	C-O	Stretching
1160	-	1160	C-O	Stretching

What follows is quantitative analysis of IR spectra for more precise study on the effect of sonication on concentration of functional groups located on CNTs surface. But beforehand, it must be emphasized that quantitative analysis while the powder sample is studied in the FTIR-ATR method, is not reliable. While size and geometry of particles which make sample are various and variable, due to change in reflection angles, intensity of the peaks is variable in different ATR measurements. Hence, in the current study, quantitative analysis is employed for achieving to a general view and understanding about effect of increasing time and energy of sonication on the functional groups.

The quantitative analyses are done based on the Beer-Lambert law according to

$$A = log\frac{I_0}{I} = \varepsilon cl,$$

(Equation 2-13). As mentioned in the chapter 2, the parameters I_0 and I can be obtained by tangential baseline method. Whereas, in this study, measurement of concentration is impossible directly, amount of the absorption (A) for each individual is calculated. According Beer-Lambert law (Equation 2-13),

$$A \sim c,$$

so changes in absorption show changes in concentration. Figure 4-14 explains measurement of absorption for C-H bond located at 2922 cm^{-1} in the spectrum of sample W_5 schematically. Also as a requirement for quantitative analysis, "**baseline correction**" operation is done for all spectra by software of FTIR device.

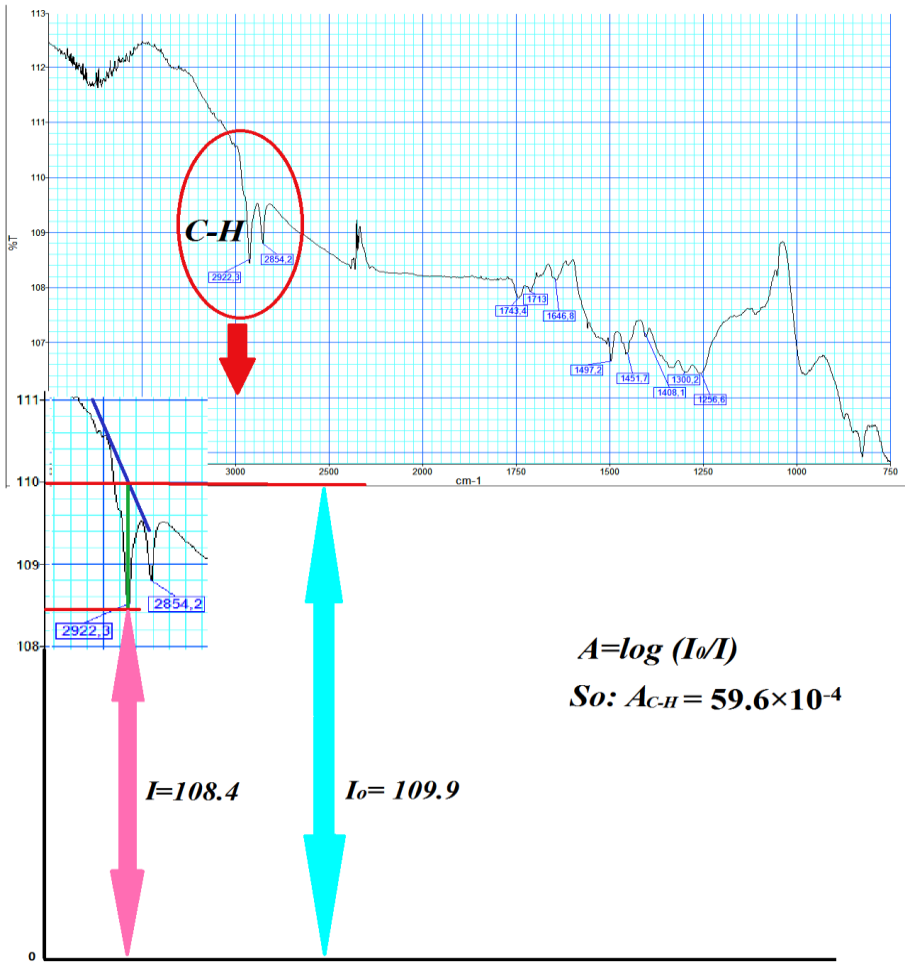

Figure 4-14: *Measurement of absorption for C-H bond located at 2922 cm^{-1} in the spectrum of sample W_5.*

Following figures (4-15 to 4-20) and tables (4-7 to 4-12) represent effect of increasing sonication time on concentration of functional groups on the CNTs interacted with DIW.

Table 4-7: *Changes of the absorption of O-H bond during increasing sonication time in the DIW medium.*

Sample Name	Peak Position (cm^{-1})	I_0	I	A
W_0	3336	102.94	102.81	5.4880×10^{-4}
W_5	~ 3330	112.10	111.98	4.6514×10^{-4}
W_{10}	~ 3330	112.20	112.08	4.6473×10^{-4}
W_{15}	~ 3330	113.92	113.80	4.5771×10^{-4}
W_{20}	~ 3330	113.86	113.68	6.8711×10^{-4}
W_{25}	~ 3330	116.30	116.13	6.3528×10^{-4}
W_{30}	~ 3330	117.50	117.20	11.1025×10^{-4}
W_{35}	~ 3330	111.22	110.95	10.5558×10^{-4}

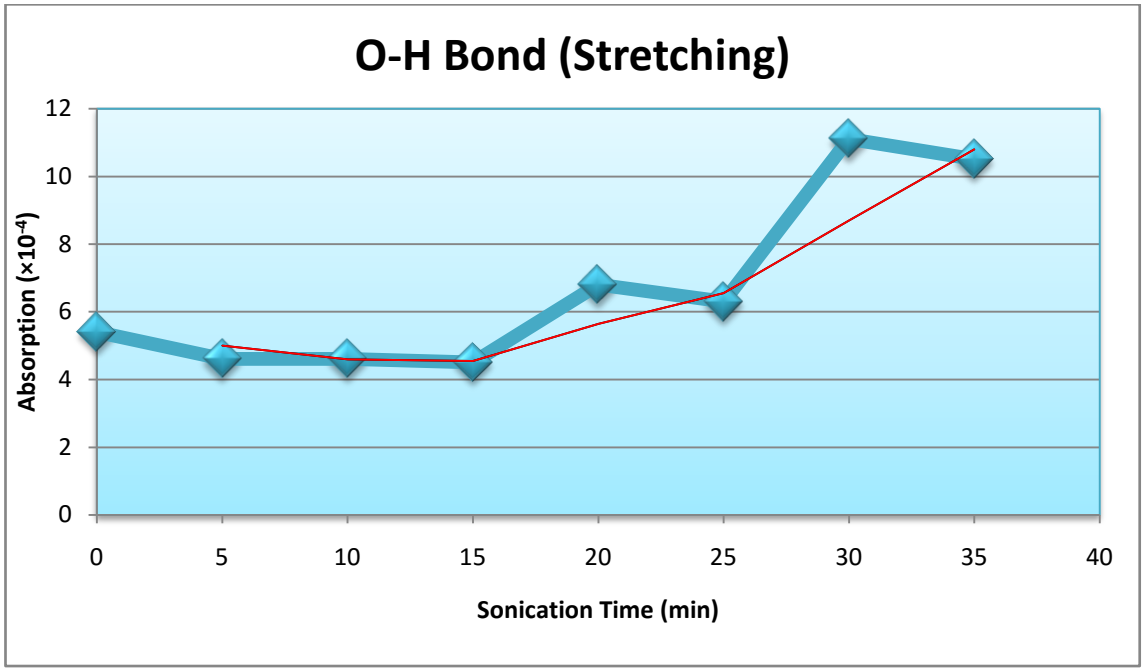

Figure 4-15: *Changes of the absorption of O-H bond during increasing sonication time in the DIW medium.*

In the each graph, moving average trend (Red line) is drawn. It gives better general view for better understanding curve trend.

Table 4-8: *Changes of the absorption of C-H bonds during increasing sonication time in the DIW medium.*

Sample	Peak Position (cm^{-1})	I_0	I	A	A_t
W_0	2926	102.10	101.00	47.043×10^{-4}	72.677×10^{-4}
	2858	101.92	101.35	25.634×10^{-4}	
W_5	2922	109.90	108.40	59.684×10^{-4}	91.50×10^{-4}
	2854	109.60	108.80	31.816×10^{-4}	
W_{10}	2926	109.60	107.70	75.948×10^{-4}	115.901×10^{-4}
	2854	109.20	108.20	39.953×10^{-4}	
W_{15}	2922	111.20	109.20	78.821×10^{-4}	124.132×10^{-4}
	2854	110.80	109.65	45.311×10^{-4}	
W_{20}	2926	111.20	109.20	78.821×10^{-4}	118.266×10^{-4}
	2858	110.60	109.60	39.445×10^{-4}	
W_{25}	2922	112.90	107.90	196.724×10^{-4}	302.416×10^{-4}
	2854	112.30	109.60	105.692×10^{-4}	
W_{30}	2922	114.40	108.30	237.975×10^{-4}	365.547×10^{-4}
	2854	114.00	110.70	127.572×10^{-4}	
W_{35}	2926	108.60	103.00	229.926×10^{-4}	356.053×10^{-4}
	2854	108.30	105.20	126.127×10^{-4}	

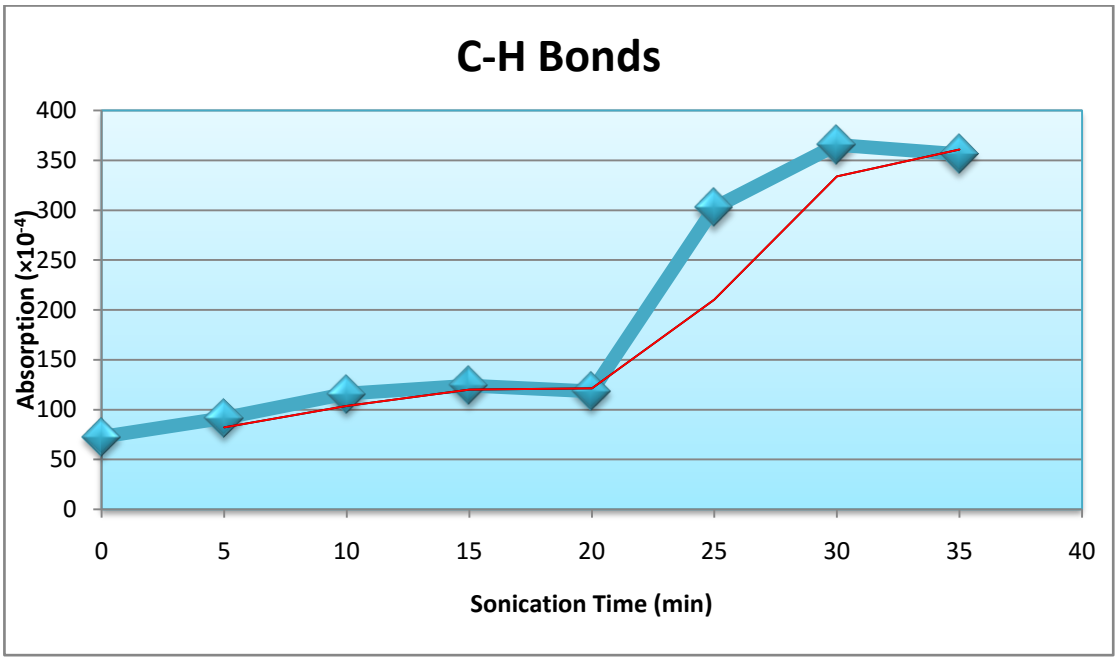

***Figure 4-16**: Changes of the absorption of C-H bond during increasing sonication time in the DIW medium.*

***Table 4-9:** Changes of the absorption of COOH group during increasing sonication time in the DIW medium.*

Sample Name	Peak Position (cm^{-1})	I_0	I	A
W_0	1745	102.23	101.94	12.3373×10^{-4}
W_5	1743	108.12	107.80	12.8727×10^{-4}
W_{10}	1745	107.00	106.60	16.2657×10^{-4}
W_{15}	1745	108.10	107.65	18.1165×10^{-4}
W_{20}	1747	107.90	107.50	16.1298×10^{-4}
W_{25}	1741	109.50	108.33	46.6537×10^{-4}
W_{30}	1745	111.20	109.75	57.0025×10^{-4}
W_{35}	1743	106.30	105.00	53.4396×10^{-4}

***Table 4-10:** Changes of the absorption of C=O bond during increasing sonication time in the DIW medium.*

Sample Name	Peak Position (cm^{-1})	I_0	I	A
W_0	1713	102.22	102.06	6.8031×10^{-4}
W_5	1713	108.20	107.93	10.8508×10^{-4}
W_{10}	1713	107.0	106.75	10.1589×10^{-4}
W_{15}	1713	108.10	107.87	9.2501×10^{-4}
W_{20}	1713	107.97	107.73	9.6644×10^{-4}
W_{25}	1709	109.33	108.67	26.2968×10^{-4}
W_{30}	1712	110.0	110.6	23.6244×10^{-4}
W_{35}	1713	105.90	105.35	22.6142×10^{-4}

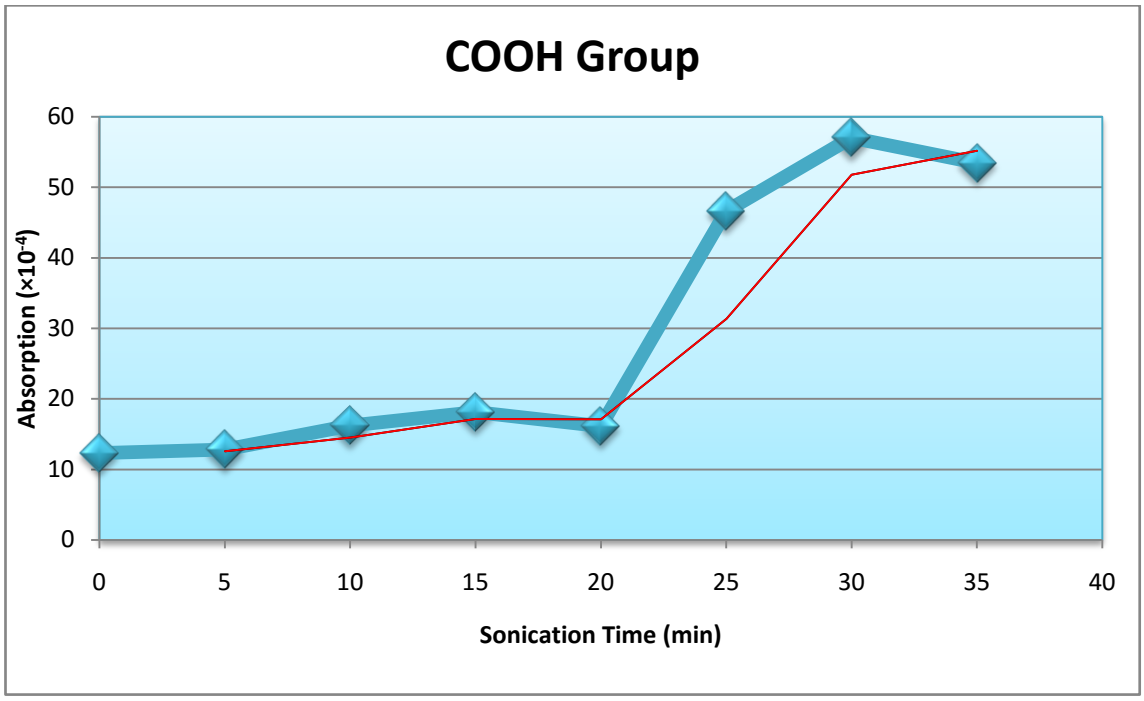

Figure 4-17: *Changes of the absorption of COOH bond during increasing sonication time in the DIW medium.*

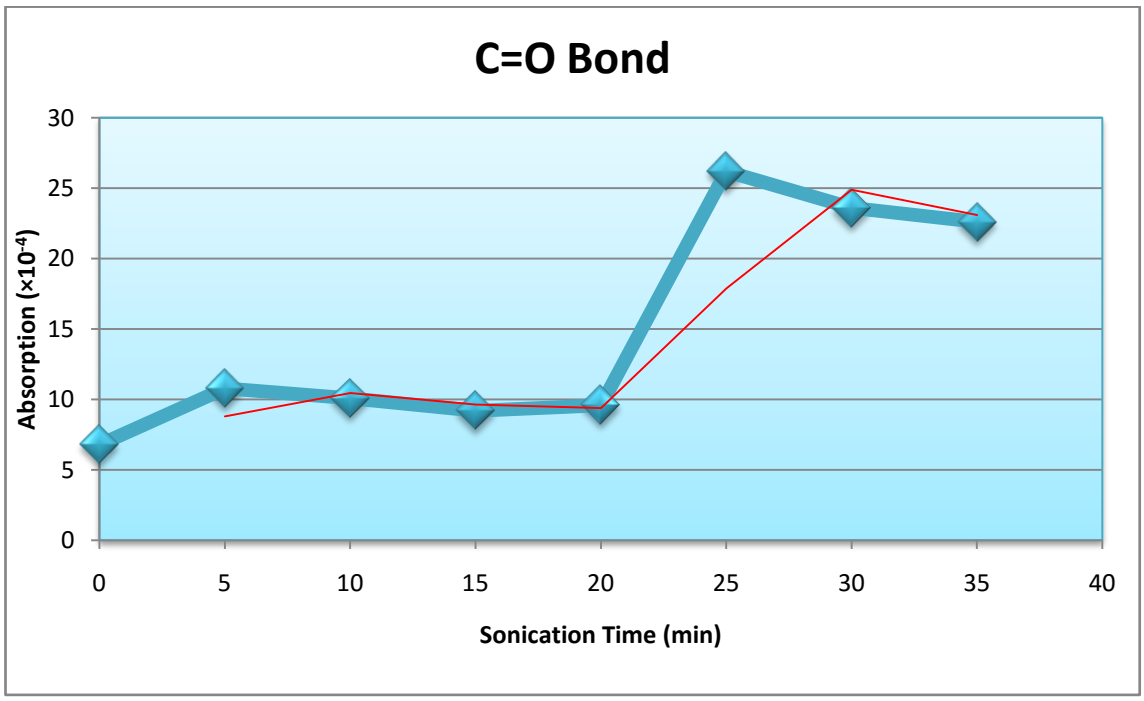

Figure 4-18: *Changes of the absorption of C=O bond during increasing sonication time in the DIW medium.*

Table 4-11: *Changes of the absorption of H-O-H bond (Bending mode) during increasing sonication time in the DIW medium.*

Sample Name	Peak Position (cm^{-1})	I_0	I	A
W_0	1651	102.40	102.32	3.3942×10^{-4}
W_5	1646	108.45	108.12	13.2351×10^{-4}
W_{10}	1646	107.40	107.12	11.3371×10^{-4}
W_{15}	1645	107.38	107.07	12.5559×10^{-4}
W_{20}	1644	108.3	108.0	12.0470×10^{-4}
W_{25}	1643	109.95	109.70	9.8860×10^{-4}
W_{30}	1646	110.6	109.6	39.4457×10^{-4}
W_{35}	1648	105.8	105.0	32.9636×10^{-4}

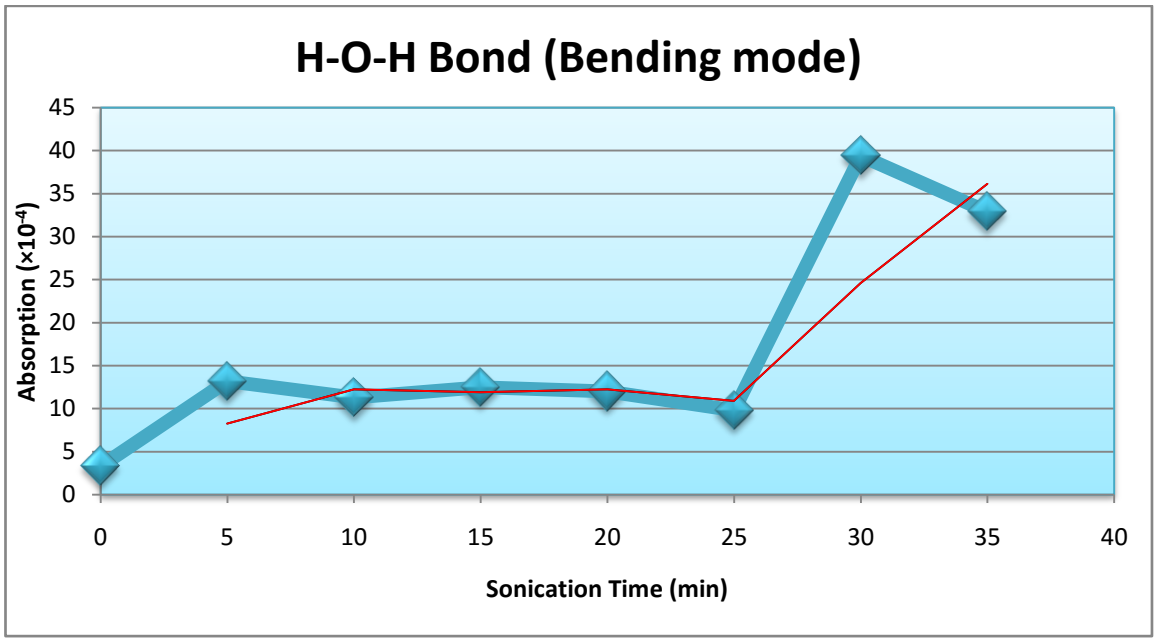

Figure 4-19: *Changes of the absorption of H-O-H bond (Bending mode) during increasing sonication time in the DIW medium.*

Table 4-12: *Changes of the absorption of C-O bond during increasing sonication time in the DIW medium.*

Sample	Peak Position (cm^{-1})	I_0	I	A	A_t
W_0	1302	101.68	101.52	6.8392×10^{-4}	18.7961×10^{-4}
	1254	101.84	101.56	11.9569×10^{-4}	
W_5	1300	106.67	106.49	7.3346×10^{-4}	30.5236×10^{-4}
	1256	106.90	106.40	20.3607×10^{-4}	
	~1165	107.52	107.45	2.8283×10^{-4}	
W_{10}	1298	105.40	105.20	8.2487×10^{-4}	30.8979×10^{-4}
	1256	105.50	105.15	14.4318×10^{-4}	
	~1165	105.80	105.60	8.2174×10^{-4}	

Table 4-12: *Changes of the absorption of C-O bond during increasing sonication time in the DIW medium.*

Sample	Peak Position (cm^{-1})	I_0	I	A	A_t
W_{15}	1300	106.25	106.00	10.2307×10^{-4}	35.5563×10^{-4}
	1254	106.35	105.93	17.1852×10^{-4}	
	1150	106.80	106.60	8.1404×10^{-4}	
W_{20}	1300	106.09	105.86	9.4255×10^{-4}	33.576×10^{-4}
	1254	106.20	105.80	16.3884×10^{-4}	
	1150	106.40	106.21	7.7621×10^{-4}	
W_{25}	1300	107.40	107.20	8.0949×10^{-4}	40.4747×10^{-4}
	1254	107.40	107.00	16.2050×10^{-4}	
	1165	107.60	107.20	16.1748×10^{-4}	
W_{30}	1300	108.40	108.20	8.0202×10^{-4}	43.7505×10^{-4}
	1252	108.40	107.70	28.1357×10^{-4}	
	1165	108.75	108.56	7.5943×10^{-4}	
W_{35}	1300	104.10	103.90	8.3518×10^{-4}	43.4228×10^{-4}
	1252	104.20	103.60	25.0796×10^{-4}	
	1165	104.44	104.20	9.9914×10^{-4}	

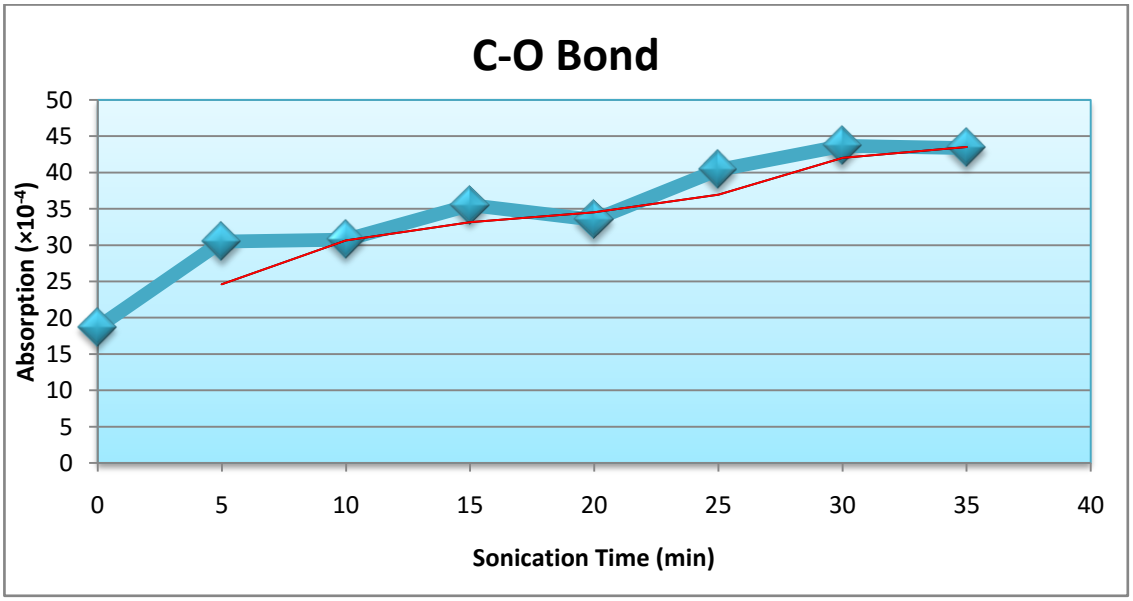

Figure 4-20: *Changes of the absorption of C-O bond during increasing sonication time in the DIW medium.*

The presented graphs (Figures 4-15 to 4-20) shows by increasing sonication time, concentration of functional groups located on the CNTs surface is raised generally. Hence it can be claimed that sonication of CNT-DIW suspension leads to oxidation and hydration of CNT surface. According to figures 4-15 to 4-20, most of the functional groups

(Except OH groups) experience significant growth in concentration after 25 min (~135 KJ energy) sonication. The OH groups enjoy significant growth in concentration after 30 min (~163 KJ energy) sonication. Hence if concentration of functional groups would be important, doing sonication more than 20 min (~110 KJ energy) is not recommended while CNT-DIW suspension is subjected.

What follows is an investigation for answering this question, "why sonication leads to increase of oxidation and hydration on the CNT surface?" For answer to this question effect of the sonication process on the suspension (water and CNTs) must be surveyed. When ultrasound waves are applied in the suspension, first event is **sonolysis** of water molecules and producing high-active radicals. Hot-spot and interfacial reaction zones provide special thermodynamic situation for thermal dissociation of oxygen, hydrogen, and hydroxide species. Different types of high-active chemical species like OH·, H·, O· and hydroperoxyl radicals (OOH·), are ready to attack to carbon surface. Following reactions represent water reactions due to sonication where '*)))*' shows ultrasonic irradiation. [43]

$$H_2O+))) \longrightarrow OH\cdot+H\cdot$$

$$O_2+))) \longrightarrow 2O\cdot$$

$$OH\cdot+O\cdot \longrightarrow OOH\cdot$$

$$O\cdot+ H_2O\cdot \longrightarrow 2OH\cdot$$

$$H\cdot+O_2 \longrightarrow OOH\cdot$$

$$OH\cdot+H\cdot \longrightarrow H_2O\cdot$$

$$2OH\cdot \longrightarrow H_2O+O\cdot$$

$$OOH\cdot+OH\cdot \longrightarrow O_2+H_2O$$

$$2OH\cdot \longrightarrow H_2O_2$$

$$2OOH\cdot \longrightarrow H_2O_2+O_2$$

$$H\cdot+H_2O_2 \longrightarrow OH\cdot+H_2O$$

$$OH\cdot+H_2O_2 \longrightarrow H_2O+OOH\cdot$$

$$2H\cdot \longrightarrow H_2$$

Water is not single part which is irritated by ultrasound waves; on the other side, also surface of CNTs is affected by sonication. Raman spectroscopy is best tool for study of CNTs surface in this situation. Raman spectroscopy provides study of the defects, and

disorders as a probable result of sonication process. Following figures (4-21 to 4-26) represent Raman spectra of samples W_0, W_4, W_6, W_8, and W_{10} that are sonicated for 0, 4, 6, 8 and 10 min respectively.

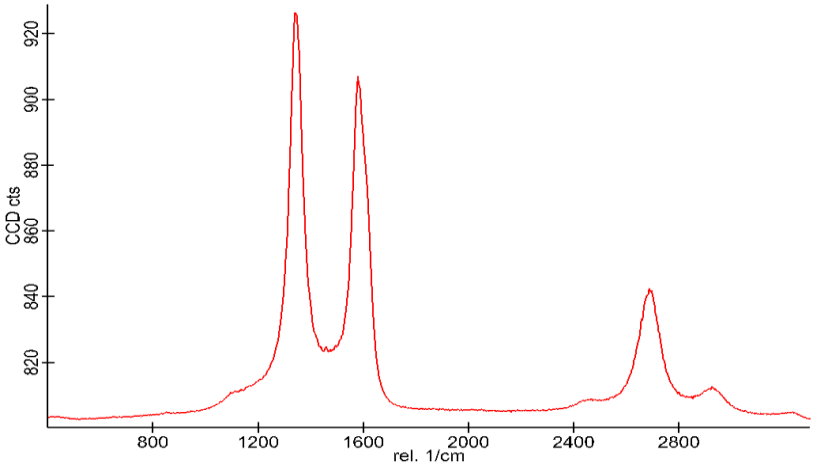

Figure 4-21: *Raman spectrum of sample W_0.*

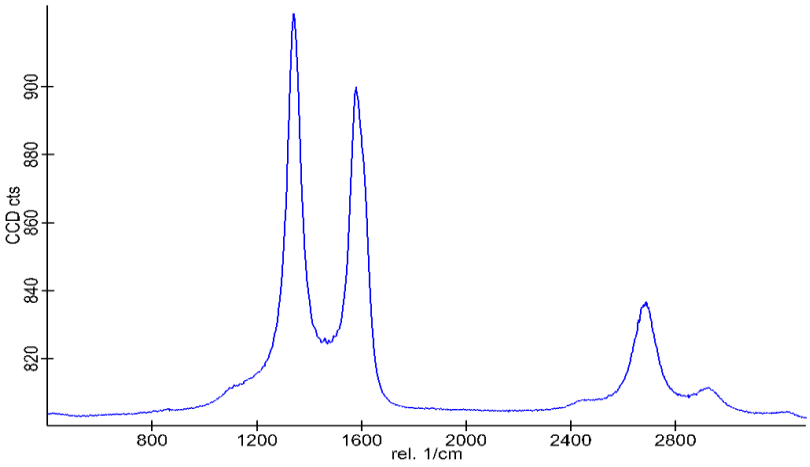

Figure 4-22: *Raman spectrum of sample W_4.*

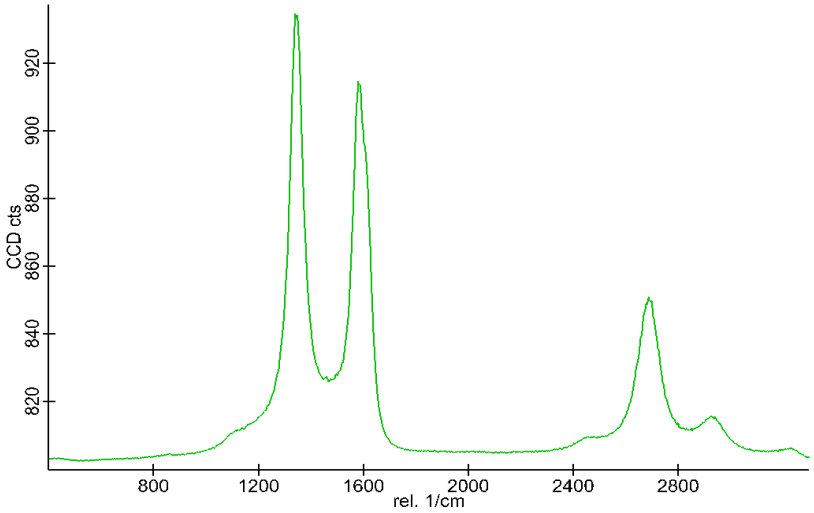

Figure 4-23: *Raman spectrum of sample W_6.*

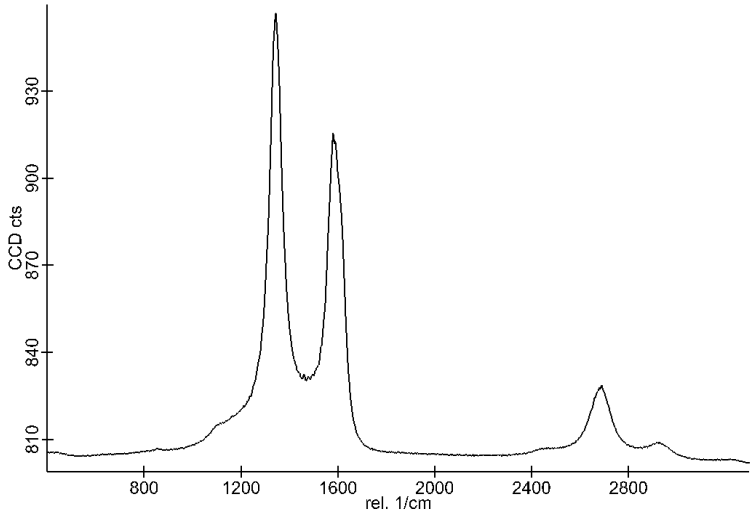

Figure 4-24: *Raman spectrum of sample W_8.*

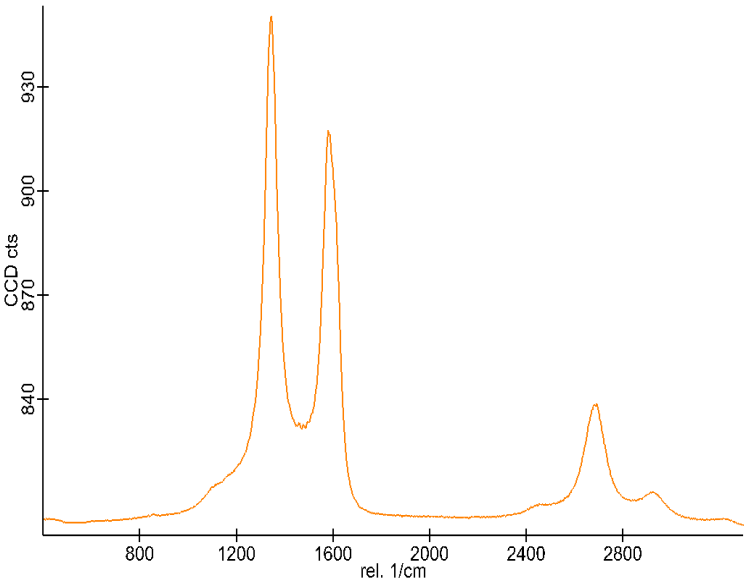

Figure 4-25: *Raman spectrum of sample W_{10}.*

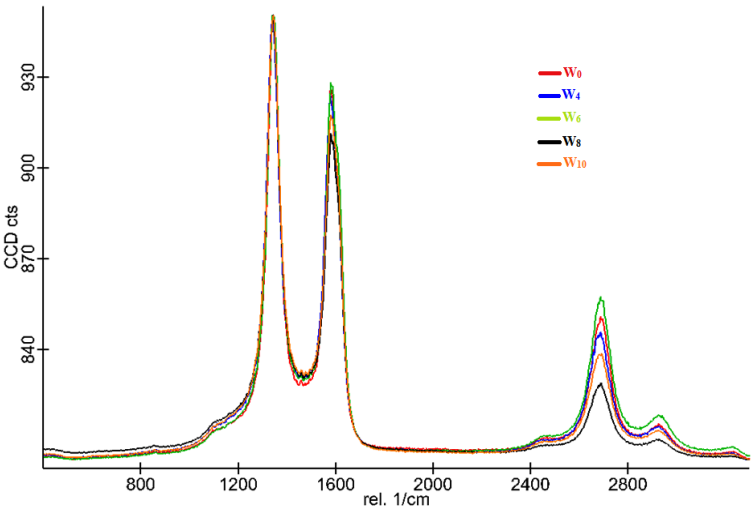

Figure 4-26: *Comparison of Raman spectra related to samples W_0, W_4, W_6, W_8, and W_{10}.*

Table 4-13 represents characteristic parameters related to presented Raman spectra.

Table 4-13: *Characteristic parameters related to Raman spectra of samples W_0, W_4, W_6, W_8, and W_{10}.*

Sample Name	D-band Position(cm^{-1})	G-band Position (cm^{-1})	2D-band Position (cm^{-1})	I_D/I_G Ratio
W_0	1342	1581	2690	1.2
W_4	1341	1580	2687	1.3
W_6	1342	1582	2690	1.2
W_8	1343	1582	2688	1.5
W_{10}	1344	1583	2688	1.4

The I_D/I_G ratio parameter is used for estimation of amount of defects, disorders and functional groups located on the CNT surface. As explained in the chapter 2, D band located around 1340 cm^{-1} shows sp^3 carbons (orbital configuration of defects and disorders) and G band settled around 1580 cm^{-1} represents sp^2 carbons. Also functionalization leads to sp^2 to sp^3 rehybridization [21]. Hence, increasing I_D/I_G ratio notices to increase either defects or functional groups. Figure 4-27 shows effect of sonication time on the I_D/I_G ratio based on obtained Raman spectra.

This graph (Fig. 4-27) explains that generally sonication process leads to create defects and disorders in the structure of CNTs especially in the long term although decrease in some points is observable. A.J. Blanch *et al.* (2010) [113] have reported similar results at Flinders (Australia) university.

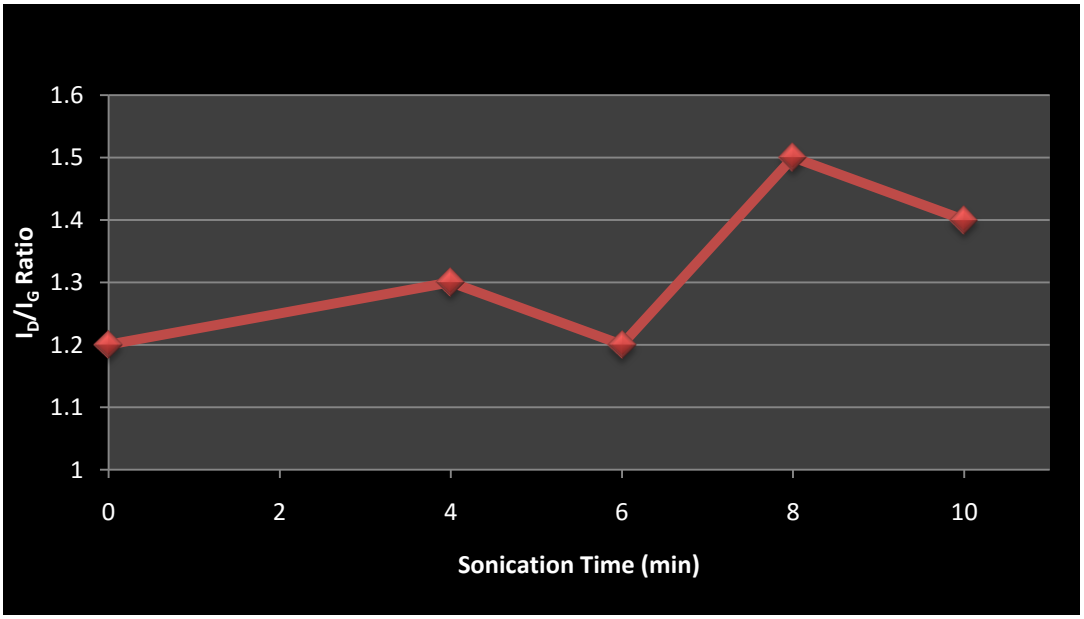

Figure 4-27: *Effect of sonication time on the I_D/I_G ratio.*

Defects and disorders are active centers with high density of unpaired electrons. Sonication process, by creating tension in the CNT structure, leads to create disorders and local rehybridization of sp^2 to sp^3. Hence sonication by increasing sp^3/sp^2 ratio and density of unpaired electrons results in increase of surface reactivity.

Tendency of functional groups to attach different defective locations is not same. Ellison *et al.* (2005) [114], at Wittenberg university (Ohio - USA), have reported similar FTIR results while CNTs are interacted with water. They used density functional theory (DFT) calculations for determining probability of tendency of water-based functional groups for absorbing to different defective locations. Based on this study, optimized geometries for absorbing these functional groups are seven-membered and five-membered rings according to figure 4-28. Hence Stone-Wales defects and non-hexagonal rings enjoy maximum density of functional groups in the surface of CNT.

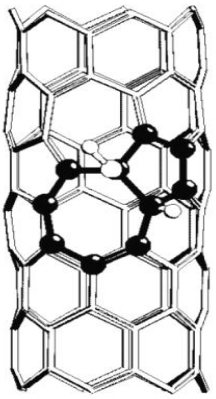

Figure 4-28: *Non-hexagonal rings, optimized geometries for absorbing functional groups* [114].

Notwithstanding that increasing sonication time leads to raise I_D/I_G ratio generally, some points do not obey this trend (Figure 4-27). Nobody has reported any reason for this phenomenon yet. For investigation about the reason, surveying some studies which focus on interaction of other types of waves with CNT is helpful.

W. Lin *et al.* (2010) [115] and Y. Ling *et al.* (2011) [105] have reported that interaction of microwave with CNT results in either improvement of functionalization or removing some functional groups which have been presented. Also they claim that, in this interaction, thermal annealing leads to reduce the defect density.[105,115]

Based on what was explained, also this justification can be compatible with sonication process. Ultrasonic irradiation can promote functionalization on the one hand, and on the other hand, remove some settled functional groups. According to Raman spectroscopy results, it is so clear that the dominant effect of sonication process on the structure of CNT is increasing disorders and defects but also as a limited effect, localized superheating produced by sonication process (Resulted from interfacial reaction zone) leads to localized annealing process to decrease the defect density. Also this theory justifies decrease of concentration some functional groups in some points during increase of so-

nication time as FTIR results show. Anyway, it is emphasized that prevailing effect of increasing sonication time is increase of concentration of functional groups and defects generally. Also several research groups [15,116–118] around the world have reported functionalization of CNTs as result of ultrasonication.

4.3 Study of CNTs Sonicated in the JD230

First of all, interaction of JD230 with CNTs without soncation will be studied. Figure 4-29 represents spectrum of sample J_0.

4-29: *IR spectrum of sample J_0*

In this spectrum, the peaks show minimum intensities. For investigation about effect of interaction of JD230 with CNT, just IR measurement is not adequate but with considering amine groups at the end of Jeffamine chains, reduction of CNT surface is not unlikely. The remarkable point of sample J_0 spectrum is related to carboxyl groups (COOH). The peak located at 1745 cm^{-1} which is available in the pristine CNT spectrum (Figure 4-2), is deleted completely in the spectrum of sample J_0 (Figure 4-29). It means JD230 reacts with carboxyl groups located on the CNT surface and dismisses them. Table 4-14 represents qualitative analysis of sample J_0.

Table 4-14: *Qualitative analysis of IR spectrum of sample J_0*

Wavenumber (cm^{-1})	Bond	Vibration Mode
3250	O-H	Stretching
2975	C-H	Stretching
2876	C-H	Stretching
1500-1340	C-H	Bending
1302	C-O	Stretching

Figure 4-30 represents IR spectrum of sample J_{10}. According to this spectrum, sonication of CNT-JD230 suspension even for 2 min (10 KJ energy) leads to oxidation and hydration on the surface of CNTs. A lot of new peaks which are created by stretching and bending vibration modes of C-H and C=O bonds notice about effect of ultrasound waves. The important peaks located around 1750, and 1715 that are related to COOH and C=O are products of sonication process in JD230 medium.

Figure 4-30: *IR spectrum of sample J_{10}.*

What follows is a study of effect of increasing sonication energy (or time) on the functional groups concentration. Figures 4-31 to 4-38 show IR spectra related to CNTs under sonication process between 20-90 KJ energy (or 3.5-15 min) in the JD230 medium.

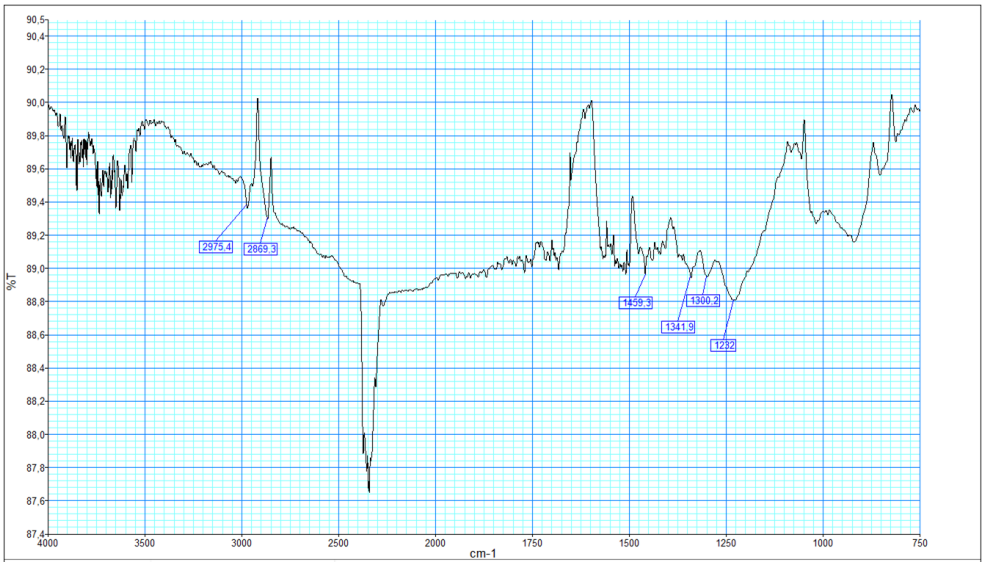

Figure 4-31: *IR spectrum of sample J_{20}.*

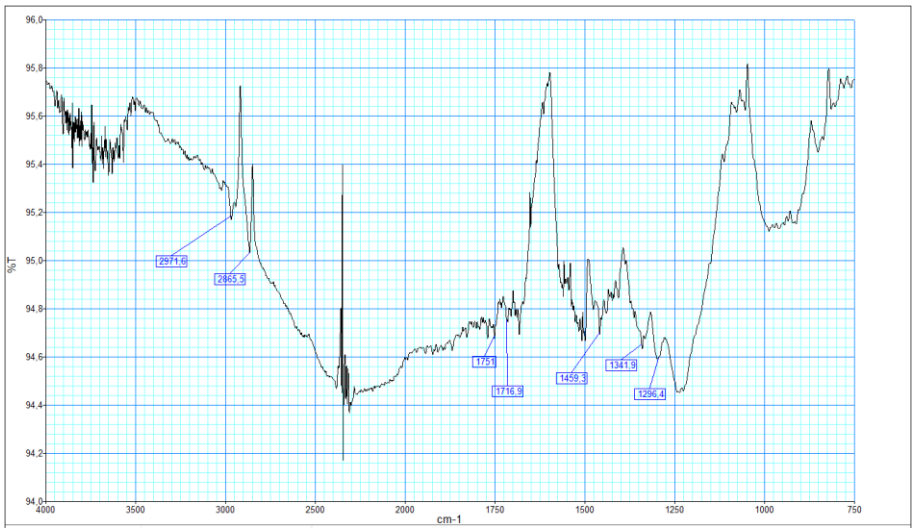

Figure 4-32: *IR spectrum of sample J_{30}.*

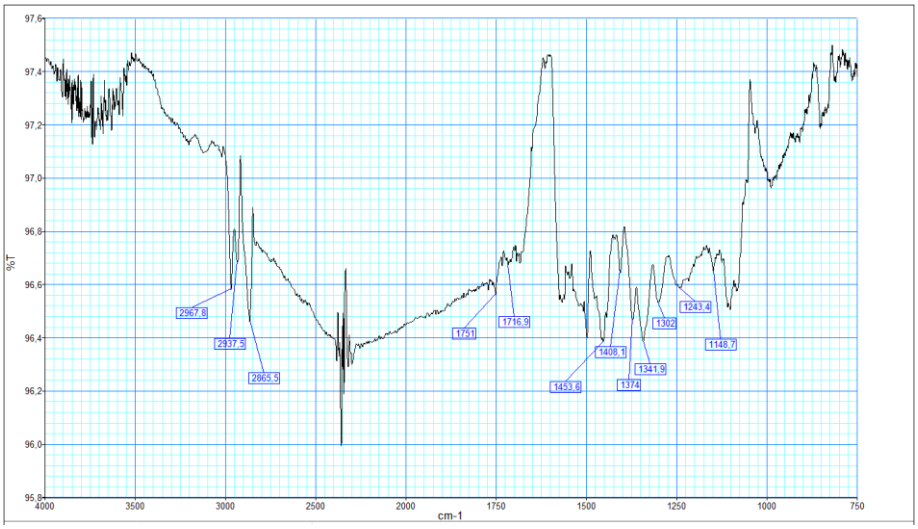

Figure 4-33: *IR spectrum of sample J_{40}.*

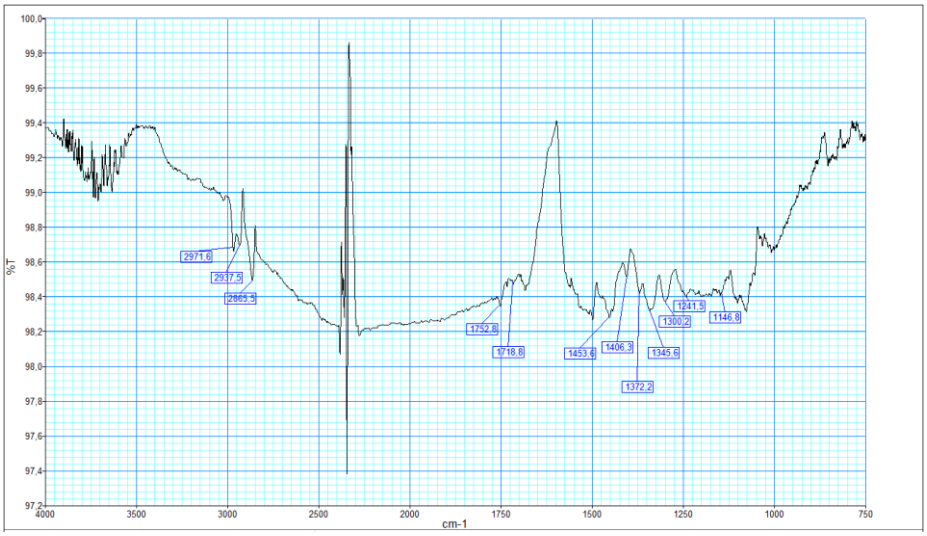

Figure 4-34: *IR spectrum of sample J_{50}.*

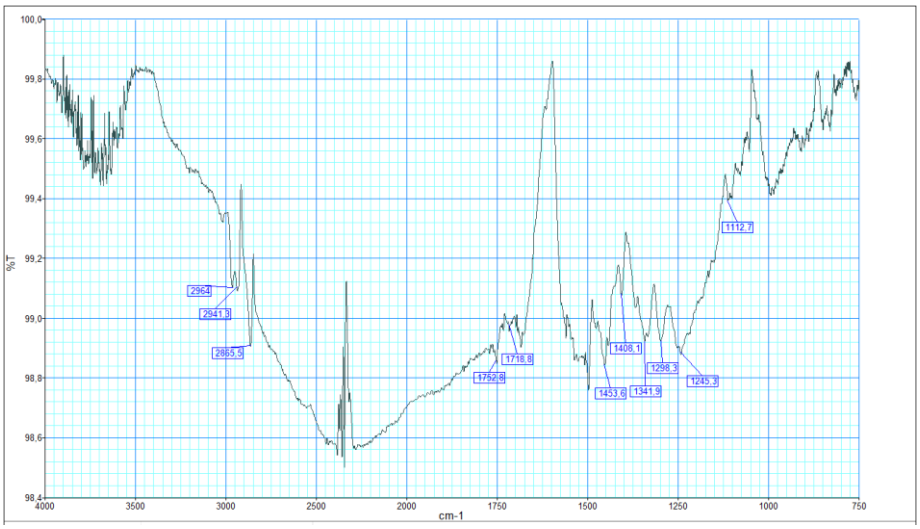

Figure 4-35: *IR spectrum of sample* J_{60}.

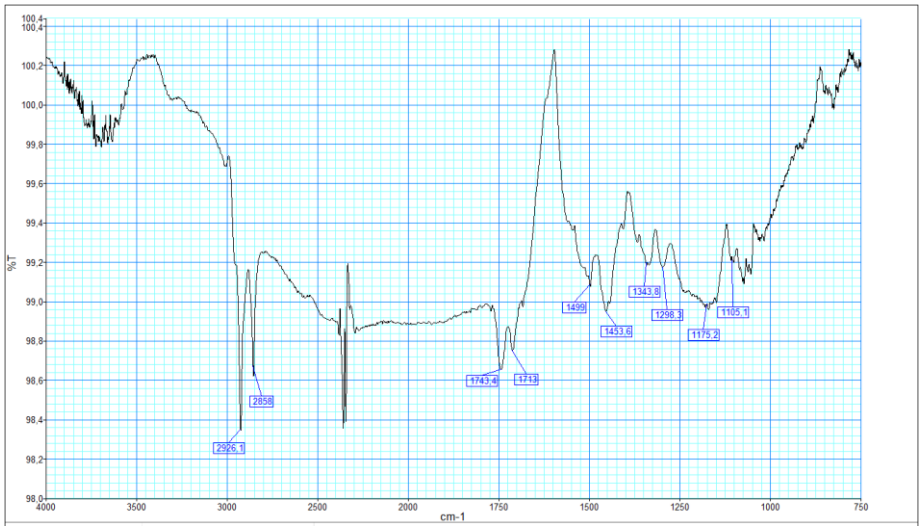

Figure 4-36: *IR spectrum of sample* J_{70}.

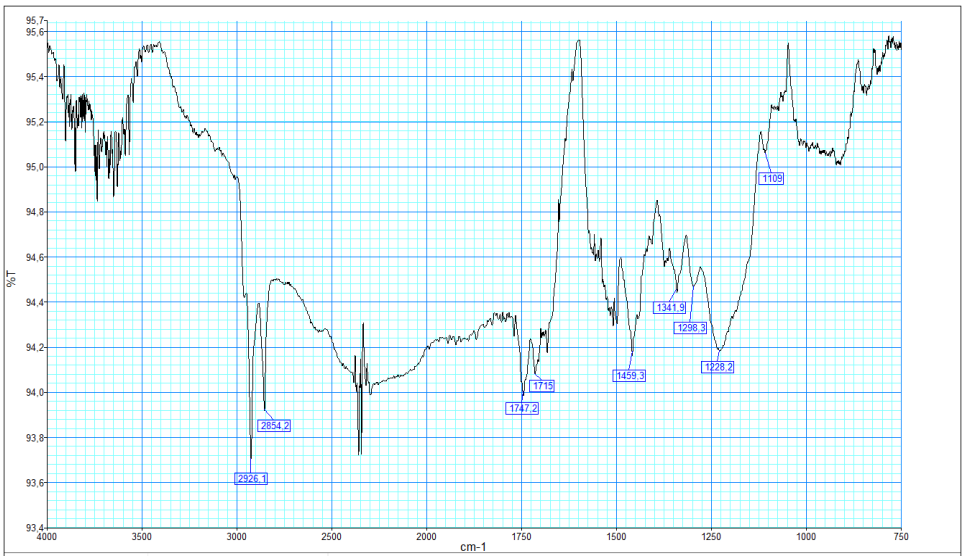

Figure 4-37: *IR spectrum of sample* J_{80}.

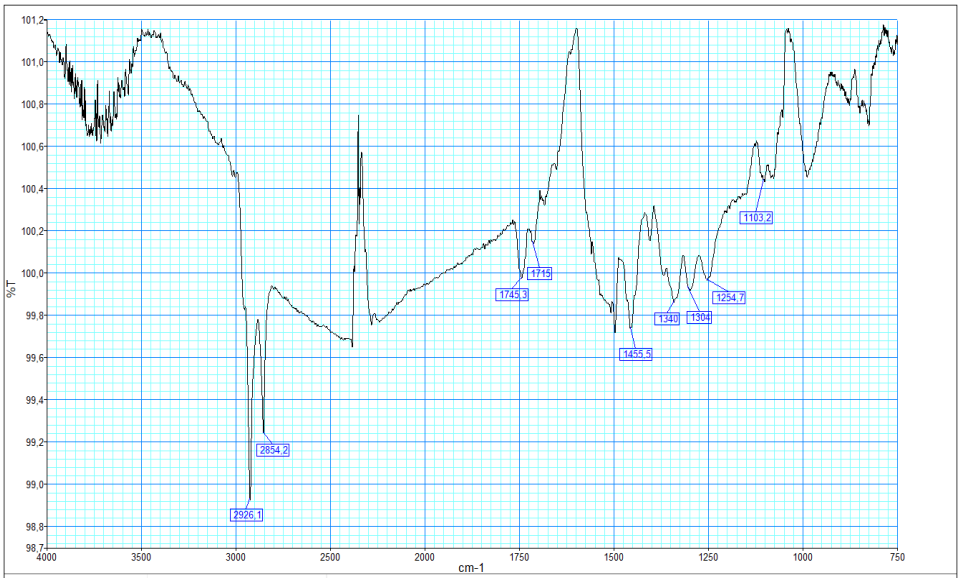

Figure 4-38: *IR spectrum of sample J_{90}.*

Table 4-15 compares qualitative analysis of three important samples J_0 (Non-sonicated), J_{10} (Minimum sonication) and J_{90} (Maximum sonication). This table for understanding effect of sonication on CNTs suspended in the JD230 medium is necessary. In the spectra of CNTs sonicated in the JD230, no sign is observed for proving nitration. This point is so important, because it shows free radicals related to jeffamine are not produced by sonication. Also, nobody has reported degradation of Jeffamine by ultrasonication process.

Table 4-15: *Qualitative analysis of IR measurements related to samples J_0, J_{10}, and J_{90}.*

Wavenumber (cm^{-1}) related to J_0	Wavenumber (cm^{-1}) related to J_{10}	Wavenumber (cm^{-1}) related to J_{90}	Bond	Vibration Mode
3250	3270	3200	O-H	Stretching
2975	2971	2926	C-H	Stretching
2876	2876	2854	C-H	Stretching
-	1751	1745	COOH	Stretching
-	1718	1715	C=O	Stretching
1500-1340	1500-1340	1500-1340	C-H	Bending
1299	1300	1304	C-O	Stretching

Further quantitative analysis of IR spectra related to J_n series samples will be surveyed. IR Spectrum of sample J_{10} (Figure 4-30) showed that minimum sonication leads to oxidation and hydration of CNTs surface while they are suspended in the JD230 medium. But, this part tries to clarify effect of continue of sonication process on the cocetration of functional groups. Although IR spectroscopy for this target is so poor method but considering a general trend by using a lot of measurements can decrease probable errors. Next figures (4-39 to 4-43) and tables (4-16 to 4-19) follow this target. In the graphs, the moving average trend is distinguishable by blue line.

Table 4-16: *Changes of the absorption of C-H bonds during increasing sonication energy in the JD230 medium.*

Sample	Peak Position (cm^{-1})	I_0	I	A	A_t
J_0	2975	101.7	101.48	9.405×10^{-4}	12.821×10^{-4}
	2876	101.6	1.1.45	4.416×10^{-4}	
J_{10}	2971	89.0	88.6	19.562×10^{-4}	39.124×10^{-4}
	2876	89.0	88.6	19.562×10^{-4}	
J_{20}	2975	89.6	89.4	9.705×10^{-4}	33.952×10^{-4}
	2869	89.8	89.3	24.248×10^{-4}	
J_{30}	2971	95.4	95.2	9.114×10^{-4}	33.456×10^{-4}
	2865	95.6	95.0	24.342×10^{-4}	
J_{40}	2967	97.1	96.57	23.769×10^{-4}	44.428×10^{-4}
	2865	96.93	96.47	20.659×10^{-4}	
J_{50}	2971	98.97	98.63	14.945×10^{-4}	31.229×10^{-4}
	2865	98.86	98.49	16.284×10^{-4}	
J_{60}	2941	99.45	99.10	15.311×10^{-4}	32.840×10^{-4}
	2865	99.30	98.90	17.529×10^{-4}	
J_{70}	2926	99.35	98.35	43.935×10^{-4}	70.282×10^{-4}
	2858	99.20	98.60	26.347×10^{-4}	
J_{80}	2926	94.60	93.70	41.515×10^{-4}	63.349×10^{-4}
	2854	94.42	93.94	22.134×10^{-4}	
J_{90}	2926	100.05	98.92	49.329×10^{-4}	75.504×10^{-4}
	2854	99.85	99.25	26.175×10^{-4}	

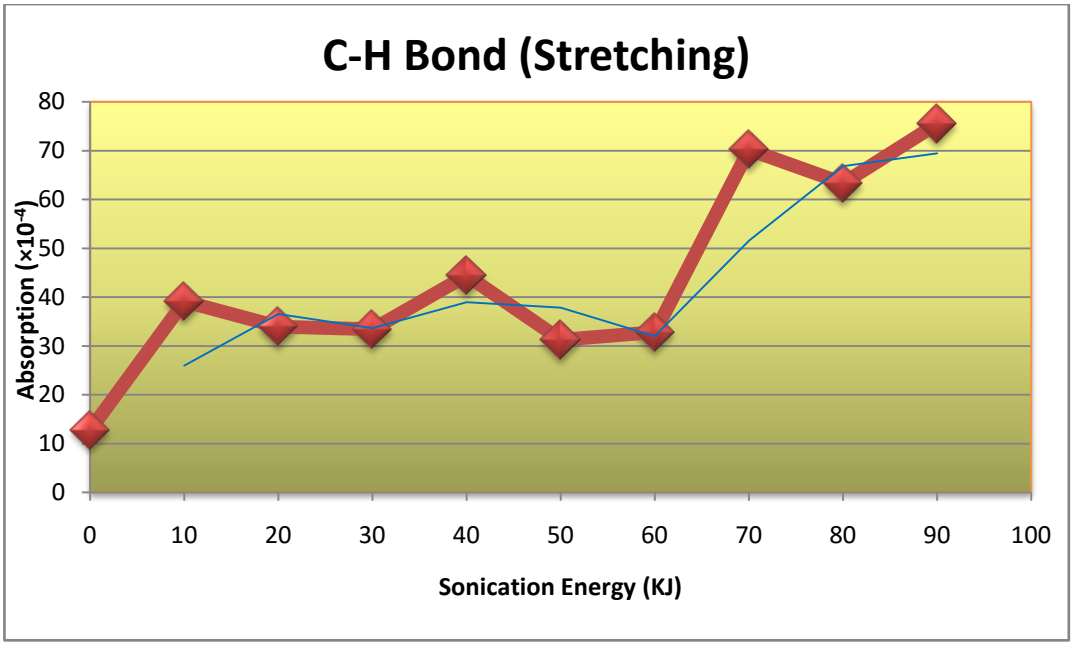

Figure 4-39: *Changes of the absorption of C-H bond during increasing sonication energy in the JD230 medium.*

Table 4-17: *Changes of the absorption of COOH group during increasing sonication energy in the JD230 medium.*

Sample Name	Peak Position (cm^{-1})	I_0	I	A
J_0	-	0	0	0
J_{10}	1751	88.330	88.253	3.7875×10^{-4}
J_{20}	1751	89.12	89.0	5.8517×10^{-4}
J_{30}	1751	94.80	94.68	5.5008×10^{-4}
J_{40}	1751	96.60	95.56	4.7009×10^{-4}
J_{50}	1751	98.44	98.34	4.4140×10^{-4}
J_{60}	1751	98.94	98.84	4.3916×10^{-4}
J_{70}	1743	98.95	98.65	13.1870×10^{-4}
J_{80}	1747	93.96	94.30	15.6868×10^{-4}
J_{90}	1745	100.24	99.965	11.9308×10^{-4}

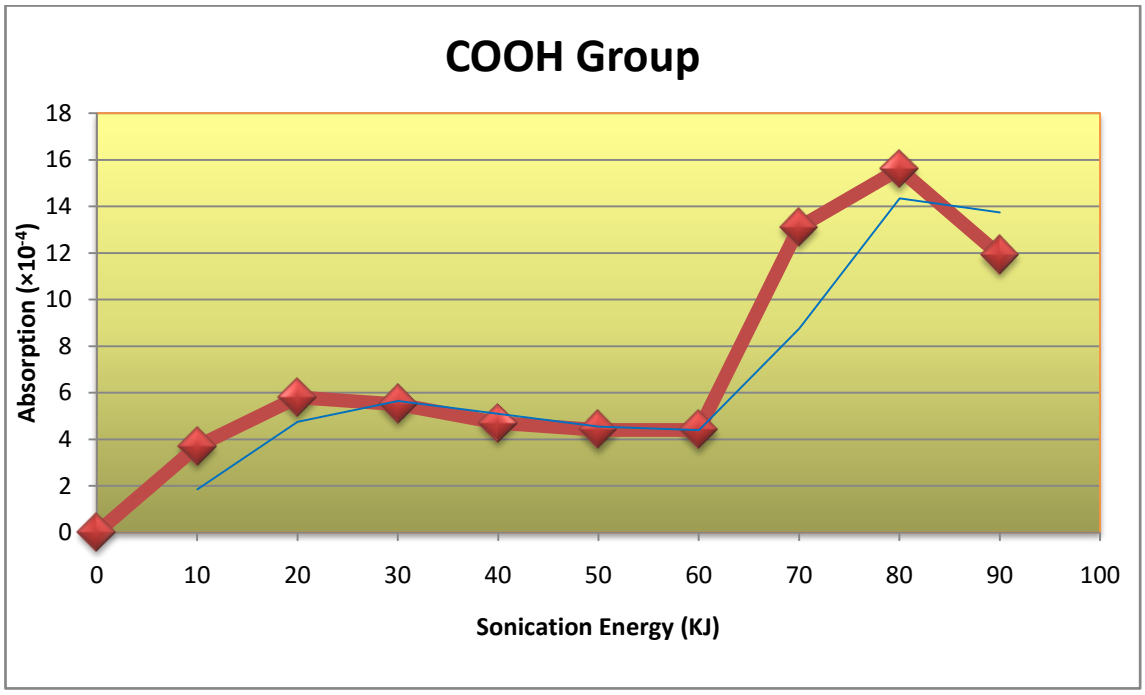

Figure 4-40: *Changes of the absorption of COOH group during increasing sonication energy in the JD230 medium.*

Figures 4-39 and 4-40 show after starting sonication, by continuation of sonication, concentration of functional groups does not change. But this trend is changed after 70 KJ sonication, whereas amount of -H and COOH groups is increased. As explained, due to absence of C-N bond, probability of degradation of JD230 is almost zero. It seems that after starting sonicaton, -H or -OH groups are products of sonolysis of the water which is existed in the jeffamine as impurity. Also, sonication process leads to entry of air flow in the suspension. During cavitation phenomenon, CNTs surface is exposed to free and active radicals.

During ultrasonication of CNT-JD230 suspension, several forces, factors and events are fighting together for and against functionalization (See in the figure 4-41). On one hand, increasing high active radicals and surficial defects, act for functionalization, and on the other hand, factors including thermal annealing of defects, separation of functional groups from surface by ultrasonic irritation, and reaction of functional groups with JD230 are against functionalization. This conflict leads to unstable trend of functionalization of surface between 2-10.5 min (10-60 KJ) sonication. In this range, neither decreasing nor increasing trends of functionalization are dominant. However, story is changed after 70 KJ sonication, and adjuvant factors of functionalization overcome.

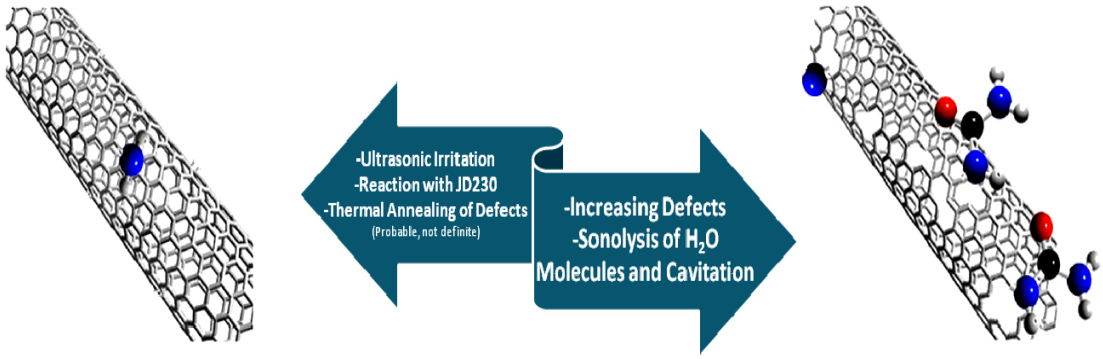

Figure 4-41: *Various events for and against functionalization during sonication.*

Following tables (4-18 and 4-19) and figures (4-42 and 4-43) study oxidation trend of CNTs surface during sonication.

Table 4-18: *Changes of the absorption of C=O bond during increasing sonication energy in the JD230 medium.*

Sample Name	Peak Position (cm^{-1})	I_0	I	A
J_0	-	0	0	0
J_{10}	1718	88.39	88.28	5.4080×10^{-4}
J_{20}	1718	89.16	89.04	5.8490×10^{-4}
J_{30}	1717	94.860	94.745	5.2682×10^{-4}
J_{40}	1717	96.74	96.67	3.1436×10^{-4}
J_{50}	1718	98.520	98.465	2.4251×10^{-4}
J_{60}	1718	99.015	98.950	2.8519×10^{-4}
J_{70}	1713	98.92	98.74	7.9098×10^{-4}
J_{80}	1715	94.26	94.08	8.3012×10^{-4}
J_{90}	1715	100.28	100.143	5.9372×10^{-4}

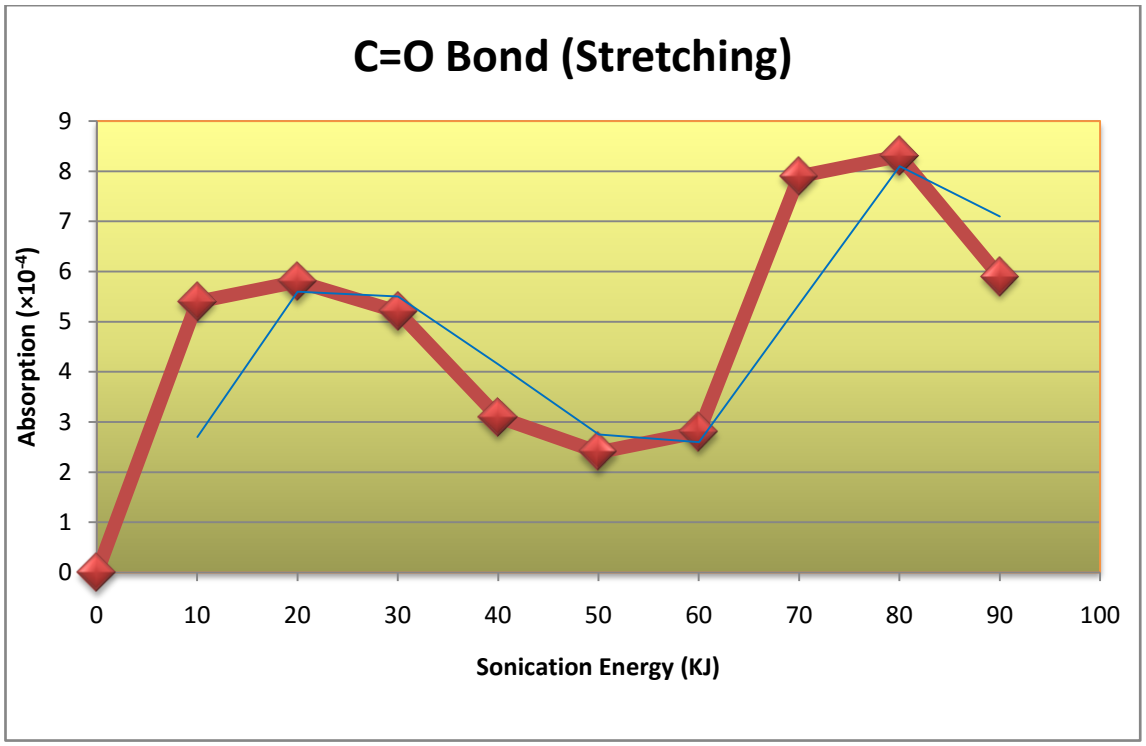

Figure 4-42: *Changes of the absorption of C=O bond during increasing sonication energy in the JD230 medium.*

Table 4-19: *Changes of the absorption of C-O bond during increasing sonication energy in the JD230 medium.*

Sample Name	Peak Position (cm^{-1})	I_0	I	A
J_0	1299	100.195	100.090	4.5536×10^{-4}
J_{10}	1300	88.40	88.24	7.8676×10^{-4}
J_{20}	1300	89.08	88.95	6.3425×10^{-4}
J_{30}	1296	94.745	94.590	7.1107×10^{-4}
J_{40}	1302	96.69	96.53	7.1925×10^{-4}
J_{50}	1300	98.55	98.37	7.9395×10^{-4}
J_{60}	1298	99.08	98.92	7.0189×10^{-4}
J_{70}	1298	99.340	99.175	7.2194×10^{-4}
J_{80}	1298	94.640	94.465	8.0380×10^{-4}
J_{90}	1304	100.08	99.92	6.9487×10^{-4}

According to these figures (4-42 and 4-43), at the beginning point of soncation, oxidation is started but in the continuation of sonication, due to low concentration of active species of oxygen, oxidation does not show significant changes.

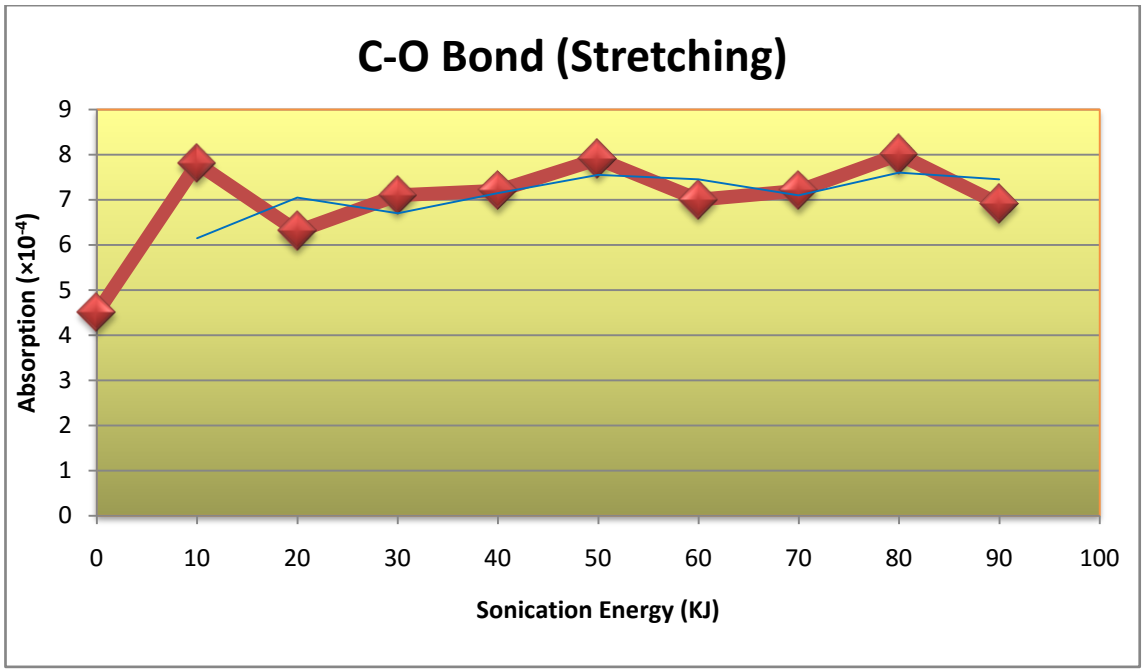

Figure 4-43: *Changes of the absorption of C-O bond during increasing sonication energy in the JD230 medium.*

5. SUMMARY AND CONCLUSION

The objective of this thesis was characterization of functional groups and defects on the surface of sonicated CNTs (in the Jeffamine D-230 polyetheramine (JD230) and deionized water (DIW) mediums) by using FTIR-ATR and Raman spectroscopy, and then investigation of relationship between sonication time and functional groups on the CNTs.

In this regard, at the first place, 10 suspensions of JD230-CNT and 11 suspensions of DIW-CNT with constant ratio of 0.25 % (wt) for sonication step were prepared. In the second step, each sample was sonicated for specific time (or energy) (Min: 2min (10 KJ) and max: 35 min (190 KJ)). In the third step sonicated CNTs were separated from liquid part by helping Büchner funnel, filter paper, and vacuum pump. Also, for completely removing of JD230 from the samples which were sonicated in the JD230 medium, they were washed by 500 cc water in the Büchner filtration system. Finally, at the last step of sample processing stage, for exiting non-bonded water, samples were dried at 50˚C for 4-5 hrs by dryer. After this process, sonicated CNTs were collected for characterization stage.

In the IR spectroscopy tests, for increasing signal-to-noise ratio (S/N) two strategies were followed. First, KBr powder as a transparent material is mixed with CNT samples (m_{CNT}/m_{KBr} was optimized to 1%) and second, diamond prism is changed to diamond - zinc selenide (Di/ZnSe) prism. Also 5 samples (Sonicated in the DIW and non-sonicated) were selected for studying effect of sonication process on the structure of CNTs by Raman spectroscopy.

CNTs sonicated in either DIW or JD230 were studied separately by IR spectroscopy. Table 5-1 summarizes IR qualitative analysis for five important samples. These samples include PCNT (Pristine CNT), W_0 (Non-sonicated CNTs, interacted with DIW), W_{35} (The CNTs enjoyed maximum sonication (35 min) in the DIW medium), J_0 (Non-sonicated CNTs, interacted with JD230), and J_{90} (The CNTs enjoyed maximum sonication (90 KJ) in the JD230 medium).

IR spectroscopy showed that just mixing CNTs with water leads to four important events. Three new peaks were created and one peak was drop. Three new peaks located at 1713, 1651, and 1254 cm^{-1}, that are related to C=O, H-O-H and C-O bonds respectively, showed that mixing CNT and water leads to oxidation and hydration of CNT. Also the peak located at 1037 which is related to anhydrides was limited due to interaction with water.

Table 5-1: *Summary of IR qualitative analysis of important samples.*

Bond	Sample PCNT	Sample W_0	Sample J_0	Sample W_{35}	Sample J_{90}
	Wavenumber (cm^{-1})				
O-H (ν)	3269	3336	3250	3330	3200
C-H (ν)	2979	2926	2975	2926	2926
	2854	2858	2876	2858	2854
COOH (ν)	1745	1745	-	1743	1745
C=O (ν)	-	1713	-	1713	1715
H-O-H (δ)	-	1651	-	1648	-
C-H (δ)	1500-1340				
C-O (ν)	1302	1302	1302	1302	1300
	-	1254	-	1251	-
	-	-	-	1160	-

By starting and continuation of sonication, significant and huge oxidation and hydration were happened. Especially, remarkable growth of the peak located around 1650 (H-O-H (δ)) and creating a new peak located around 1160 cm^{-1} C-O (ν) showed effect of sonication on the surface chemistry of CNTs while they were suspended in the DIW medium. Also the other peaks which are related to O-H, C-H, COOH, C=O and C-O bonds experienced growth during increasing sonication time, especially after 25 min (~135 KJ energy).

Based on what was claimed, sonication process leads to functionalization. This phenomenon happens due to two important reasons. First, ultrasound waves lead to sonolysis of water molecules and producing high-active radicals such as OH·, H·, O·, OOH·, and H_2O· that are ready to attack to carbon surface. Second reason was revealed when Raman spectroscopy results were surveyed. Raman spectroscopy showed that generally sonication process creates defects and disorders in the structure of CNTs although decrease happens in some points.

Defects are active sites having high density of unpaired electrons. Ultrasonication creates disorders and local rehybridization of sp^2 to sp^3 leads to increase in surface reactivity. Based on Raman spectroscopy results, the dominant effect of sonication process on the structure of CNT is increase in defects (sp^3 hybridization). But also as a limited effect it can be truth that localized superheating can result in localized annealing to decrease the defect density (Probable, not definite).

After investigation about CNTs sonicated in the water medium, similar studies were done while CNTs were sonicated in the JD230 medium. IR spectroscopy showed mixing CNTs and JD230 leads to decrease of functional groups on the CNT surface. Espe-

cially, this effect is remarkable about carboxyl groups (COOH). As table 5-1 shows, carboxyl groups peak located at 1745 cm^{-1} is available in the pristine CNT spectrum, but this peak has disappeared completely in the spectrum of sample J_0. It seems JD230 has reacted with carboxyl groups located on the CNT surface and dismissed them.

By starting sonication, even at the beginning points (10 KJ energy or 2 min), oxidation and hydration of the surface of CNTs were started. The peaks located around 1750, and 1715 that are related to COOH and C=O were created due to sonication. The IR spectra did not show nitration of surface (C-N bond), hence it can be claimed that free radicals related to jeffamine were not produced by sonication (Sonication did not lead to JD230 degradation).

After starting sonication, by continuation of sonication, concentration of functional groups did not change. But this trend was changed after 70 KJ (12.5 min) sonication, whereas amount of -H and COOH groups was increased. With regarding to no degradation of JD230, free radicals which attack to the surface are produced by sonolysis of the water existed in the jeffamine on one side, and on the other side, entry of air flow and then cavitation phenomenon.

As discussed during this thesis, in a general trend, ultrasonic dispersion leads to increase of defects and functionalization. By considering that concentration of defects and functional groups affects on hydrophobicity, thermal, electrical and mechanical properties of CNT, while functional properties of CNTs are subjected, using ultrasonication as dispersion method must be warily.

REFERENCES

1. Iijima S. Helical microtubules of graphitic carbon. Nature. 1991;354:56–8.
2. Kong J, Franklin NR. Nanotube Molecular Wires as Chemical Sensors. Science (80-). 2000;287(5453):622–5.
3. Collins PG. Extreme Oxygen Sensitivity of Electronic Properties of Carbon Nanotubes. Science (80-) [Internet]. 2000;287(5459):1801–4. Available from: http://www.sciencemag.org/cgi/doi/10.1126/science.287.5459.1801
4. Dettlaff-Weglikowska U, Benoit J-M, Chiu P-W, Graupner R, Lebedkin S, Roth S. Chemical functionalization of single walled carbon nanotubes. Curr Appl Phys. 2002;2(6):497–501.
5. Bandosz TJ. Surface chemistry of activated carbons and its characterization. Activated Carbon Surfaces in Environmental Remediation. Elsevier Ltd; 2006. p. 159–229.
6. Hielscher K. Ultrasonic Milling and Dispersing Technology for Nano-Particles. Hielscher Ultrasonics GmbH. Teltow, Germany; 1998;
7. Huang YY, Terentjev EM. Dispersion of carbon nanotubes: Mixing, sonication, stabilization, and composite properties. Polymers (Basel). 2012;4:275–95.
8. Jeon I, Chang DW. Functionalization of Carbon Nanotubes. Carbon Nanotub - Polym Nanocomposites. 1991;91–110.
9. Choudhary V, Singh BP, Mathur RB. Carbon Nanotubes and Their Composites. Syntheses and Applications of Carbon Nanotubes and Their Composites. InTech; 2013. p. 193–222.
10. Petrea C, Gârea SA, Iovu H. The Influence of Different Types of Carbon Nanotubes on the Synthesis and Properties of Epoxy-based Nanocomposite Materials. Mater Plast. 2008;45(1):34–7.
11. Yıldırım A, Seçkin T. In Situ Preparation of Polyether Amine Functionalized MWCNT Nanofiller as Reinforcing Agents. Adv Mater Sci Eng [Internet]. 2014;2014:1–6. Available from: http://www.hindawi.com/journals/amse/2014/356920/
12. Bradley M, Izzia F. Carbon Black Analysis. Thermo Sci. 2008;
13. Hirsch A. Functionalization of single-walled carbon nanotubes. Angew Chemie - Int Ed. 2002;41(11):1853–9.
14. Schmidt G, Gallon S, Esnouf S, Bourgoin J-P, Chenevier P. Mechanism of the Coupling of Diazonium to Single-Walled Carbon Nanotubes and Its Consequences. Chem - A Eur J. 2009;15(9):2101–10.
15. Ávila-orta CA, González-morones P, Espinoza-gonzález CJ, Martínez-colunga JG, Neira-velázquez MG, Sáenz-Galindo A. Toward Greener Chemistry Methods

for Preparation of Hybrid Polymer Materials Based on Carbon Nanotubes. In: Suzuki S, editor. Syntheses and Applications of Carbon Nanotubes and Their Composities. INTECH; 2013. p. 167–92.

16. T.W. Odom, J. H. Hafner CML. Scanning Probe Microscopy Studies of Carbon Nanotubes. Carbon Nanotub Springer-Verlag Berlin Heidelb. 2001;80:173–211.

17. Britz DA, Khlobystov AN. Noncovalent interactions of molecules with single walled carbon nanotubes. Chem Soc Rev [Internet]. 2006;35(7):637–59. Available from: http://www.ncbi.nlm.nih.gov/pubmed/16791335

18. Sanchez-Valencia JR, Dienel T, Gröning O, Shorubalko I, Mueller A, Jansen M, et al. Controlled synthesis of single-chirality carbon nanotubes. Nature. 2014;512:61–4.

19. Prasek J, Drbohlavova J, Chomoucka J, Hubalek J, Jasek O, Adam V, et al. Methods for carbon nanotubes synthesis—review. J Mater Chem. 2011;21:15872.

20. Physicsworld. Mission: Tomorrow » Scientists delve deeper into carbon nanotubes – physicsworld.com [Internet]. [cited 2015 Mar 7]. Available from: http://missiontomorrow.tv/scientists-delve-deeper-into-carbon-nanotubes-physicsworld-com/

21. Gebhardt B. Type Selective Functionalization of Single-Walled Carbon Nanotubes. der Friedrich-Alexander-Universität Erlangen-Nürnberg Tag; 2012.

22. Peschel G. Carbon-carbon bonds Hybridization. Freie Univ Berlin website. Berlin, Germany; 2005;

23. Vernetztes Studium - Chemie, Chemie für Mediziner: Hybridisierung [Internet]. TORVS research team website. [cited 2016 Jan 27]. Available from: http://www2.chemie.uni-erlangen.de/projects/vsc/chemie-mediziner-neu/bindung/hybridisierung.html

24. SP2 Hybridization [Internet]. Pearson Education Website. [cited 2016 Jan 27]. Available from: http://wps.prenhall.com/wps/media/objects/724/741576/Instructor_Resources/Chapter_01/Text_Images/FG01_15.JPG

25. Dagotto E. Physical Properties of Carbon Nanotubes. University of Tennessee. 2010.

26. Yu O, Jing-Cui P, Hui W, Zhi-Hua P. The rehybridization of electronic orbitals in carbon nanotubes. Chinese Phys B [Internet]. 2008;17(8):3123–9. Available from: http://stacks.iop.org/1674-1056/17/i=8/a=059

27. Launois a LP, Roche PPS, Salvetat J. Understanging Carbon Nanotubes From Basics to Application. The Lecture Notes in Physics. Springer; 2006.

28. Double-Walled-CNT [Internet]. Nanoshel Website. [cited 2016 Jan 28]. Available from: http://www.nanoshel.com/wp-content/uploads/2015/09/Double-Walled-CNT.jpg

29. Eloranta J. Undergraduate Quantum Chemistry. California State, USA: California State University, Northridge; 2015. 156 p.

30. Ghosh S, Beckingham KM, Weisman RB. Carbon Nanotubes, Basic Concepts

and Physical Properties. WILEY-VCH Verlag CmbH & Co. KCaA; 2004.

31. Boris, Yakobson, Avouris. Mechanical Properties of Carbon Nanotubes. Carbon Nanotub. 2001;80(Appl. Phys.):287–327.

32. Collins PG. Defects and Disorder in Carbon Nanotubes. Oxford Handbook of Nanoscience and Technology: Frontiers and Advances. Oxford Univ. Press; 2009.

33. Grierson DS, Sumant A V, Konicek AR, Friedmann TA, Sullivan JP, Carpick RW. Thermal stability and rehybridization of carbon bonding in tetrahedral amorphous carbon. Appl Phys. 2010;107.

34. D.Hornbaker. Electronic Structure of Carbon Nanotube Systems Measured with Scanning Tuneling Microscopy. University of Illinois at Urbana-Champaign; 2003.

35. Orlikowski D, Buongiorno Nardelli M, Bernholc J, Roland C. Theoretical STM signatures and transport properties of native defects in carbon nanotubes. Phys Rev B. 2000;61(20):14194–203.

36. Niyogi S, Hamon MA, Hu H, Zhao B, Bhowmik P, Sen R, et al. Chemistry of Single-Walled Carbon Nanotubes. Acc Chem Res. 2002;35:1105–13.

37. Park S, Srivastava D, Cho K. Generalized chemical reactivity of curved surfaces: Carbon nanotubes. Nano Lett. 2003;3(9):1273–7.

38. Columbia University. larry-scott-CNT [Internet]. Columbia University Website. [cited 2016 Feb 1]. Available from: http://ftp.columbia.edu/cu/chemistry/////ance/scott-2014/larry-scott-graphic.jpg

39. Gómez MD. Polystyrene grafting of CNx nanotubes for the elaboration of polystyrene-based nanocomposites. IPICYT; 2007.

40. Toma FM. Covalently functionalized carbon nanotubes and their biological applications. SISSA. SISSA; 2009.

41. Jorio, A., Dresselhaus M. Carbon Nanotubes: Advanced Topics in the Synthesis, Structure, Properties and Applications. Dresselhaus G, editor. Springer; 2008.

42. Pan B, Xing B. Adsorption mechanisms of organic chemicals on carbon nanotubes. Environ Sci Technol. 2008;42(24):9005–13.

43. Wu TY, Guo N, Teh CY, Hay JXW. Theory and Fundamentals of Ultrasound. Advances in Ultrasound Technology for Environmental Remediation. Springer; 2013.

44. Pang YL, Abdullah AZ, Bhatia S. Review on sonochemical methods in the presence of catalysts and chemical additives for treatment of organic pollutants in wastewater. Springer; 2011.

45. Taurozzi JS, Hackley V a, Wiesner MR. Preparation of Nanoparticle Dispersions from Powdered Material Using Ultrasonic Disruption Preparation of Nanoparticle Dispersions from Powdered Material Using Ultrasonic Disruption. NIST Spec Publ 1200-2. 2012;

46. A. Hind. An Introduction to Optical Spectroscopy. Agilent’s Spectroscopy. Melbourne, Australia; 2011;

47. Harvey D. Spectroscopic methods. Analytical chemestry. 1971. p. 543–666.

48. Workman J. Applied Spectroscopy: A Compact Reference for Practitioners. Academic Press; 1998.

49. Stuart B. Infrared Spectroscopy: Fundamentals and Applications. Wiley; 2004.

50. Capria M. Physics before and after Einstein. IOS Press. 2005.

51. Roy SC, Kissel L, Pratt RH. Elastic scattering of photons. Radiat Phys Chem. 1999;56:3–26.

52. IUPAC. Compendium of Chemical Terminology. 2nd ed. 1997.

53. Technische Universitat Braunschweig. Molecular Spectroscopy [Internet]. [cited 2015 Mar 22]. Available from: http://www.pci.tu-bs.de/aggericke/PC4e_osv/Molecular-Spectroscopy.pdf

54. Infrared and Raman spectroscopy [Internet]. [cited 2015 Jun 9]. Available from: https://serc.carleton.edu/NAGTWorkshops/mineralogy/mineral_physics/raman_ir.html

55. Carey FA. Spectroscopy. Organic Chemistry. McGraw-Hill Companies; 2001.

56. ThermoNicoletCorporation. Introduction to Fourier Transform Infrared Spectrometry. Worldwide [Internet]. 2001; Available from: http://mmrc.caltech.edu/FTIR/FTIRintro.pdf

57. P. Griffiths, Hasseth JA De. Fourier Transform Infrared Spectrometry. 2nd ed. Wiley Blackwell; 2007.

58. J. NEAL. Fourier Transform Infrared Spectroscopy. Encyclopedia of Materials Characterization. Elsevier Inc; 1992. p. 416–27.

59. K. LANGHOLZ. Transmission and Reflection (ATR) Far-Infrared Spectroscopy Applied in the Analysis of Cultural Heritage Materials. Università di Bologna; 2009.

60. Gillie JK, Hochlowski J, Arbuckle-Keil G. Infrared spectroscopy. Anal Chem. 2000;72:71–9.

61. J. Paula, P. Atkins. Molecular Interactions. Physical Chemistry. 9th ed. Oxford; 2009.

62. W.D. Perkins. Fourier Transform-Infrared Spectroscopy. J Chem Educ. 1986;63(Chemical Instrumentation):A5–10.

63. Bracewell RN. The Fourier Transform and Its Applications. 3rd ed. McGrawHill; 2000.

64. Monsef Khoshhesab Z. Reflectance IR Spectroscopy. In: Theophile T, editor. Infrared Spectroscopy - Materials Science, Engineering and Technology. InTech; 2012. p. 233–44.

65. T. J. Matula, P. L. Marston, J. Acoust. Scattering of acoustic evanescent waves by circular cylinders: Partial wave series solution. Acoust Soc Am J. 2002;111(5):2378–2378.

66. PikeTechnologies. ATR – Theory and Applications. PIKE Technologies [Internet]. Madison, USA; 2011; Available from:

http://www.piketech.com/files/pdfs/ATRAN611.pdf

67. Wikipedia the free encyclopedia. File:ATR path-en.svg - Wikimedia Commons [Internet]. [cited 2015 Mar 15]. Available from: http://commons.wikimedia.org/wiki/File:ATR_path-en.svg

68. J. Mendham, R. C. Denney, J. D. Barnes, M. J. K. Thomas. Vibrational Spectroscopy. Vogels's Quantitive Chemical Analysis. 6th ed. Pearson Education Limited; 2000. p. 692–716.

69. White WB. Raman Spectroscopy. Encyclopedia of Materials Characterization. Elsevier Inc; 1992. p. 428–41.

70. Princeton Instruments. Raman spectroscopy basics. 2012;

71. Smith E, Geoffrey D. Modern Raman Spectroscopy – A Practical Approach. England: John Wiley & Sons Ltd; 2005.

72. Raman transitions [Internet]. Princeton Instruments Website. [cited 2015 Jun 9]. Available from: http://www.princetoninstruments.com/Uploads/Princeton/Images/raman_fig4.png

73. Le Ru EC, Etchegoin PG. A quick overview of surface-enhanced Raman Spectroscopy. Princ Surface-Enhanced Raman Spectrosc. 2009;1–28.

74. Chen K-H. Spontaneous Raman and Coherent Anti-Stokes Raman Spectroscopy. Harvard University; 1989.

75. Schwartz DT. Raman Spectroscopy : Introductory Tutorial. University of Washington. Washington, USA; 2009.

76. M.Reichenbacher, J.Popp. Chalenegs in molecular structure determination. Berlin: springer; 2012. 74 p.

77. A. Fadini, F.M. Schnepel. Vibrational Spectroscopy: Methods and Applications. Ellis Horwood Ltd; 1989.

78. Hahn DW. Raman Scattering Theory. Dep Mech Aerosp Eng Univ Florida. 2007;

79. ROA D. Basic Theory and Measurement of Raman Scattering. Molecular Catalysis and In-Situ Characterization Group. Dalian, China; 2010.

80. Codrich D. Applications and limits of Raman spectroscopy in the study of colonic and pulmonary malformations. UNIVERSITA' DEGLI STUDI DI TRIESTE; 2007.

81. Spectroscopy Facilities [Internet]. The Prashant Kamat lab at the University of Notre Dame. [cited 2015 Jun 16]. Available from: http://www3.nd.edu/~kamatlab/facilities_spectroscopy.html

82. Introduction to Raman Spectroscopy. Thermo Fisher Scientific Inc. USA; 2008;

83. Mayo D, Miller F, Hannah R. Course notes on the interpretation of infrared and Raman spectra. Hoboken, New Jersey: John Wiley & Sons, Inc; 2003.

84. Raman spectroscopy [Internet]. Department of Chemistry of University of California website. [cited 2014 Oct 17]. Available from: http://www.chem.uci.edu/~dmitryf/manuals/Fundamentals/Raman microscopy.pdf

85. Horiba. Raman Spectroscopy for Analysis and Monitoring. Jobin Yvon. Kyoto, Japan;

86. Lazar G, Zellama K, Vascan I, Stamate M, Lazar I, Rusu I. Infrared absorption properties of amorphous carbon films. J Optoelectron Adv Mater. 2005;7(2):647–52.

87. Vanyorek L, Meszaros R, Barany S. Surface and electrosurface characterization of surface-oxidized multi-walled N-doped carbon nanotubes. Colloids Surfaces A Physicochem Eng Asp. Elsevier B.V.; 2014;448(1):140–6.

88. Hodkiewicz J. Characterizing Carbon Materials with Raman Spectroscopy. Thermo Fish Sci. 2010;

89. Casiraghi C, Pisana S, Novoselov KS, Geim a. K, Ferrari a. C. Raman fingerprint of charged impurities in graphene. Appl Phys Lett. 2007;91(23):23–5.

90. Arvani M, Aghajanloo M. Multi-wavelength Raman characterization of back-gated monolayer and bilayer graphene. Halmstad University, Sweden; 2012.

91. Moorfield. Graphene - nanoCVD.co.uk [Internet]. NanoCVD Website (Moorfield Nano Technology). [cited 2016 Feb 1]. Available from: http://www.nanocvd.co.uk/graphene_material_nanoCVD.html

92. Allen PB. Electrons in graphene – massless Dirac electrons and Berry phase. Phys 556. 2007;

93. Piscanec S, Lazzeri M, Mauri F, Ferrari a. C. Optical phonons of graphene and nanotubes. Eur Phys J Spec Top. 2007;148(1):159–70.

94. Goler S, Yan J, Pellegrini V, Pinczuk A. Raman spectroscopy of magneto-phonon resonances in graphene and graphite. Solid State Commun. 2012;152(15):1289–93.

95. Lui CH, Malard LM, Kim S, Lantz G, Laverge FE, Saito R, et al. Observation of layer breathing modes in few-layer graphene through the combination Raman scattering. Nano Lett. 2012;

96. Jiang J-W, Wang B-S, Rabczuk T. Acoustic and breathing phonon modes in bilayer graphene with Moiré patterns. Appl Phys Lett. 2012;101(2).

97. Jespersen TS. Raman scattering in carbon nanotubes. University of Copenhagen; 2007.

98. Lui CH, Heinz TF. Measurement of layer breathing mode vibrations in few-layer graphene. Phys Rev B - Condens Matter Mater Phys. 2013;87(12):1–7.

99. Kuzmany H, Plank W, Hulman M, Kramberger C, Grüneis a., Pichler T, et al. Determination of SWCNT diameters from the Raman response of the radial breathing mode. Eur Phys J B. 2001;22(3):307–20.

100. Dresselhaus MS, Dresselhaus G, Saito R, Jorio a. Raman spectroscopy of carbon nanotubes. Phys Rep. 2005;409(2):47–99.

101. Costa S. Characterization of carbon nanotubes by Raman spectroscopy. Cent Knowl Based Nanomater Technol Inst Chem Environ Eng Szczecin Univ Technol Pol. 2008;

102. Datsyuk V, Kalyva M, Papagelis K, Parthenios J, Tasis D, Siokou a., et al.

Chemical oxidation of multiwalled carbon nanotubes. Carbon N Y. 2008;46(6):833–40.

103. Costa S, Borowiak-Palen E. Raman study on doped multiwalled carbon nanotubes. Acta Phys Pol A. 2009;116(1):32–5.

104. Jaeger BK. Single Walled Carbon Nanotube Raman and Infrared Spectroscopy , and Nanotube application in Gas Chromatography. Chemistry 400: Senior Seminar. 2010.

105. Ling Y, Deokar A. Microwave-Assisted Preparation of Carbon Nanotubes with Versatile Functionality. Carbon Nanotub Appl Electron Devices [Internet]. 2011;127–42. Available from: http://www.intechopen.com/books/carbon-nanotubes- applications-on-electron-devices/microwave-assisted-preparation-of-carbon-nanotubes-with-versatile- functionality

106. Nanocyl-TM NC7000 series - Product Datasheet – Thin Multi-Wall Carbon Nanotubes. Nanocyl-TM. 2009 Mar;1–2.

107. HUNTSMAN. Jeffamine ® D-230 Polyetheramine. 2008;1–2.

108. Lide DR. CRC Handbook of Chemistry and Physics. CRC Press LLC; 2005.

109. Mills B. Büchner funnel [Internet]. Wikipedia, The free encyclopedia. [cited 2015 Jul 26]. Available from: https://en.wikipedia.org/wiki/B%C3%BCchner_funnel

110. Cui Y, Van Duijneveldt JS. Adsorption of polyetheramines on montmorillonite at high pH. Langmuir. 2010;26(22):17210–7.

111. faculty of chemistry. Raman spectrometer Witec alpha 300 [Internet]. Krakow University Website. 2015. Available from: http://www2.chemia.uj.edu.pl/zor/inst_en.php

112. OChemOnline. Infrared spectroscopy absorption table [Internet]. OChemOnline Website. [cited 2015 Jul 29]. Available from: http://www.ochemonline.com/Infrared_spectroscopy_absorption_table

113. Blanch a. J, Lenehan CE, Quinton JS. Optimising surfactant aided dispersions of carbon nanotubes in aqueous solution. 2010 Int Conf Nanosci Nanotechnol [Internet]. 2010;132–5. Available from: http://ieeexplore.ieee.org/lpdocs/epic03/wrapper.htm?arnumber=6045209

114. Ellison MD, Good AP, Kinnaman CS, Padgett NE. Interaction of water with single-walled carbon nanotubes: reaction and adsorption. J Phys Chem B [Internet]. 2005;109(21):10640–6. Available from: http://www.ncbi.nlm.nih.gov/pubmed/16852291

115. Lin W, Moon KS, Zhang S, Ding Y, Shang J, Chen M, et al. Microwave makes carbon nanotubes less defective. ACS Nano. 2010;4(3):1716–22.

116. Chen W, Tao X. Ultrasound-induced functionalization and solubilization of carbon nanotubes for potential nanotextiles applications. MRS Proc. 2006;920.

117. Aravind, S. S. J., Baskar, P., Baby, T. T., Sabareesh, R. K., Das, S., & Ramaprabhu S. Investigation of Structural Stability, Dispersion, Viscosity, and Conductive Heat Transfer Properties of Functionalized Carbon Nanotube Based Nanofluids. J Phys Chem C. 2011;115:16737–44.

118. C. Alvarado, A. Galindo, L. Lopez, C. Orta. Surface modification of (MWCNT) with ultrasound H_2SO_4/HNO_3. Afinidad. 2011;68:370–4.

APPENDICES

Appendix A: IR Absorptions by Frequency Regions

4000-3000 cm^{-1}					
3700-3584	medium	sharp	O-H	stretching	alcohol
3700-3100	strong	broad	O-H	stretching	water
3550-3200	strong	broad	O-H	stretching	alcohol
3500-3400	medium		N-H	stretching	primary amine
3400-3250	medium		N-H	stretching	aliphatic primary amine
3350-3310	medium		N-H	stretching	secondary amine
3333-3267	strong	sharp	C-H	stretching	alkyne
3300-2500	strong	broad	O-H	stretching	carboxylic acid
3200-2700	weak	broad	O-H	stretching	alcohol
3100-3000	medium		C-H	stretching	alkene
3000-2000 cm^{-1}					
3000-2840	medium		C-H	stretching	alkane
3000-2800	strong	broad	N-H	stretching	amine salt
2830-2695	medium		C-H	stretching	aldehyde
2600-2550	weak		S-H	stretching	thiol
2349	strong		O=C=O	stretching	carbon dioxide
2275-2250	strong	broad	N=C=O	stretching	isocyanate
2260-2222	weak		C≡N	stretching	nitrile
2260-2190	weak		C≡C	stretching	alkyne
2175-2140	strong		S- C≡N	stretching	thiocyanate
2160-2120	strong		N=N=N	stretching	azide
2150			C=C=O	stretching	ketene
2145-2120	strong		N=C=N	stretching	carbodiimide
2140-2100	weak		C≡C	stretching	alkyne
2140-1990	strong		N=C=S	stretching	isothiocyanate
2000			C=C=N	stretching	ketenimine
2000-1670 cm^{-1}					
2000-1900	medium		C=C=C	stretching	allene
2000-1650	weak		C-H	bending	aromatic compound
1818-1750	strong		C=O	stretching	anhydride
1815-1785	strong		C=O	stretching	acid halide

1800-1770	strong	C=O	stretching	conjugated acid halide
1780-1770	strong	C=O	stretching	vinyl / phenyl ester
1775-1720	strong	C=O	stretching	conjugated anhydride
1760	strong	C=O	stretching	carboxylic acid
1750-1735	strong	C=O	stretching	esters or δ-lactone
1745	strong	C=O	stretching	cyclopentanone
1740-1720	strong	C=O	stretching	aldehyde
1730-1715	strong	C=O	stretching	α, β-unsaturated ester
1725-1705	strong	C=O	stretching	aliphatic ketone
1720-1706	strong	C=O	stretching	carboxylic acid
1710-1685	strong	C=O	stretching	conjugated anhydride
1710-1680	strong	C=O	stretching	conjugated acid
1690	strong	C=O	stretching	primary amide
1690-1640	medium	C=N	stretching	imine / oxime
1685-1666	strong	C=O	stretching	conjugated ketone
1680	strong	C=O	stretching	secondary or tertiary amide
1670-1400 cm^{-1}				
1678-1648	weak-medium	C=C	stretching	alkene
1650	strong	C=O	stretching	δ-lactone
1650-1600	medium	C=C	stretching	conjugated alkene
1650-1580	medium	N-H	bending	amine
1650-1566	medium	C=C	stretching	cyclic alkene
1648-1638	strong	C=C	stretching	alkene
1644-1594	strong	O-H	bending	water
1620-1610	strong	C=C	stretching	α, β-unsaturated ketone
1600-1500	strong	N-O	stretching	nitro compound
1465	medium	C-H	bending	alkane
1450-1375	medium	C-H	bending	alkane
1440-1395	medium	O-H	bending	carboxylic acid
1400-1000 cm^{-1}				
1420-1330	medium	O-H	bending	alcohol
1415-1380	strong	S=O	stretching	sulfate

1400-1000	strong		C-F	stretching	fluoro compound
1390-1380	medium		C-H	bending	aldehyde
1390-1310	medium		O-H	bending	phenol
1385-1365	medium		C-H	bending	alkane
1372-1335	strong		S=O	stretching	sulfonate sulfonamide
1372-1290	strong		N-O	stretching	nitro compound
1350-1342	strong		S=O	stretching	sulfonic acid
1350-1300	strong		S=O	stretching	sulfone
1342-1266	strong		C-N	stretching	aromatic amine
1310-1250	strong		C-O	stretching	aromatic ester
1275-1200	strong		C-O	stretching	alkyl aryl ether
1250-1020	medium		C-N	stretching	amine
1225-1200	strong		C-O	stretching	vinyl ether
1210-1163	strong		C-O	stretching	ester
1205-1124	strong		C-O	stretching	tertiary alcohol
1204-1177	strong		S=O	stretching	sulfonyl chloride
1200-1185	strong		S=O	stretching	sulfate
1195-1168	strong		S=O	stretching	sulfonate
1075-1020	strong		C-O	stretching	alkyl aryl ether vinyl ether
1170-1150	strong		S=O	stretching	sulfonamide sulfonic acid
1160-1120	strong		S=O	stretching	sulfone
1150-1085	strong		C-O	stretching	aliphatic ether
1124-1087	strong		C-O	stretching	secondary alco-hol
1085-1050	strong		C-O	stretching	primary alcohol
1070-1030	strong		S=O	stretching	sulfoxide
1050-1040	strong	broad	CO-O-CO	stretching	anhydride
1000-500 cm^{-1}					
995-960	strong		C=C	bending	alkene
950-910	medium		O-H	bending	carboxylic acids
915-885	strong		C=C	bending	alkene
900-650	strong		C-H	bending	
850-550	strong		C-Cl	stretching	halo compound
840-790	medium		C=C	bending	alkene
730-665	strong		C=C	bending	alkene
690-515	strong		C-Br	stretching	halo compound
600-500	strong		C-I	stretching	halo compound